

FDR4ATMOS Uncertainty Characterisation Document

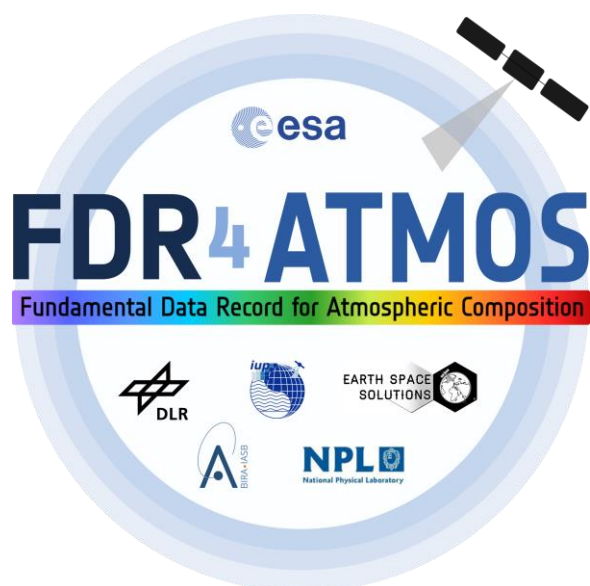
FDR4ATB-TN-NPL-020

Issue 1.1

19 July 2024



Deutsches Zentrum
für Luft- und Raumfahrt e.V.
in der Helmholtz-Gemeinschaft



Distribution List

Name	Affiliation	Copies
Angelika Dehn	ESA	1
Gabriele Brizzi	Serco	1
<i>Number of Copies</i>		2

Author and Compilation List

	Name	Affiliation	Signature
Author	Pieter De Vis Paul Green Sander Slijkhuis Klaus Bramstedt	NPL NPL DLR IUP	
Checked	Gunter Lichtenberg	DLR	
Approved	Angelika Dehn	ESA	

Change Record

Issue	Date	Page	Description of Change
draft	11/08/23	all	completely new
V0.6	14/02/24	all	Describe results based on analysis presented in PM13
V0.7	18/03/24	all	Update results based on feedback from Sander Slijkhuis
V0.8	30/03/24	all	Preliminary compete draft for internal review
V1.0	16/05/24	all	First issue
V1.1	19/07/24	all	Comments from Gabriele Brizzi addressed

Table of Contents

1	Introduction.....	5
1.1	Purpose and Scope of the document.....	6
1.2	Documents.....	8
1.2.1	References	8
1.3	Abbreviations and Acronyms.....	9
1.4	Document Overview	9
2	Uncertainty Calculation	10
2.1	Basics of uncertainty analysis.....	10
2.2	Metrological Framework	10
2.3	Guidance overview	10
2.4	Measurement Functions.....	12
2.5	Effects Tables.....	14
2.6	Propagating covariances through measurement functions.....	16
3	Results.....	18
3.1	SCIAMACHY	18
3.1.1	Irradiance	18
3.1.2	Radiance	22
3.1.3	Reflectance	27
3.2	GOME.....	29
3.2.1	Irradiance	29
3.2.2	Radiance	33
3.2.3	Reflectance	36
4	Limitations of approach	38
5	Future plans and recommendations.....	40
	Appendix A: GOME / SCIAMACHY L1b FDR Uncertainty analysis: Measurement Function, and	
	Uncertainty Effects Table (FDR4ATB.TN.DLR.016)	41

1 Introduction

FDR4ATMOS Uncertainty Characterisation Document

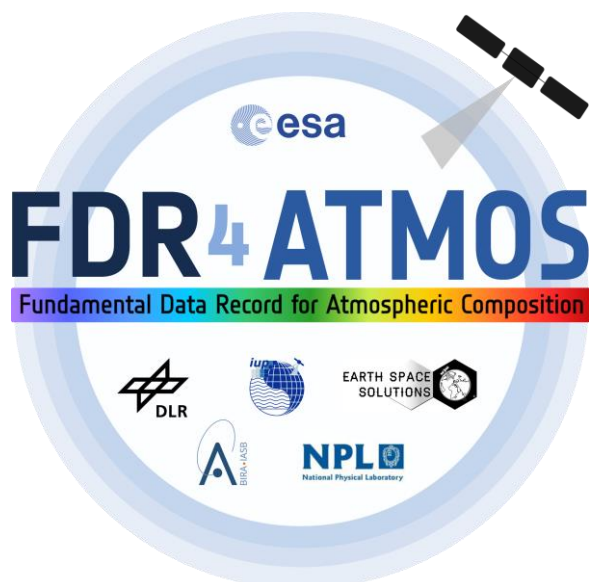
FDR4ATB-TN-NPL-020

Issue 1.1

19 July 2024



Deutsches Zentrum
für Luft- und Raumfahrt e.V.
in der Helmholtz-Gemeinschaft



1.1 Purpose and Scope of the document

The ESA FDR4ATMOS project aimed to assess the feasibility of and establish a pathway for the generation of Fundamental Data Records (FDRs) that target O₃, SO₂ and NO₂ from GOME-1 and SCIAMACHY data onboard the ERS-2 and ENVISAT platforms respectively.

A Fundamental Data Record (FDR) is defined as:

... a long, stabilised record of uncertainty-quantified sensor observations that are calibrated to physical units and located in time and space, together with all ancillary and lower-level instrument data used to calibrate and locate the observations and to estimate uncertainty.

FDRs are the fundamental output of a satellite sensor (Level 1 data). They are provided for two reasons:

1. to record all the information needed by contemporaneous use of the FDR to generate climate data records or thematic data products from the FDR, and
2. for the long-term preservation of the data set, including all the information that future scientists will need to know to understand how the data set was determined.

The purpose of generating a FDR for these two missions is to allow the data records to be used together as a single long-term record of observations with the data merging performed in metrologically rigorous ways, such that the impact of the various correction steps necessary can be quantified and made available with the new FDRs.

The general approach of the work was to

- Review the currently available data sets, the processing algorithms and their uncertainty information provision, using the extensive experience of the DLR and IUP Bremen teams and available literature.
- Identify gaps & limitations in the current uncertainty provision, and the propagation of the uncertainties through them, creating a work plan to best address the findings, focusing on data quality and calibration aspects.
- Work with the user community to determine an optimum data format and specification for the FDR, including the needs for the L2 experts at BIRA, IUP and DLR.
- The proposed FDRs are to be designed according to the QA4EO guidelines [RD-01] and provide the evidence base for the FDR construction, including the assumptions and limitations and an assessment of the overall accuracy and performance. Specifically:
 - The FDR should be easy to use and limit the number of parameters (≤ 10) contained besides the required metadata, and in the NetCDF file format.
 - The uncertainty specifications of FDR shall be complete, quantitative and traceable; ideally per-datum and include correlations in the spectral, spatial and temporal regimes that allow quantitative propagation of uncertainties.
 - Established metrological protocols and best scientific practice shall be employed, including the use of visualisations, consistent terminology, and general data descriptors consistent with the QA4EO guidelines.

- Produce an Uncertainty Characterization Report [This document] that describes the theoretical specifications and details the methodology used to derive uncertainty budgets for the specific data types and products.
- The initial dataset to be assessed was the documentation of the GOME evolution project [RD-02] and the Level 1 error review done during the QWG Phase F [RD-03] as well as the available Algorithm Theoretical Baseline Documents (ATBD) for the respective missions [RD-04, RD-05].

This document is the Uncertainty Characterization Report for the FDR4ATMOS products and describes the methods and results of the uncertainty analysis undertaken.

1.2 Documents

1.2.1 References

- [RD-1] QA4EO website <https://qa4eo.org/>
- [RD-2] D. Loyola and GOME-EVL team. GOME Evolution Final Report. Tech. rep. DLR-IMF, Nov. 2018.
- [RD-3] S. Slijkhuis and G. Lichtenberg. SCIAMACHY L1b product error analysis (ENV-TN-DLR-SCIA-0134). Tech. rep. 2. DLR-IMF, Nov. 2018.
- [RD-4] GOME/ERS-2 Level 0 to 1b ATBD, GOME-DLR-L1-ATBD, Issue 7, 20.06.2016 <https://earth.esa.int/web/sppa/mission-performance/esa-missions/ers2/gome/products-and-algorithms/products-information>
- [RD-5] SCIAMACHY L0-1c Processing ATBD - Algorithm Theoretical Baseline Document for Processor V.9, ENV-ATB-DLR-SCIA-0041, Issue 7, 2018-11-23
- [RD-6] 'General guidance on a metrological approach to fundamental data records (FDR)', FDR4ATMOS project deliverable D-B1-07
- [RD-7] GOME / SCIAMACHY L1b FDR Uncertainty analysis: Measurement Function, and Uncertainty Effects Table, FDR4ATB.TN.DLR.016 (See Appendix A)
- [RD-8] Coddington, O. M., Richard, E. C., Harber, D., Pilewskie, P., Woods, T. N., Chance, K., Liu, X., and Sun, K.: The TSIS-1 Hybrid Solar Reference Spectrum, Geophys. Res. Lett., 48, e2020GL091709, <https://doi.org/10.1029/2020GL091709>, 2021.

1.3 Abbreviations and Acronyms

ATBD	Algorithm Theoretical Baseline Document
BIRA	Belgisch Instituut voor Ruimte-Aeronomie (Belgian Institute for Space Aeronomy)
DLR	Deutsches Zentrum für Luft- und Raumfahrt e.V.
EO	Earth Observation
ESA	European Space Agency
FDR	Fundamental Data Record
GOME	Global Ozone Monitoring Experiment
IUP	Institute für Umweltphysik (Bremen)
MC	Monte Carlo
NPL	National Physical Laboratory, UK
QA	Quality Assurance
QWG	Quality Working Group
SCIAMACHY	Scanning Imaging Absorption spectroMeter for Atmospheric CHartography

1.4 Document Overview

- Section 1: Introduction (this section)
- Section 2: Uncertainty Calculation
- Section 3: Results
- Section 4: Limitations of approach
- Section 5: Future plans and recommendations
- Section 6: Summary and Conclusions
- Annex A:

2 Uncertainty Calculation

2.1 Basics of uncertainty analysis

The uncertainty analysis for the GOME and SCIAMACHY data products follows the QA4EO guidelines [RD-01] and is described in the 'General guidance on a metrological approach to fundamental data records (FDR)' document that formed deliverable D-B1-07 of this project [RD-06]. Since its issuance in 2020, the guidance has been developed and maintained on the QA4EO website, to ensure access to the current version (including the manual for the CoMet toolkit). The following is given as a summary of the guidance; full details are available in RD-01 and RD-06.

2.2 Metrological Framework

The Quality Assurance framework for Earth Observation ([QA4EO](#)) was established by the Committee on Earth Observation Satellites (CEOS) to define processes and procedures to achieve the QA4EO principle. These guidelines are based on the principles of metrology (the science of measurement). Metrology is responsible for maintaining the SI (the International System of Units) and the measurement systems derived from it. These measurements must be stable over centuries and equivalent all over the world, which can be achieved through the key principles of metrological traceability, uncertainty analysis and comparison.

A framework has been developed to act as a set of guidelines for how to apply the QA4EO principles to generate metrologically-rigorous data products. Guidelines have been developed such that it can be applied to:

- Fundamental Data Records (FDRs);
- Fiducial Reference Measurements (FRMs);
- Thematic Data Products (TDPs).

The QA4EO principle is:

Critical for ensuring that data and derived products are easily accessible in an open manner and have associated with them an indicator of quality traceable to reference standards (preferably SI) so users can assess suitability for their applications, i.e. the 'fitness for purpose'.

where the quality indicators are defined as

A Quality Indicator (QI) shall provide sufficient information to allow all users to readily evaluate the fitness for purpose of Earth observation data or derived products.

with a quality indicator traceability defined as

A QI shall be based on documented and quantifiable assessments of evidence demonstrating the level of traceability to internationally agreed (where possible SI) reference standards.

2.3 Guidance overview

The guidance is now held online and to promote consistency and minimize obsolescence, this guidance document will cite the on-line resources, as opposed to reproduce it here.

The overview of the guidance is provided in the [QA4EO executive summary](#) [RD-02] detailing the

overarching principles for applying meteorological principles to satellite data records. This document covers the definitions of metrologically-rigorous dataset types with the core principles of

- Documentation of the chain of traceability (to SI)
- A systematic approach to uncertainty analysis
- Use of comparisons to validate uncertainty statements

The document continues in discussing the particularities of working with EO data (as opposed to laboratory data) where the measurement configuration (observation and illumination geometry, for example) and measurand (observed from sensor in motion) continually vary, providing multiple dimensions of correlations that need to be considered within a data record and considered through the processing of data from L0/L1 to the higher geophysical products.

Ideally, a detailed systematic analysis of all steps to the creation of a data products is needed to provide the most complete picture of its uncertainty. However, it is recognized that almost no product meets this 'gold standard' definition due to lack of knowledge, historical record keeping, a complete physical understanding of every process or the time and budget required to make such an in-depth analysis. Pragmatically, the approach asks only that what is known is documented, with the rationale behind any assumptions, approximations or 'worst case' estimates stated communicating the degree of maturity of the analysis.

The executive summary concludes with the core principles of applying the approach

1. Define the measurand and measurement model
2. Define traceability with a diagram
3. Document each source of uncertainty with the core information needed to propagate it.
4. Calculate the product and its uncertainty
5. Practical documentation

More detailed documentation then follows.

The [Metrology Theoretical Basis](#) [RD-02] document starts with definitions of metrological vocabulary used throughout the document (and the metrological community) and the metrological underpinning principles set out in the Guide to the Expression of Uncertainty in Measurement (the GUM) and International Vocabulary of Metrology (the VIM).

The measurement model is described, that not only describes the algorithm from input parameters to output product, but also all quantities that affect the uncertainty in the output product. These could include environmental sensitivities (e.g., to temperature) and algorithm approximations.

Propagation of uncertainties is discussed, via analytical and Monte Carlo methods, with the practicalities of the propagation of correlations in the multivariant measurands found in EO resulting in some correlation parameterisation the pragmatic choice in the majority of cases. A later section in the document expands these ideas with practical options. The concept of correlation dimensions is introduced, aligned to the inherent cycles of sensor observation and/or calibration which allow a more intuitive route to understand how correlations influence the product uncertainty over increasing spatial and temporal scales. This concept adds a third error form, called 'structured' between the book-stopping terms 'random' and 'systematic'. Structured errors are correlated on some scales but become random

over longer scales and are generalised to in association with the periodicity of the underlying cause, for example, a scan, calibration cycle or orbit. The document goes on to describe common forms of this correlation in EO sensors and efforts made to make this parameterisation easier to handle – including the CoMet toolkit proposed to be used in this project.

Vocabulary and notation rules are outlined.

The [Uncertainty Analysis Process](#) [RD-02] document provides a practical guide to applying the approach.

1. How to define the measurand and measurement model
2. The different types of traceability diagram and suitably to the process structure
3. Documenting each source of uncertainty, including:
 - a. The term (identifier and notation)
 - b. Uncertainty magnitude
 - c. Sensitivity co-efficient
 - d. The probability distribution function for the uncertainty
 - e. Correlations with other effects
 - f. The form of each characteristic correlation dimension or length
 - g. A maturity statement describing how the effect has been evaluated
4. Calculate the product and its uncertainty – via the CoMet toolkit in this case.
5. Practical documentation

The [CoMet toolkit](#) was developed to streamline uncertainty storage and propagation. Uncertainties can be propagated manually or first stored in digital effects tables and then propagated (examples for both options are available on <https://www.comet-toolkit.org/examples/>).

2.4 Measurement Functions

The GOME and SCIAMACHY L1b reflectances and irradiances measurement functions and process chains are described in full in ‘GOME / SCIAMACHY L1b FDR Uncertainty analysis: Measurement Function, and Uncertainty Effects Table’ [RD-07] and it is not the author’s intention to duplicate this information here. In summary:

The general measurement function for calibrated irradiance is given by:

$$I(\lambda_i) = \frac{S_i - SS_i - DS_i - MEC_i}{BPDF_0(\lambda_i) \cdot m_{BPDF,t}(\lambda_i) \cdot (RR_{0,i}/PPG_{0,i})(\lambda_i) \cdot PPG_{t,i} \cdot m_t(\lambda_i) \cdot E_t(\lambda_i)} \quad (1)$$

where

S_i - measured signal at detector pixel i

λ_i - wavelength of detector pixel i

$I(\lambda_i)$ - incident radiation as function of wavelength

SS_i - straylight signal at detector pixel i (depending on all signals in the channel)

DS_i - dark signal of detector pixel i
 MEC_i - correction term for memory effect or non-linearity of detector pixel i
 $BPDF_0(\lambda_i)$ - bi-directional scattering distribution function of the diffuser; includes neutral density filter for SCIAMACHY
 $(RR_{0,i}/PPG_{0,i})(\lambda_i)$ - smooth part of the radiance response function as function of wavelength, for unpolarised input
 $PPG_{t,i}$ - pixel-to-pixel part of response function at detector pixel i
 $m_t(\lambda_i)$ - RR degradation monitoring factor as function of wavelength
 $E_t(\lambda_i)$ - etalon change as function of wavelength
 $m_{BPDF,t}(\lambda_i)$ - BPDF degradation monitoring factor

The general calibration equation for calibrated radiance may be written as:

$$I(\lambda_i) = \frac{S_i - SS_i - DS_i - MEC_i}{c_{pol}(\lambda_i, p_t(\lambda_i)) \cdot (RR_{0,i}/PPG_{0,i})(\lambda_i) \cdot PPG_{t,i} \cdot m_t(\lambda_i) \cdot E_t(\lambda_i)} \quad (2)$$

where subscript 0 denotes the quantity at a reference time $t = 0$ and subscript t denotes the quantity at the time of measurement, and:

S_i - measured signal at detector pixel i
 λ_i - wavelength of detector pixel i
 $I(\lambda_i)$ - incident radiation as function of wavelength
 SS_i - straylight signal at detector pixel i (depending on all signals in the channel)
 DS_i - dark signal of detector pixel i
 $(RR_{0,i}/PPG_{0,i})(\lambda_i)$ - smooth part of the radiance response function as function of wave-length, for unpolarised input
 $c_{pol}(\lambda_i, p_t(\lambda_i))$ - polarisation correction factor as function of wavelength and input polarisation
 $PPG_{t,i}$ - pixel-to-pixel part of response function at detector pixel i
 $m_t(\lambda_i)$ - degradation monitoring factor as function of wavelength
 $E_t(\lambda_i)$ - etalon change as function of wavelength

Within [RD-07], uncertainties are discussed for irradiance (using equation 1) and for radiance/reflectance (using equation 2). For the latter, the focus is on the uncertainty contributions that apply to reflectance. Any uncertainties common to radiance and irradiance are not considered here, because they will cancel in the reflectance.

Equations (1) and (2) form the basis of the analysis including discussion of the magnitude of the L1b uncertainty and the determination of the L2 product and considerations of the dominant terms (and those that cancel to first order as a result of the fitting process). Figure 1 shows the irradiance process chains for GOME and SCIAMACHY respectively, showing the importance of the order of the various correction terms and the predominate similarities of the method employed to both sensors L1b irradiance product.

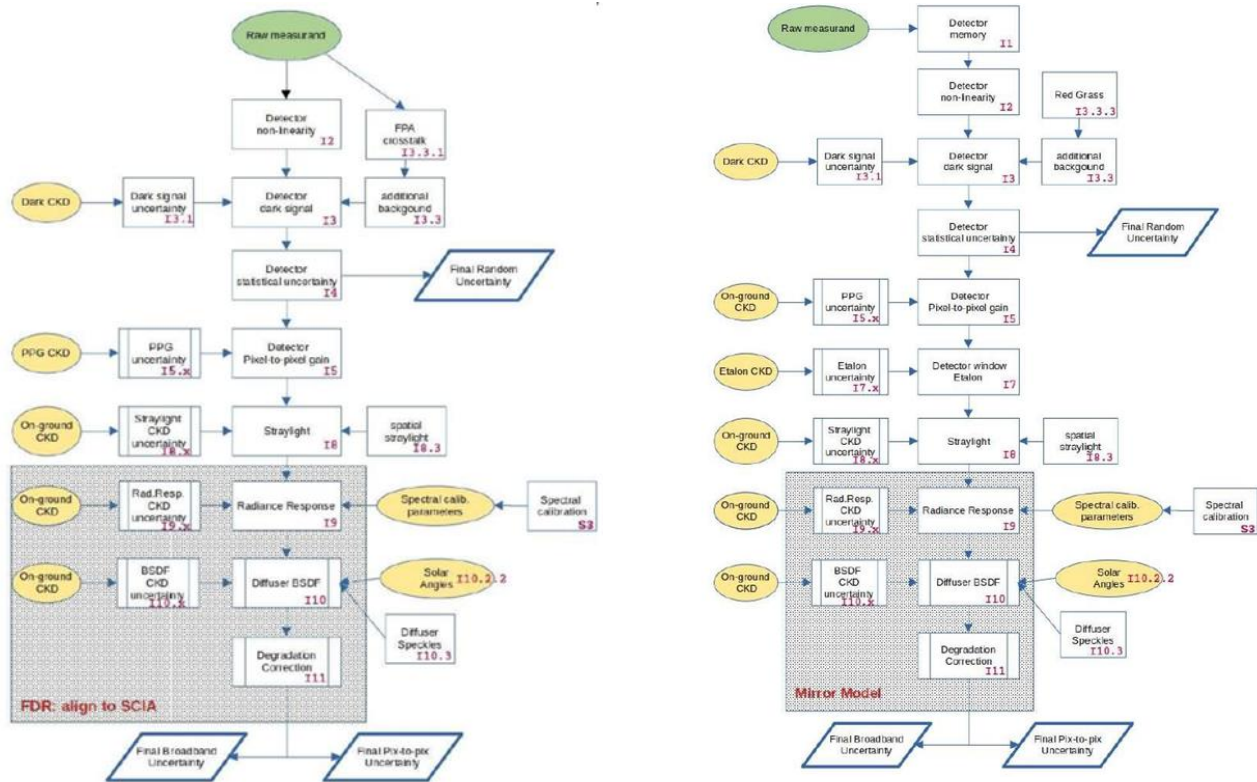


Figure 1 The GOME (left) and SCIAMACHY (right) process chain diagrams for the irradiance product uncertainties.

2.5 Effects Tables

For each quality and uncertainty in the L1b product, an effects table summarises the pertinent information necessary to propagate the uncertainty to the final product. Analysis of the contributors was prioritized based on their relevance to the products. Not all contributors were fully assessed, and some information remains incomplete. However, the dominant terms that drive the overall uncertainty magnitude have been addressed. A recommendation for future study is to fully address the incomplete data, providing validation of the assumptions made in this project. The effects table template, provided in RD-06 is given in Figure 2. Summary effects tables for SCIAMACHY and GOME are provided in RD-07 (provided here as appendix A).

Table descriptor		Value/Parameter	Notes
Name of effect		A unique name to describe the effect	
Effect identifier		A unique number used to identify the position in the uncertainty tree or process chain	
Affected term in measurement function		Name and standard symbol of affected term	Usually an effect will only affect a single term, though there may be exceptions. The next higher-level identifier should be reported.
Maturity of analysis	Maturity of uncertainty estimate	0 – Effect identified, no quantification performed (no further information in cells below) 1 – Rough estimates only 2 – Some analysis performed to estimate values 3 – Rigorous analysis performed	This allows for the fact in the FDR/CDR we haven't thought everything through in detail and makes that very clear to users. If the maturity is low, we may still be able to estimate if it is negligible or minor, or if it's possibly significant (and therefore needs more work soon)
	Maturity of correlation scale estimate	0 – Not done 1 – Estimated 2 – Based on analysis, unsure about correlation shape 3 – Strong evidence	Reference to the evidence for the maturity assessment, e.g. publication, report, weblink etc.
	If maturity of estimate is 0 or 1, how significant do you expect this effect to be?	Negligible, Minor or Significant? For pixel level results and for long-term / large scale results	
Correlation type and form	From level xx	Select one of the types defined in §6.3 and Table 4	See §6.3 Define the level of analysis from, then to, e.g. level 0 to level1, and the relevant scales, e.g. per scan, orbit, calibration cycle etc. If there is a correlation with another effect, state its identifier.
	temporal scale type & form [time]		
	spatial scale type & form [geospatial coordinates]		
	Spectral type & form		
Correlation scale	From level xx	What is the correlation scale	See §6.4
	temporal scale [time]		
	spatial scale [geospatial coordinates]		
	Spectral scale		
Uncertainty	PDF shape	Functional form of estimated error distribution for the term, see Table 3	
	units	Units in which PDF shape is expressed (units of term, or can be a percentage etc)	See comment in §5.3.1 where uncertainty and sensitivity cannot be separated
	magnitude	Value(s) or parameterisation estimating width of PDF	
Sensitivity coefficient		Value, equation or parameterisation of sensitivity of measurand to term Can also flag "included in uncertainty" (by making this equal 1)	Where the uncertainty and sensitivity coefficient cannot be separated the sensitivity coefficient should be one and the uncertainty is in units of the measurand.
Validation		A description of any validation of the uncertainty at effect level.	The source of the uncertainty information and validation should also be identified.

Figure 2. Effects table template for the GOME and SCIAMACHY product uncertainty contributors.

2.6 Propagating covariances through measurement functions

To characterise the typical uncertainties for the SCIAMACHY and GOME FDRs, we do a detailed uncertainty propagation for a few example files using a custom FDR4ATMOS uncertainty characterisation tool which is developed in Python. The uncertainty propagation itself is done using the **punpy tool** (<https://punpy.readthedocs.io/en/latest/>), which is part of the CoMet toolkit (www.comet-toolkit.org). In order to propagate the uncertainties, each of the measurement functions detailed in Section 2.4 are implemented as Python functions within the FDR4ATMOS uncertainty characterisation tool. As an example, we provide the implementation for the dark signal in Figure 3.

```
class DarkSignal:
    def function_SCIA(self, f_coadd, FPNi, PETi, LCiT):
        """
        This function implements the measurement function.
        Each of the arguments can be either a scalar or a vector (1D-array).

        :param f_coadd: coadding factor for the cluster containing detector pixel i
        :param FPNi: FPN (=offset) for detector pixel i
        :param PETi: pixel exposure time (single-readout integration time) at detector pixel i
        :param LCiT: leakage current of detector pixel i at detector temperature T
        :return: dark signal of detector pixel i
        """
        DSi = f_coadd * (FPNi + PETi * LCiT)
        return DSi
```

Figure 3 Example of the Python implementation of a measurement function (Dark Signal).

These measurement functions take a number of input quantities, here provided as arguments to the Python function. The input quantities for the various measurement functions come from either an input file provided by the user, or from the output of another measurement function (which in turn has its own input quantities which again can come from inputs or further measurement functions). Each input quantities can in this way be traced back (through the measurement functions), to values provided in the input files.

For each of the input quantities in the input file, uncertainties are provided as well in the same file. The provided uncertainty contributions match those listed in the effects tables in RD-07 (provided here as appendix A) where possible. The effects tables also allow to determine the error-correlation information associated with each uncertainty contribution.

For SCIAMACHY, two example files are used for irradiance (on the 27th of February 2003 and on the 27th of February 2012), and four for radiance (an Atlantic scene on the 25th of April 2003 and the 17th of April 2010, and a scene over Mauretania on the 12th of April 2003 and the 17th of April 2010). For GOME, three irradiance files (on the 3rd of July 1997, 27th of February 2003 and 20th of July 2010), and two example radiance files are used (one Atlantic scene and one scene over Mauretania, both from 2003). Only input data for wavelengths within the FDR ranges are used, i.e. $313 \text{ nm} < \lambda < 347 \text{ nm}$, $424 \text{ nm} < \lambda < 495 \text{ nm}$ or $754 \text{ nm} < \lambda < 776 \text{ nm}$.

The FDR4ATMOS uncertainty characterisation tool reads in the input quantities and their uncertainties from the input files for above examples and combines them with the error-correlation information from the effects tables. These are then propagated through the various measurement functions in order to get uncertainties as well as error correlation information on the final radiance, irradiance and reflectance values. This is done using a Monte Carlo approach (implemented in punpy - <https://punpy.readthedocs.io/en/latest/content/atbd.html#monte-carlo-method>).

In addition to providing the total uncertainties together with an error-correlation matrix, the FDR4ATMOS uncertainty characterisation tool also propagates different uncertainty components independently, separating them based on their error-correlations. The first decomposition is based on the spectral error correlation, and the total uncertainty is decomposed into random, systematic and structured uncertainties. This division into these separate components is especially important for the harmonisation of GOME to SCIAMACHY. This process has different effects on the various types of uncertainties: the systematic uncertainties in GOME will be removed, and instead the SCIAMACHY systematic uncertainties will apply to the harmonized GOME data. Random uncertainties will be 'smoothed out' in the harmonisation process. For structured uncertainties, we need to consider the spectral correlation scales to determine whether or not they will affect the harmonisation.

On top of this separation into random, systematic and structured uncertainties, the FDR4ATMOS uncertainty characterisation tool also separates into temporally fully correlated and non-correlated components, as well as separates between components that are correlated between radiance and irradiance (i.e. both measurands are affected by a single effect in the same way), and components that independently affect radiance and irradiance. The latter is important as when reflectance is calculated, the uncertainties for effects that are correlated between radiance and irradiance will become negligible when taking the ratio between the two measurands.

Results presented in Section 3 will separate these various components, as well as investigate the dominant sources of uncertainties coming from the input files, for both the total uncertainties and the random uncertainties.

3 Results

3.1 SCIAMACHY

3.1.1 Irradiance

We start by performing a sanity check that the measurement functions have been correctly implemented. This is done by calculating the irradiance from the input quantities in the input file and comparing to the irradiance (Sun Mean Reference spectrum, which is the mean over 172 individual measurements) in the same file. We do not expect these to be exactly the same as the angles used are not exact and polarisation is not taken into account. In the top panel of **Figure 4** it is shown the calculated irradiance has the expected shape, and the bottom panel shows the differences with the Sun Mean Reference spectrum are sufficiently small (similar to expected differences due to simplification in measurement functions like lack of polarisation).

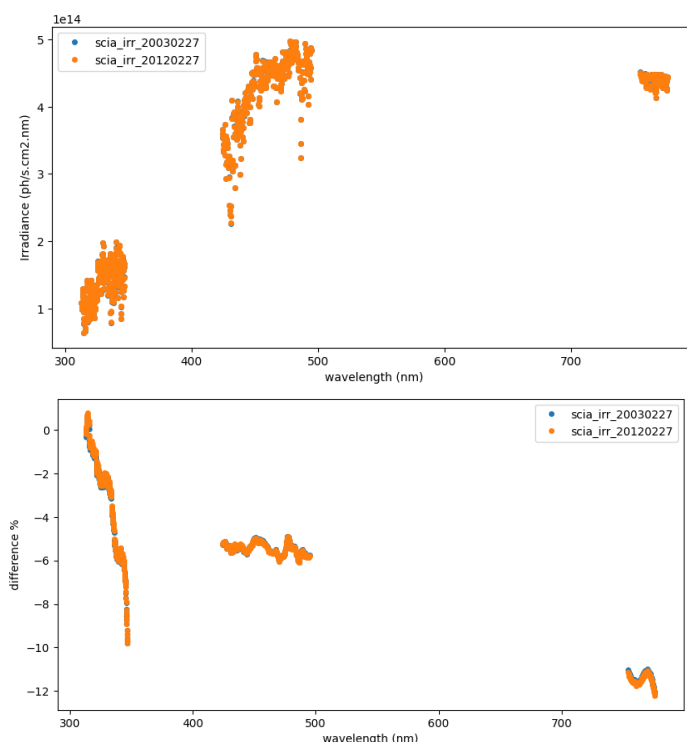


Figure 4: *Top: Calibrated SCIAMACHY irradiance as calculated by the measurement functions in the FDR4ATMOS uncertainty characterisation tool. Bottom: Difference in percent between the calculated irradiance and the expected Sun Mean Reference spectrum. The observed difference is expected as the angles used are not exact and polarisation is not taken into account.*

The combined irradiance uncertainties and error-correlation for the two SCIAMACHY example files are given in **Figure 5**. We can see that the uncertainties for the two examples are very similar and are both between 2% and 3%. The error-correlations are nearly identical as well and only one example is shown. In order to calculate these error correlation matrices, we first add the error covariance matrices for each uncertainty contribution, and then derive the error correlation matrix from the combined error covariance matrix. In these error-correlation matrices, values close to 1 mean the errors for two (spectral) pixels are highly correlated, values of zero mean errors are not correlated, and values of -1 mean errors

are anti-correlated (though note that none of the values in the error correlation matrix in Figure 5 are negative). We can see the uncertainties within the same band are fairly constant, and the errors are very correlated.

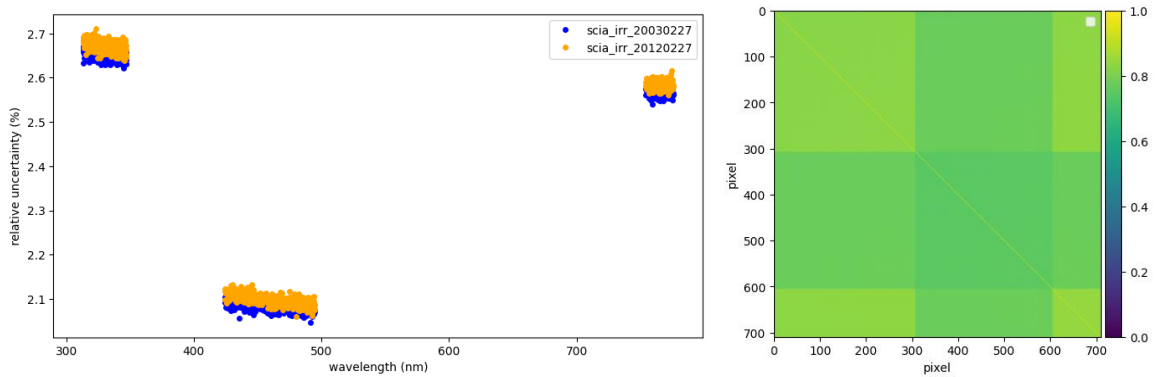


Figure 5: Left: Combined uncertainties on irradiance for the 2 example input files for SCIAMACHY. Right: error-correlation matrix with respect to spectral pixels for the input file from 2003. The errors for the different wavelengths are highly correlated, especially within the same band.

In **Figure 6**, the uncertainties are decomposed into components with random, systematic and structured error-correlations with respect to wavelength. The systematic uncertainties dominate (in line with the error correlation matrix shown in **Figure 5**), and the random and structured uncertainties are approximately equally important. The results for the 2003 and 2012 examples are very similar. This type of decomposition is relevant to understand the uncertainties expected for L2 products. The L2 retrievals rely on relative differences. The spectrally systematic uncertainties will thus only have a small or negligible effect on the L2 products.

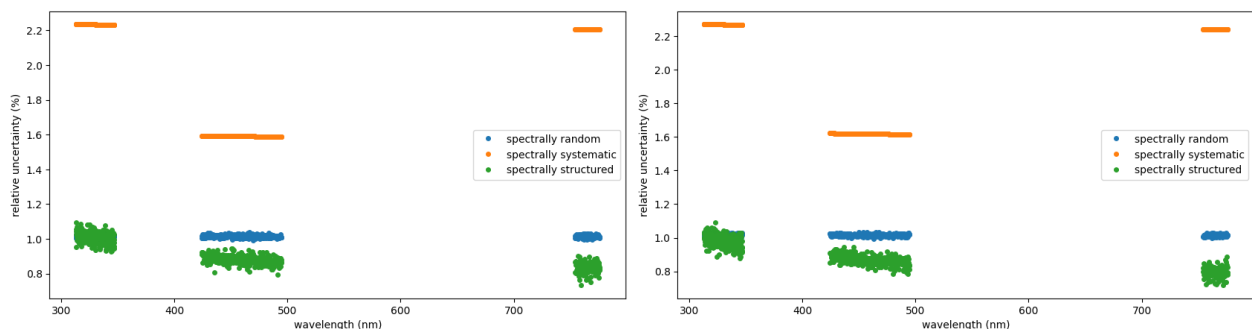


Figure 6: SCIAMACHY irradiance uncertainties decomposed into components for which the errors are spectrally uncorrelated (random - blue), spectrally fully correlated (systematic - orange), or spectrally somewhat correlated (structured - green) for the input file from 2003 (left) and 2012 (right).

Next, we investigate the decomposition into temporally random and systematic uncertainties in **Figure 7**. The systematic uncertainties again dominate (even somewhat more so than when decomposing by the spectral error-correlation). Most uncertainties will thus be entirely in common with other wavelengths/ repeated measurements.

In **Figure 7**, the irradiance uncertainties are also decomposed into uncertainties with errors that are fully correlated between radiance and irradiance, and those that are independent between radiance and irradiance. The uncertainty components with correlated errors are slightly larger than those with the independent errors. The uncertainty components that are correlated between radiance and irradiance will become negligible when propagated to reflectance, as they mostly ‘cancel out’ with the errors on radiance (see also next section).

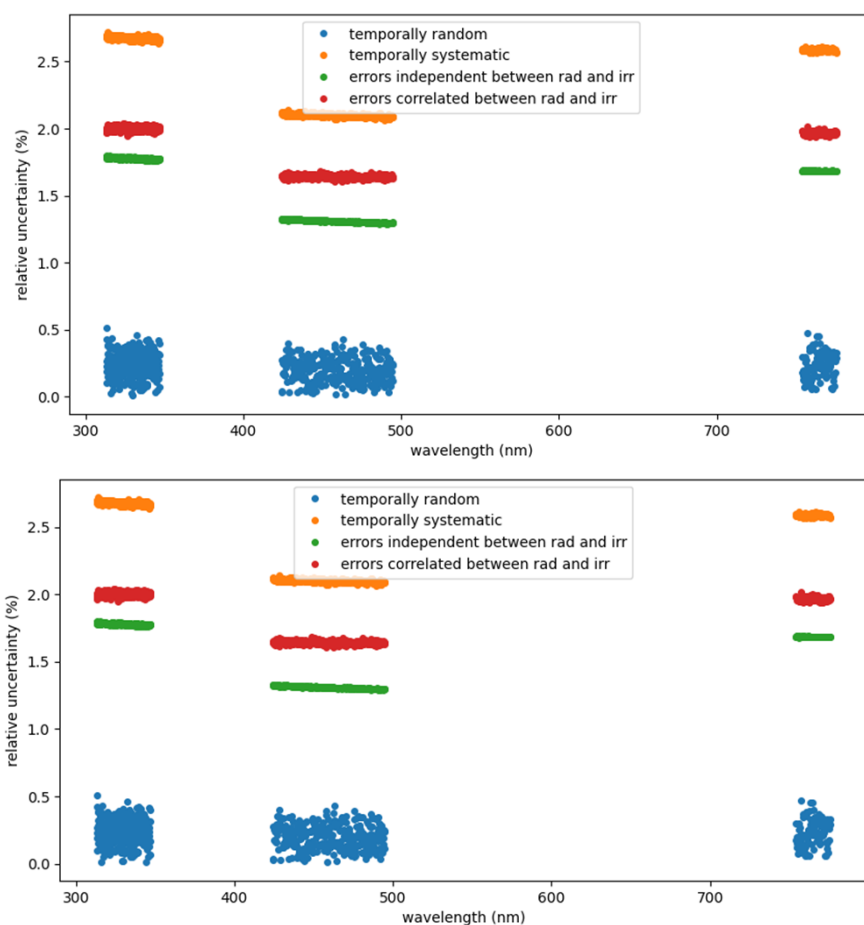


Figure 7: *SCIAMACHY irradiance uncertainties decomposed into components for which the errors are temporally uncorrelated (random - blue) and temporally fully correlated (systematic - orange). In addition, the uncertainties are also decomposed into a component for which the errors are independent (green) between radiance and irradiance, and a component that is correlated (red) between radiance and irradiance. Results for the input file from 2003 (top) and from 2010 (bottom).*

To better understand what drives the irradiance uncertainties, in **Figure 8** we plot the irradiance uncertainties originating from different sources. Here the input quantities in Equation (1) are combined in a few different categories. u_{signal} includes all the terms in the numerator of Equation (1). Their combined contribution is small. Next, u_{radresp} provides uncertainty on the radiance response. This component gives the largest contribution. Specifically, the on ground calibration distance and standard deviation are the largest contributors to this component. The $u_{\text{degradation}}$ component includes all the degradation terms, such as the radiance response degradation, BSDF degradation, etalon changes as well as the PPG uncertainties. This combined component is also rather small (<0.5%). Finally, there is

also an uncertainty component u_{bsdf} on the BSDF correction, which is the second largest contribution.

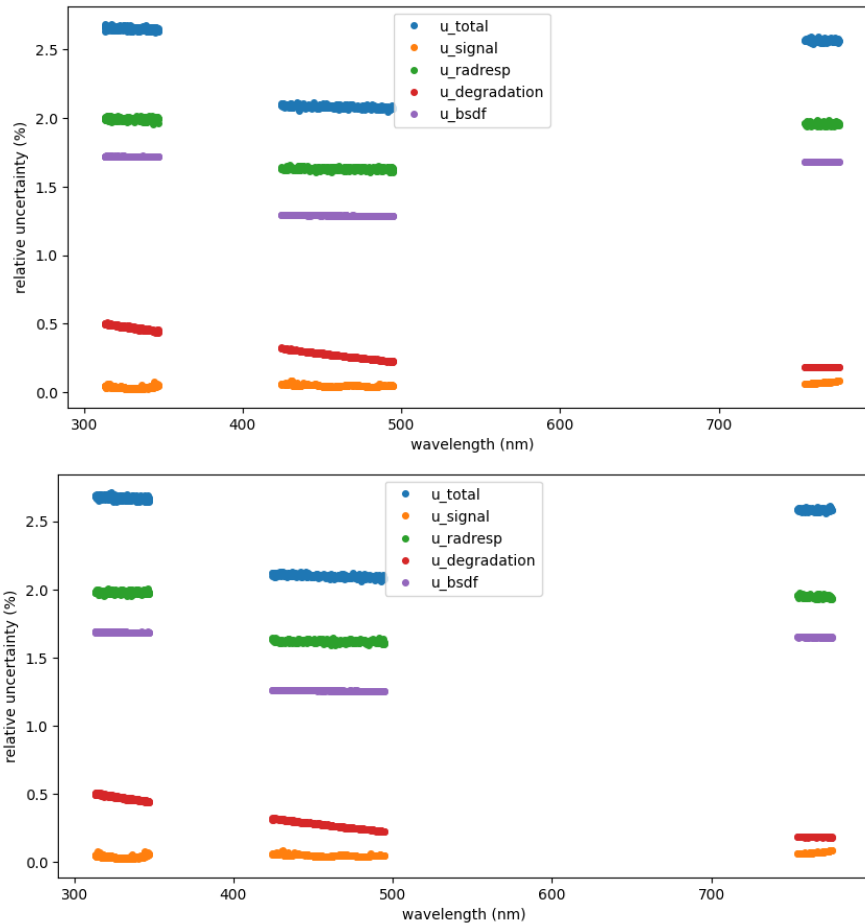


Figure 8: *SCIAMACHY irradiance uncertainties decomposed into components originating from uncertainties on different input quantities. for the input file from 2003 (top) and 2010 (bottom).*

In **Figure 9**, we repeat the same decomposition, but now only including the sources of uncertainty that have a random spectral error correlation (as these are the ones that will be important for the L2 products). We see that it is still the radiance response that is the dominant contribution. The BSDF correction uncertainty now becomes very small ($\sim 0.1\%$). The degradation uncertainty is unmodified, but now contributes a larger proportion of the total random uncertainty.

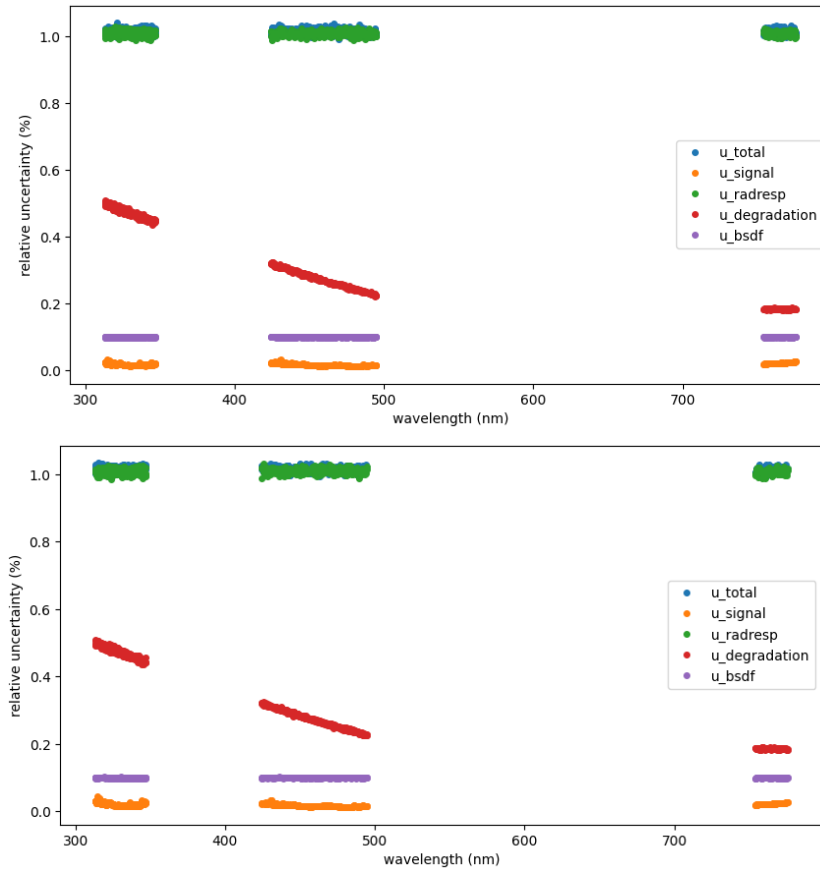


Figure 9: *SCIAMACHY irradiance uncertainties decomposed into components originating from uncertainties on different input quantities, where only uncertainties with a spectrally random error correlation are included, for the input file from 2003 (top) and 2012 (bottom).*

3.1.2 Radiance

Next, uncertainties are propagated for the radiance example products. Here, two dates will be considered (April 2003 and April 2010) for two different scenes (Atlantic and Mauretania). We again start by performing a sanity check in that the measurement functions have been correctly implemented. This is done by calculating the radiance from the input quantities in the input files and comparing to the calibrated radiance also present in the same file (**Figure 10**). We do not expect these to be exactly the same as the angles used are not exact and polarisation is not taken into account. The UV channel shows the largest differences, which could be caused by polarisation effects. The visible and NIR channels show small differences.

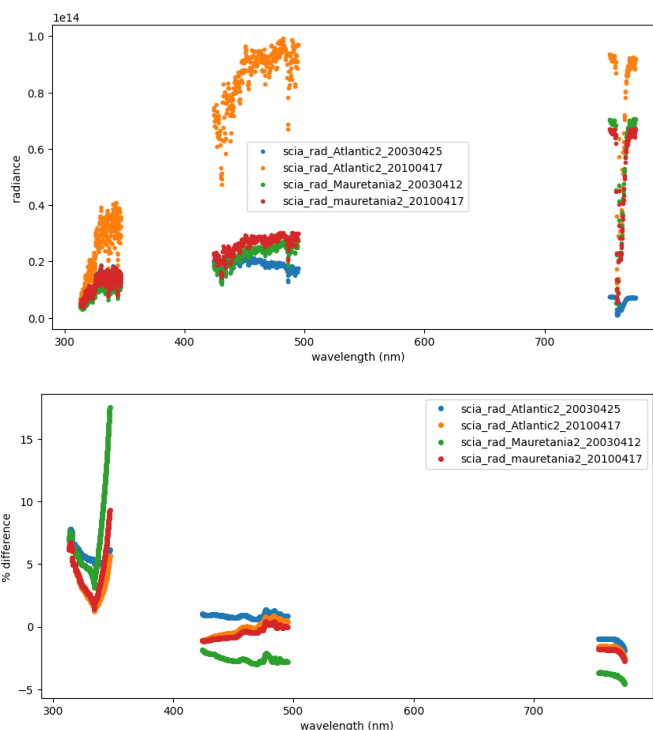


Figure 10: Top: Calibrated SCIAMACHY radiance as calculated by the measurement functions in the FDR4ATMOS uncertainty characterisation tool.

The total radiance uncertainties and error-correlation for the four example files are given in **Figure 11**. We can see that the uncertainties for the four examples are very similar and are both between 1.5 and 2.5%. The radiance uncertainties are thus smaller than the irradiance uncertainties. We note the focus of the uncertainty analysis (as described in RD-07), was on reflectance rather than radiance. Some radiance uncertainty contributions have thus been omitted, as they do not affect the reflectance. The error-correlations are nearly identical for each of the 4 examples and only one example is shown in the right panel of **Figure 11**. We can see the uncertainties within the same band are fairly constant, and the errors are very correlated (especially for UV and NIR bands).

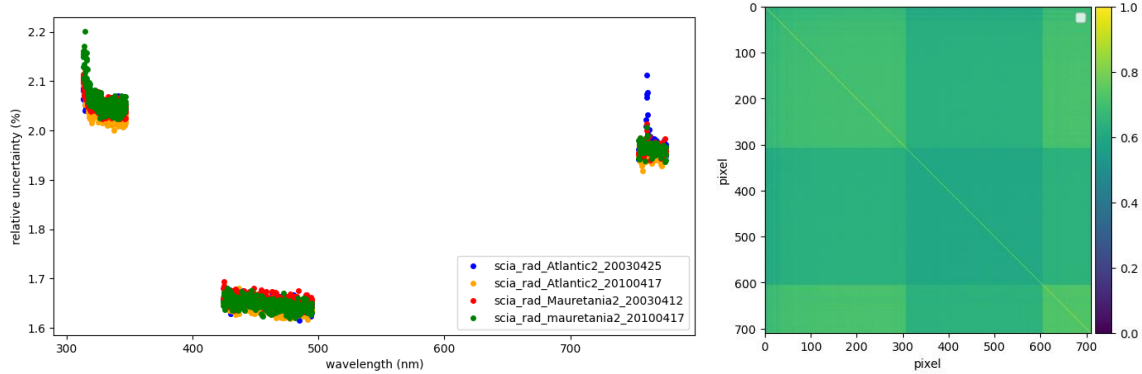


Figure 11: Left: Combined uncertainties on radiance for the 4 example input files for SCIAMACHY. Right: error-correlation matrix with respect to spectral pixels for the Atlantic input file for the scene in April 2003. The errors for the different wavelengths are highly correlated.

In **Figure 12**, the radiance uncertainties are decomposed based on their spectral error correlation. Just as for the irradiance uncertainties, we find the systematic uncertainties dominate. The random radiance uncertainties have similar values to the random irradiance uncertainties (1%). The systematic and structured radiance uncertainties are somewhat lower than for irradiance. The results for the 4 different examples are all similar.

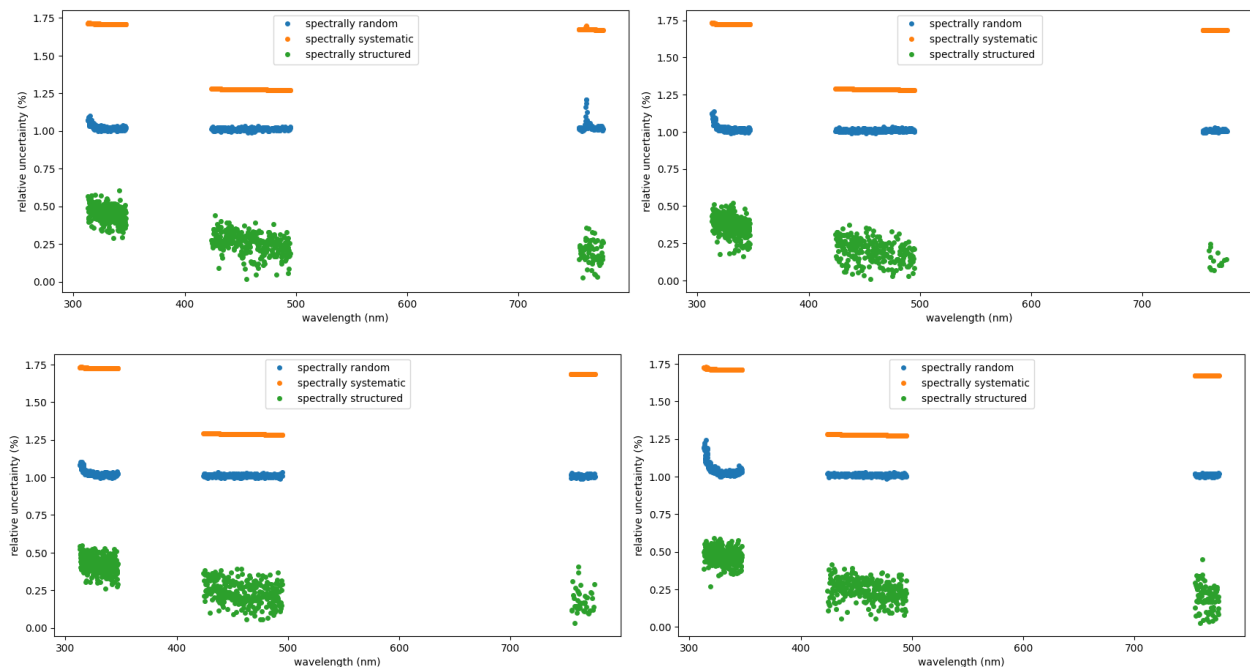


Figure 12: SCIAMACHY radiance uncertainties decomposed into components for which the errors are spectrally uncorrelated (random), spectrally fully correlated (systematic), or spectrally somewhat correlated (structured) for the Atlantic input file (top) and Mauretania input file (bottom) for the scene in April 2003 (left) and April 2010 (right).

Next, in **Figure 13** we decompose the radiance uncertainties by their temporal error correlation and by whether or not the radiance and irradiance errors are correlated. Uncertainties that have a systematic temporal error correlation dominate over random components and uncertainties for which the errors are correlated between radiance and irradiance dominate uncertainties for which the errors are independent. These are similar results as for the irradiance uncertainties, but for radiance these components dominate even stronger. Here again, the results are similar for the 4 different examples.

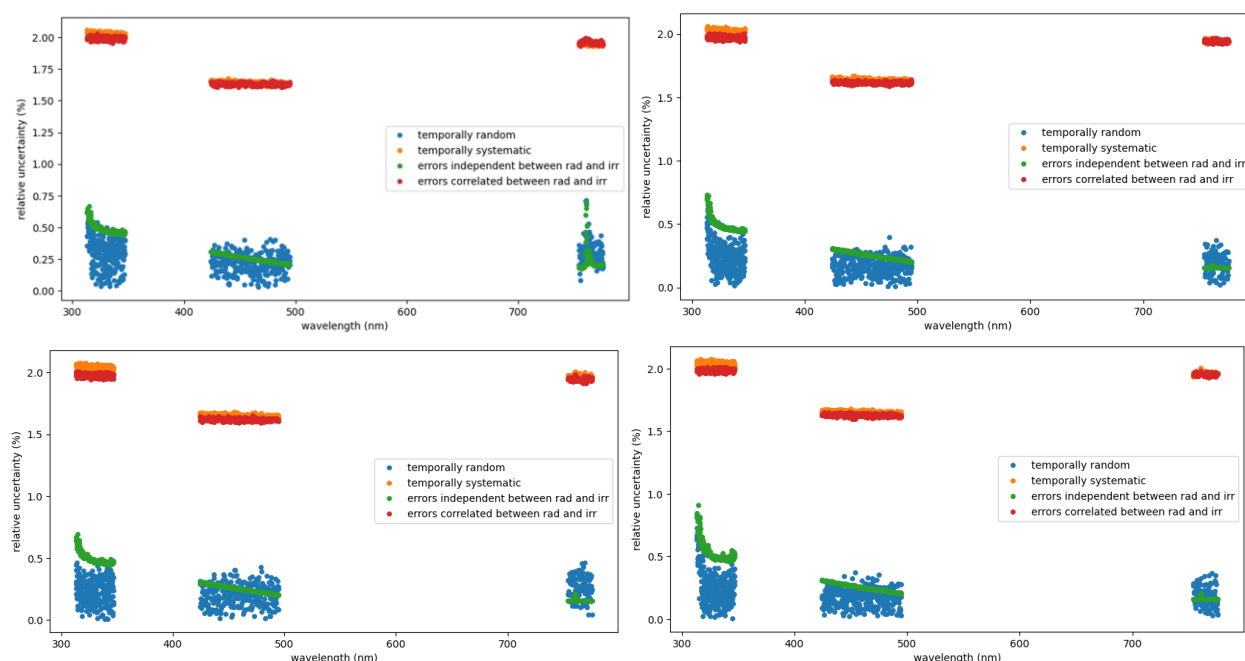


Figure 13: *SCIAMACHY radiance uncertainties decomposed into components for which the errors are temporally uncorrelated (random) and temporally fully correlated (systematic). In addition, the uncertainties are also decomposed into a component for which the errors are independent between radiance and irradiance, and a component that is correlated between radiance and irradiance. Results for the Atlantic input file (top) and Mauretania input file (bottom) for the scene in April 2003 (left) and April 2010 (right).*

In **Figure 14**, the uncertainties are decomposed based on the source of uncertainty (i.e. which group of input quantities they came from). The same categories are used for radiance as for irradiance, with the exception of the BSDF correction uncertainty. This term only applies in the irradiance measurement function and is thus not included here for radiance. The u_{signal} component includes all the terms in the numerator of Equation (2). Their combined contribution is small, though larger than was the case for irradiance. Next u_{radresp} provides uncertainty on the radiance response. This component gives the largest contribution. Specifically, the calibration distance and standard deviation are the largest contributors to this component. The $u_{\text{degradation}}$ component includes all the degradation terms, such as the radiance response degradation, BSDF degradation, etalon changes as well as the PPG uncertainties. This combined component is also rather small ($<0.5\%$). Overall, this uncertainty decomposition is very similar as for irradiance, with the exception of BSDF uncertainties not being included.

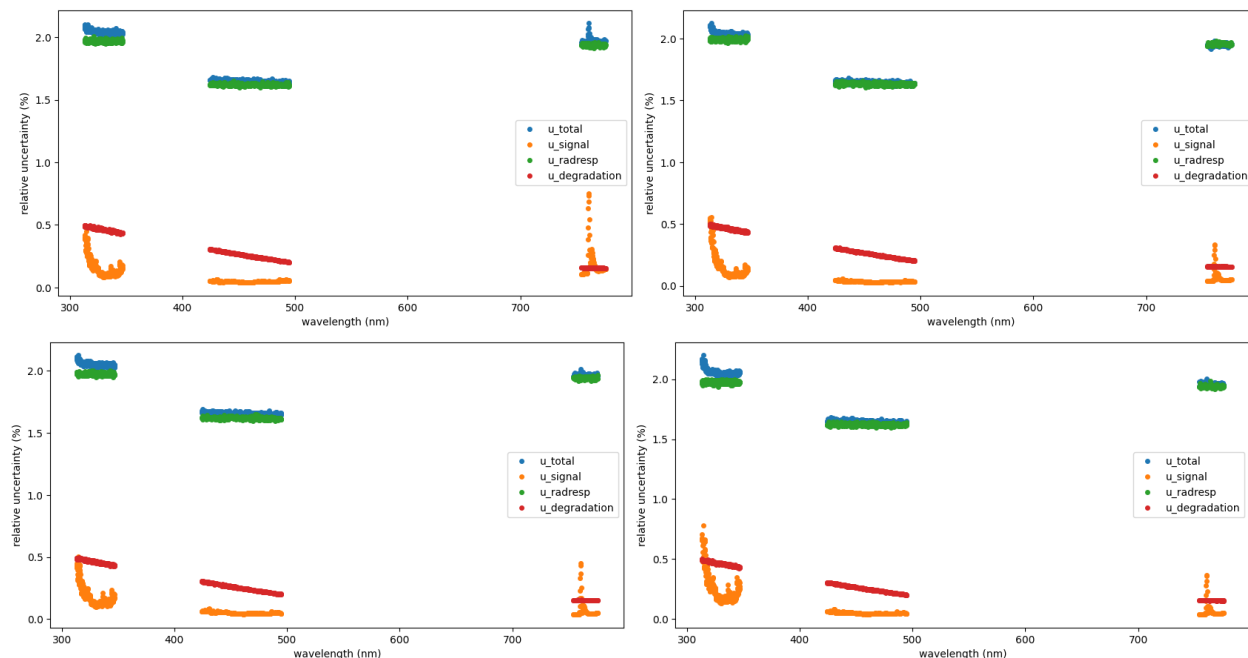


Figure 14: *SCIAMACHY radiance uncertainties decomposed into components originating from uncertainties on different input quantities. for the Atlantic input file (top) and Mauretania input file (bottom) for the scene in April 2003 (left) and April 2010 (right).*

In **Figure 15**, the same analysis is repeated for the (spectrally) random uncertainties only (since these are the most affecting the L2 products). Again, a similar picture emerges as was the case for irradiance. The decomposed uncertainties are similar, with the exception of somewhat larger u_{signal} uncertainties, and no BSRF uncertainties on radiance.

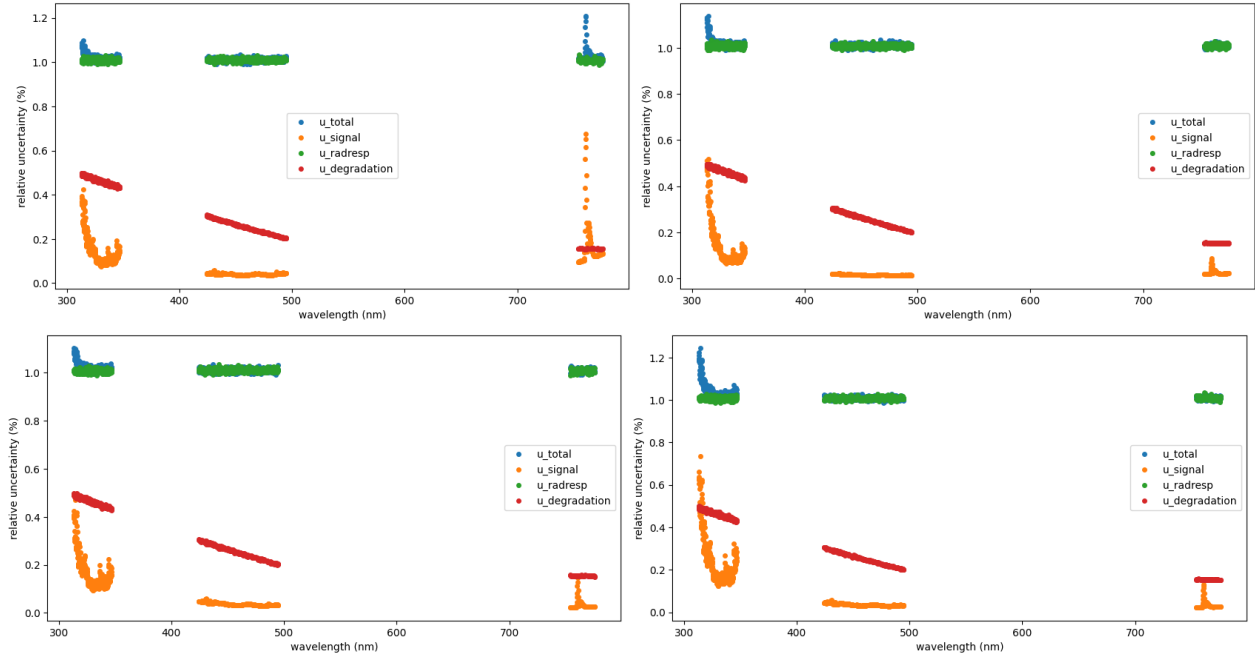


Figure 15: *SCIAMACHY radiance uncertainties decomposed into components originating from uncertainties on different input quantities, where only uncertainties with a temporally random error correlation are included, for the Atlantic input file (top) and Mauretania input file (bottom) for the scene in April 2003 (left) and April 2010 (right).*

3.1.3 Reflectance

In the remainder of this section, we propagate the irradiance and radiance uncertainties discussed in the previous sections to reflectance. First, we again verify the shape of our calculated reflectance as a sanity check. **Figure 16** shows that the reflectances have the expected spectral shape and are accurate enough for our uncertainty analysis purposes.

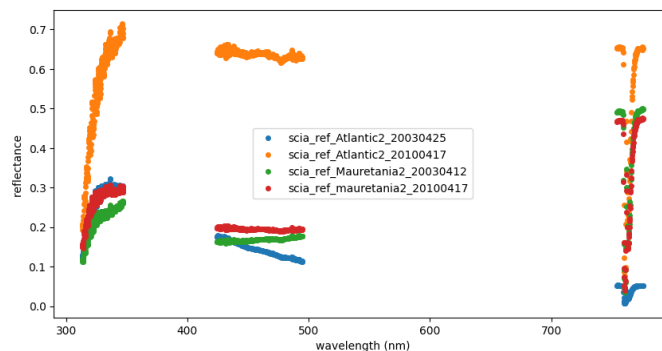


Figure 16: *SCIAMACHY reflectance as calculated by the measurement functions in the FDR4ATMOS uncertainty characterisation tool.*

Next, the combined uncertainties and error-correlation for the four example files are given in **Figure 17**. We can see that the uncertainties for the four examples are similar and are all between 1.2 and 2.2%. The error-correlations are nearly identical as well, therefore only one example is shown. We can see the uncertainties within the same band are fairly constant, and the errors are very correlated. These uncertainties are slightly lower than the radiance uncertainties. This is because the uncertainties for errors that were in common between radiance and irradiance ‘cancel out’ and become negligible.

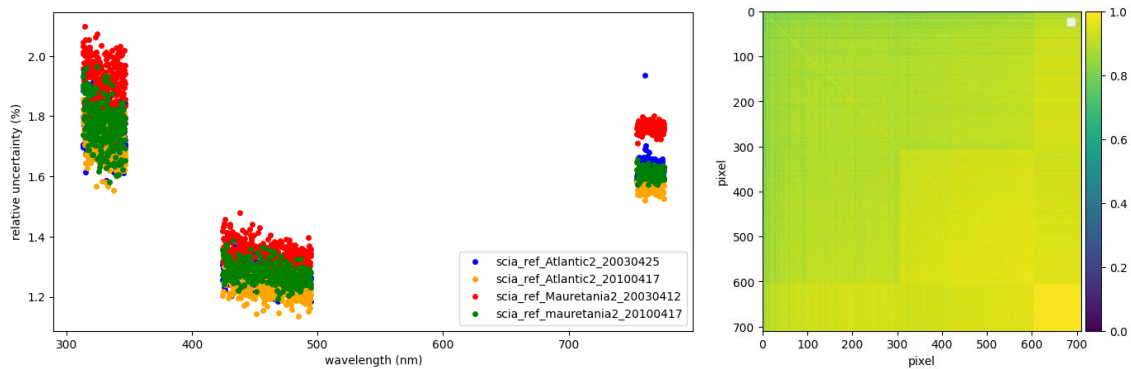


Figure 17: Left: Combined uncertainties on reflectance for the 4 example input files for SCIAMACHY. Right: error-correlation matrix with respect to spectral pixels for the Atlantic input file from 2003. The errors for the different wavelengths are highly correlated.

In the DOAS retrievals for the L2 products, the most important are uncertainties that are both spectrally and temporally random. Therefore, we again recreate the same plot, but this time only including the spectrally random uncertainties. In **Figure 18**, we show these uncertainties, which are quite low (<1%) and similar for each of the analysed scenes.

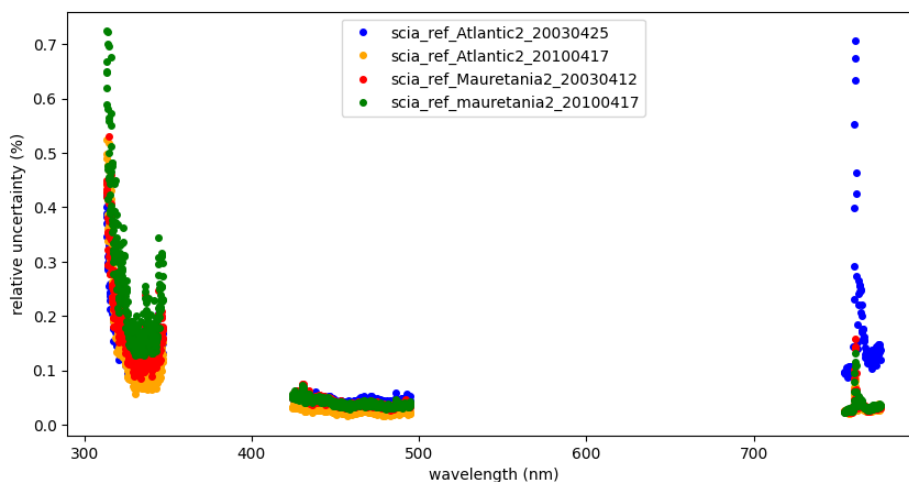


Figure 18: Combined spectrally-random uncertainties on reflectance for the 4 example input files for SCIAMACHY.

The reflectance uncertainties can also be decomposed into the sources of error (i.e. input quantity

categories). The decomposed categories now include terms for irradiance and for radiance. From **Figure 19**, we see that the signal uncertainties are still smallest, with the radiance signal uncertainties smaller than the irradiance signal uncertainties. The radiance and irradiance degradation uncertainties are also still fairly small and are very similar to each-other. The dominant contribution is the irradiance BSDF uncertainty. Note that the radiance response, which was the dominant term in the radiance and irradiance uncertainties, is in common between radiance and irradiance and has thus cancelled out.

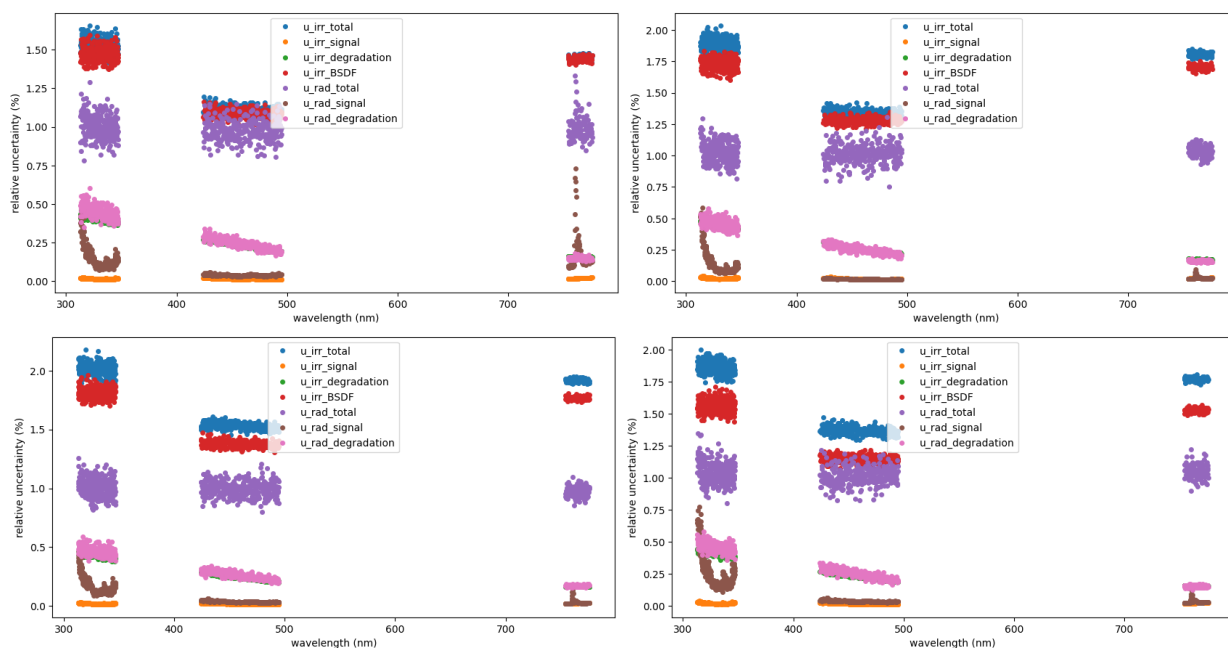


Figure 19: *SCIAMACHY reflectance uncertainties decomposed into components originating from uncertainties on different input quantities for the Atlantic input file (top) and Mauretania input file (bottom) for the scene in April 2003 (left) and April 2010 (right).*

3.2 GOME

3.2.1 Irradiance

We repeat entirely the same analysis for GOME as was performed for SCIAMACHY. Here the GOME uncertainties are for the FDR product, i.e. after harmonisation. By harmonising the GOME irradiances and radiances to the SCIAMACHY irradiances and radiances respectively, any temporally systematic uncertainties are removed from GOME and replaced by the SCIAMACHY temporally systematic uncertainties. In the remainder of the following sections, when we are discussing the GOME uncertainties, it has to be kept in mind that these are the uncertainties after the harmonisation process.

We start by performing a sanity check that the GOME measurement functions have been correctly implemented. This is done by calculating the irradiance from the input quantities in the input file and checking they have the correct spectral shape. When the spectral shape of the calculated irradiances in **Figure 20** is inspected, we find the same shape as for the SCIAMACHY irradiances. The absolute levels of irradiance are not quite the same, but this type of constant differences is of little importance for the

uncertainty analysis.

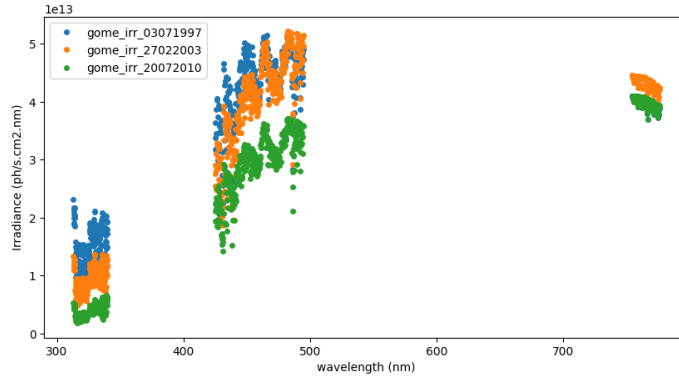


Figure 20: Top: GOME calibrated irradiance as calculated by the measurement functions in the FDR4ATMOS uncertainty characterisation tool. The observed spectral shape is as expected.

The combined uncertainties and error-correlation for the three GOME irradiance example files are given in **Figure 21**. We can see that the uncertainties for the three examples are very similar and are between 2 and 2.7%. The error-correlations are nearly identical as well and only one example is shown. We can see the uncertainties within the same band are fairly constant, and the errors are highly correlated for the UV channel, but less correlated for the visible and the NIR channels.

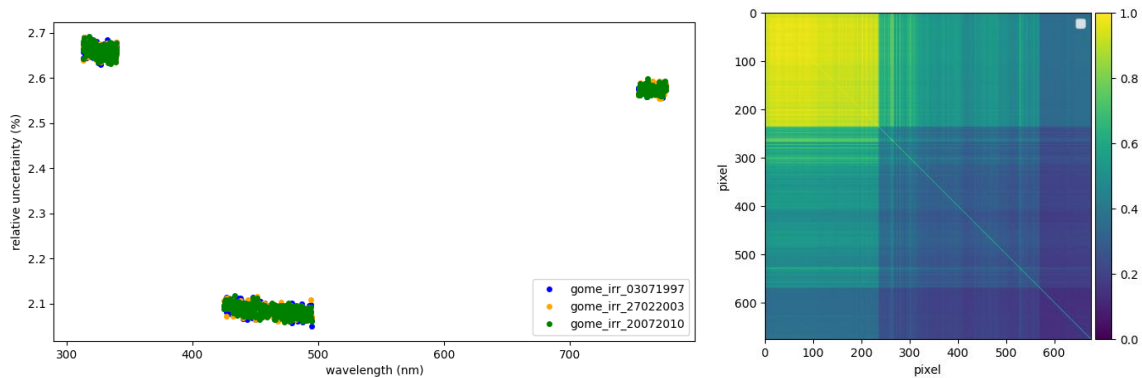


Figure 21: Left: Combined uncertainties on irradiance for the 3 example input files for GOME. Right: Error-correlation matrix with respect to spectral pixels for the input file from 2003. The errors for the different wavelengths are highly correlated, especially within the same band.

In **Figure 22**, we again decompose the uncertainties by their spectral error correlation. The systematic uncertainties are again the dominant contribution for the GOME irradiance uncertainties, followed by random and then structured uncertainties. The results are again very similar for the three different input files.

When separating between temporally random and systematic uncertainties in **Figure 23**, it is now the random uncertainties that are largest. The largest contribution seems thus to have errors that are

spectrally correlated, but temporally uncorrelated, which is somewhat uncommon, but realistic, nonetheless.

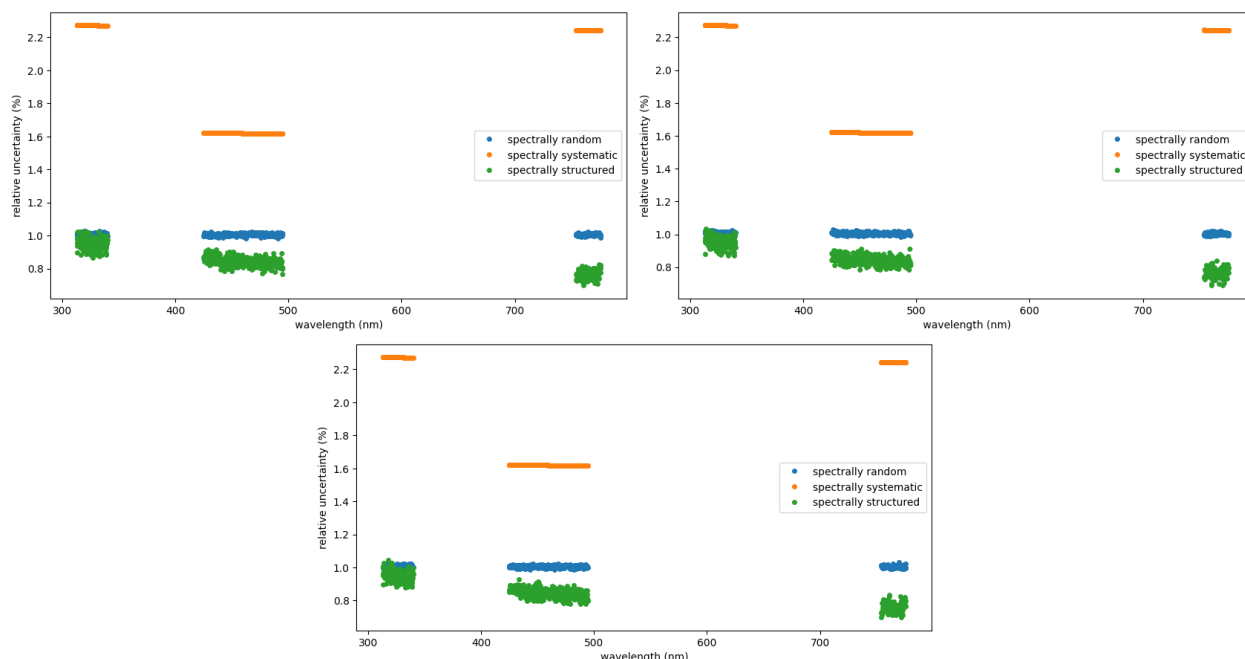


Figure 22: GOME irradiance uncertainties decomposed into components for which the errors are spectrally uncorrelated (random), spectrally fully correlated (systematic), or spectrally somewhat correlated (structured) for the input file from 1997 (top left), 2003 (top right) and 2010 (bottom).

Figure 23 also separates between the contributions for which errors are correlated between radiance and irradiance, and those that are independent. The uncertainties with errors correlated between radiance and irradiance dominate, with only a negligible contribution from those with independent errors. Most of the GOME irradiance uncertainties will thus be significantly reduced when propagating to reflectance.

In **Figure 24**, we again decompose by the source of uncertainty (i.e. input quantity categories). We find that the (temporally) systematic uncertainties from SCIAMACHY are the largest contributor to the GOME irradiance uncertainties, followed by the radiance response uncertainties (1%) and very small contributions from the PPG uncertainties and the signal (includes dark and straylight) uncertainties.

In **Figure 25**, the same is shown for the spectrally random uncertainties only. Here the largest contribution is from radiance response (again at 1%), with small contributions from PPG and signal.

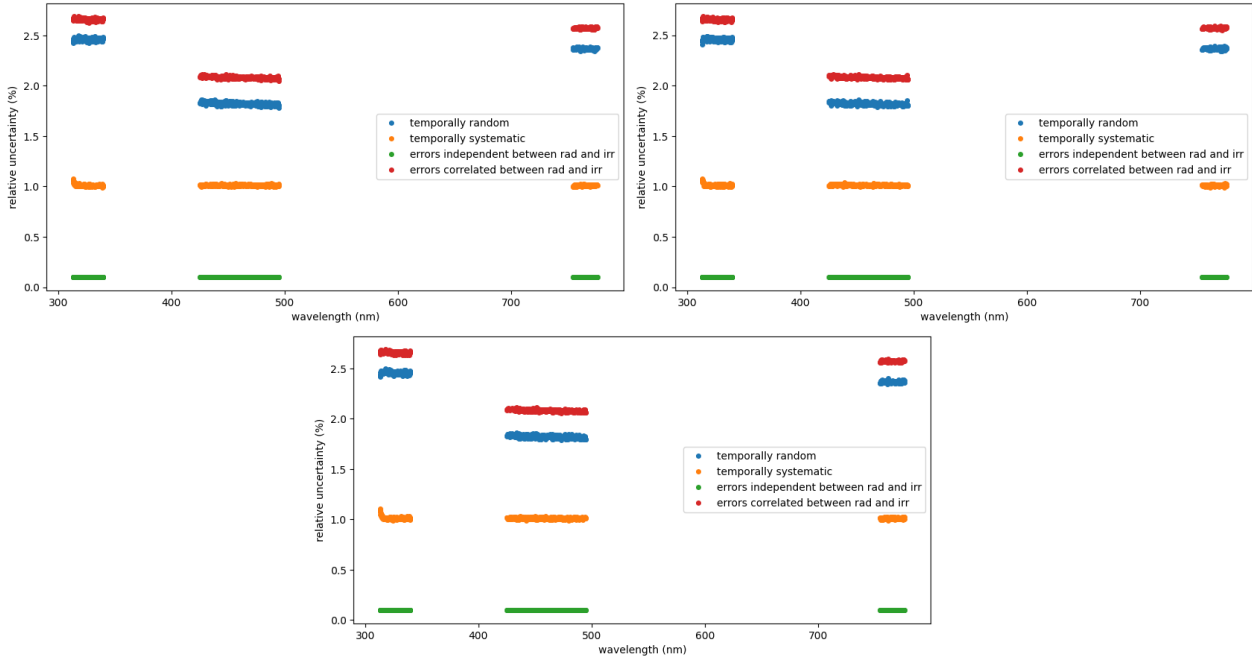


Figure 23: GOME irradiance uncertainties decomposed into components for which the errors are temporally uncorrelated (random) and temporally fully correlated (systematic). In addition, the uncertainties are also decomposed into a component for which the errors are independent between radiance and irradiance, and a component that is correlated between radiance and irradiance. Results for the input file from 1997 (top left), 2003 (top right) and 2010 (bottom)

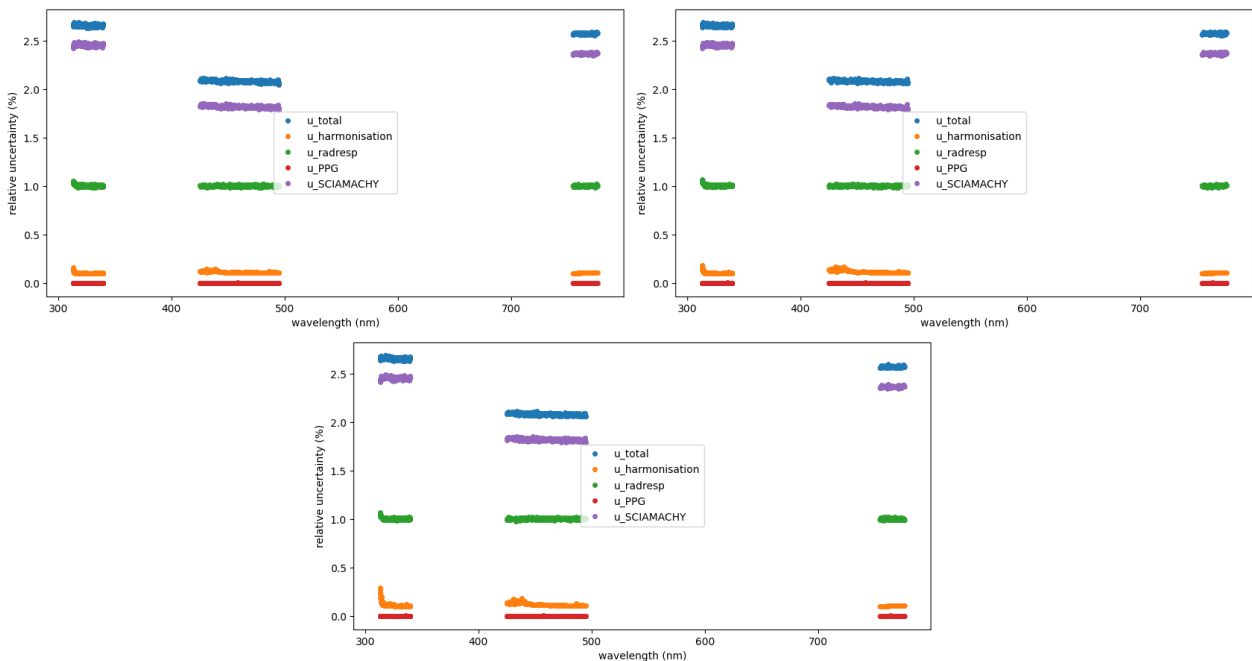


Figure 24: GOME irradiance uncertainties decomposed into components originating from uncertainties on different input quantities from 1997 (top left), 2003 (top right) and 2010 (bottom)

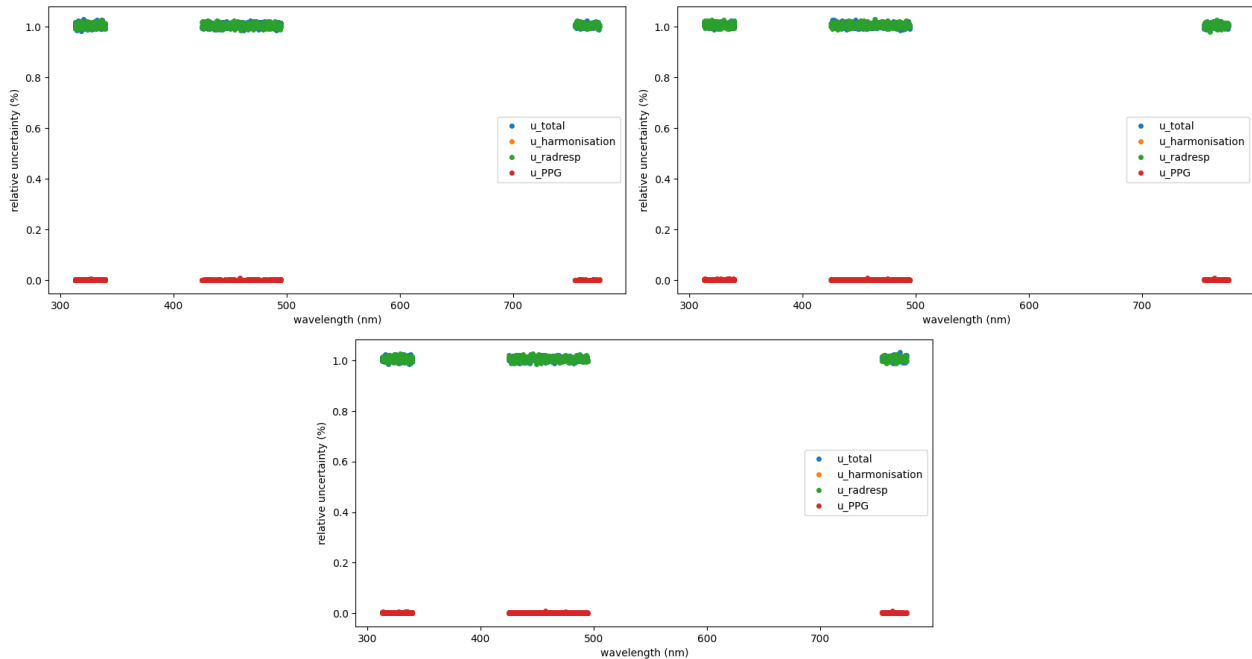


Figure 25: GOME irradiance uncertainties decomposed into components originating from uncertainties on different input quantities, where only uncertainties with a temporally random error correlation are included, for the input file from 1997 (top left), 2003 (top right) and 2010 (bottom).

3.2.2 Radiance

For the GOME radiance uncertainties, we again first confirm the spectral shape of the calculated radiances in **Figure 26** matches the spectral shape of the SCIAMACHY radiances in **Figure 16**. Next, the uncertainties for the two used scenes (Atlantic1 and Mauretania1) in 2003 are shown in **Figure 27**, together with the error correlation. Here, larger uncertainties between 4.5 and 6.5 % are found, and the error correlation (similar for both the scenes) shows a less correlated structure, where nearby spectral pixels (up to about 100 pixels) are correlated, but further pixels are uncorrelated.

In **Figure 28**, the GOME radiance uncertainties are decomposed by their spectral error correlation. In this case, the structured uncertainties dominate (4.5-6%), with systematic uncertainties around 1-2% and random uncertainties around 1%. When decomposing by temporal error-correlation (**Figure 29**), the systematic component dominates (4.5-6%) over the random component (1-2%). The same is found for the component that is independent between radiance and irradiance (4.5-6%), and the correlated errors between radiance and irradiance component (1-2%).

Figure 30 shows the decomposition by source of uncertainty (groups of input quantities). We find the same dominant component (4.5-6.5%) in the signal uncertainties, which were always a small contribution in previous sections. In the case of the GOME radiances, these uncertainties become large due to the scene variability in the harmonisation process. The radiance response contributes around 1% and the degradation correction is negligible. When only including the random uncertainties in **Figure 32**, we find the radiance response (1%) dominates.

The above results were all for the nadir viewing direction in the input files. Similar results are found when using different viewing geometries. In **Figure 32**, the radiance uncertainties for east and west viewing directions are shown. The radiance uncertainties are around 9% for east and 5-6.6 % for the

west viewing directions. It is the spectrally structured uncertainty from the scene variability of the harmonisation factor (which is temporally systematic and independent from irradiance uncertainties) that is different between the different viewing directions. The other components remain the same.

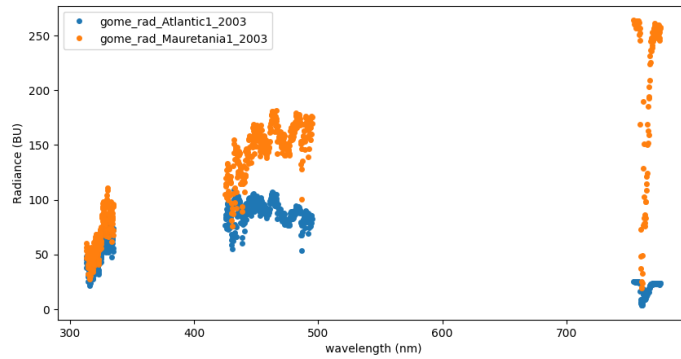


Figure 26: Top: Calibrated radiance as calculated by the measurement functions in the FDR4ATMOS uncertainty characterisation tool.

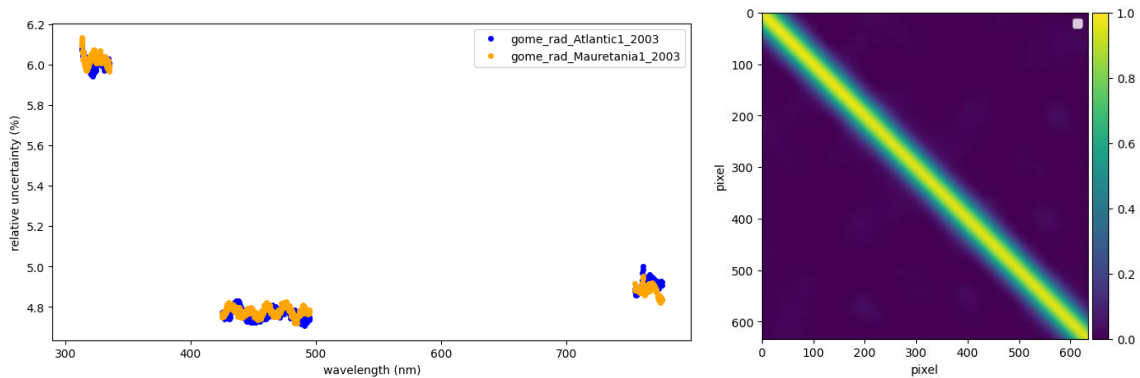


Figure 27: Left: Combined uncertainties on radiance for the 2 example input files for GOME. Right: error-correlation matrix with respect to spectral pixels for the input file from Atlantic1. The errors for the different wavelengths are not very correlated.

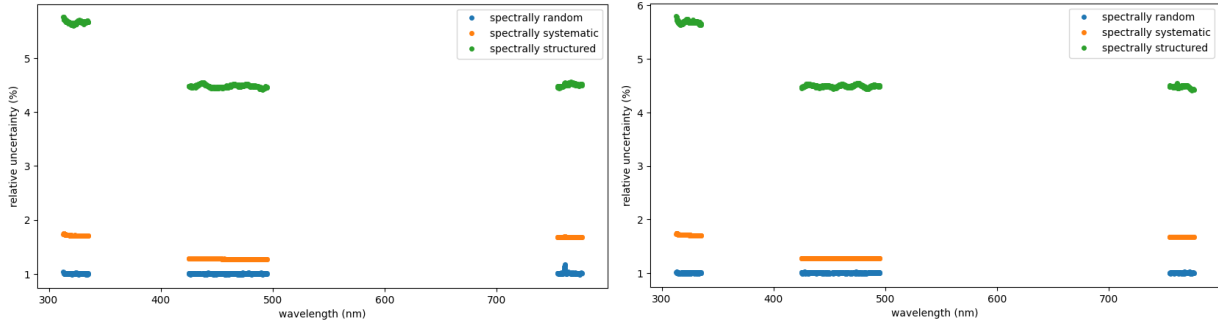


Figure 28: GOME radiance uncertainties decomposed into components for which the errors are spectrally uncorrelated (random), spectrally fully correlated (systematic), or spectrally somewhat correlated (structured) for the Atlantic input file (left) and Mauretania input file (right).

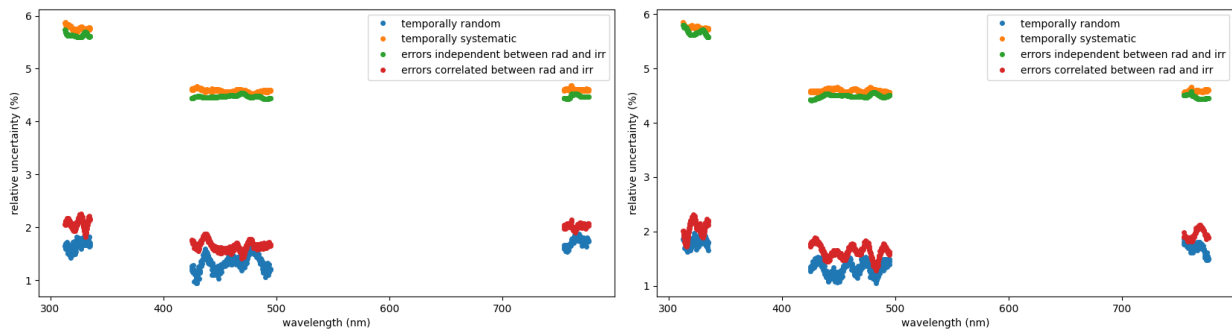


Figure 29: GOME radiance uncertainties decomposed into components for which the errors are temporally uncorrelated (random) and temporally fully correlated (systematic). In addition, the uncertainties are also decomposed into a component for which the errors are independent between radiance and irradiance, and a component that is correlated between radiance and irradiance. Results for the Atlantic input file (left) and Mauretania input file (right).

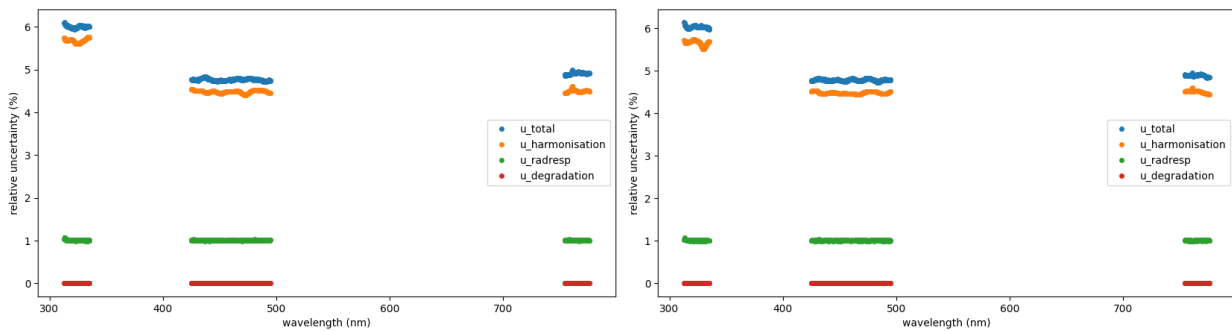


Figure 30: GOME radiance uncertainties decomposed into components originating from uncertainties on different input quantities for the Atlantic input file (left) and Mauretania input file (right).

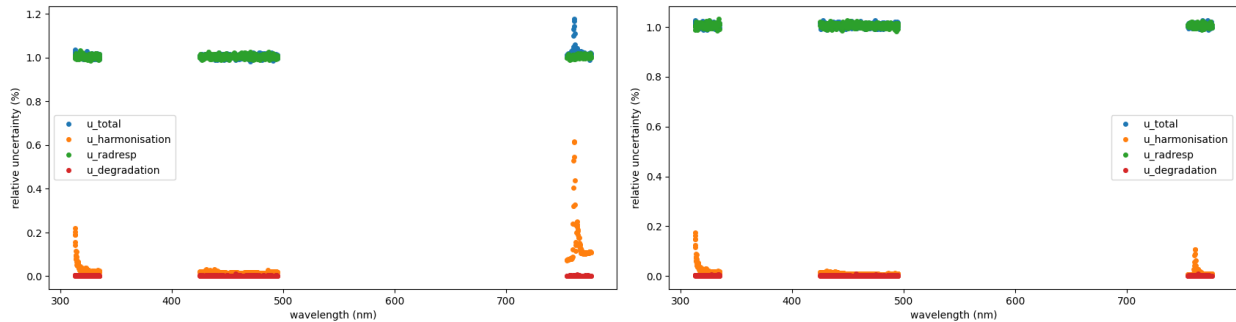


Figure 31: GOME radiance uncertainties decomposed into components originating from uncertainties on different input quantities, where only uncertainties with a temporally random error correlation are included, for the Atlantic input file (left) and Mauretania input file (right).

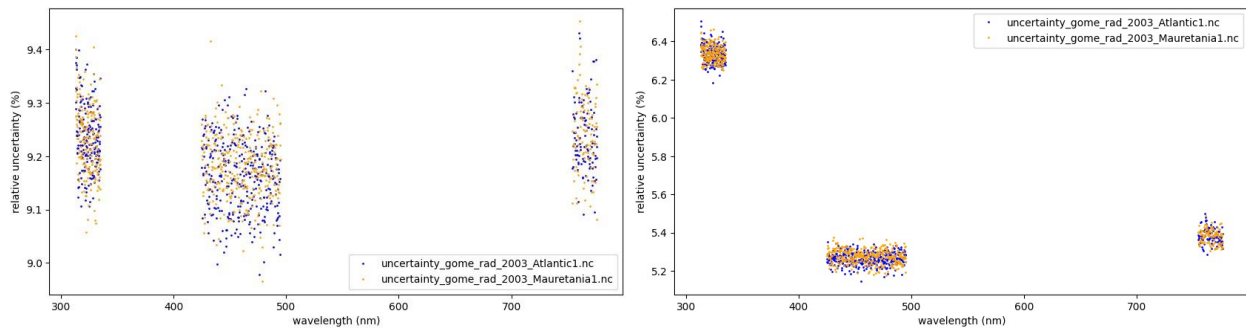


Figure 32: GOME radiance uncertainties for the east (left) and west (right) viewing direction.

3.2.3 Reflectance

For the GOME reflectances, the same picture emerges as for the radiances. The dominant structured uncertainty on the GOME radiances originating from the scene variability uncertainty of the harmonisation factor propagates to reflectance and dominates its uncertainty budget. In **Figure 33**, we see the uncertainties are again around 4-6.5%, and the error correlation matrix shows the same structure where nearby wavelengths are correlated, but further separated wavelengths are not. Rather than repeating the same decompositions as in previous sections, in this case we can simplify as there are only two non-negligible components. These two components are the large 4-6.5% spectrally structured, temporally systematic radiance uncertainties originating in the scene variability uncertainty of the harmonisation factor (see Section 3.2.2) and the 1.5-2.5% systematic SCIAMACHY irradiance uncertainties that propagated through the harmonisation process. The radiance response uncertainties are in common between radiance and irradiance and become negligible for reflectance. The degradation uncertainties, and irradiance signal uncertainty were already negligible in the previous sections and thus will be negligible for the GOME reflectance as well.

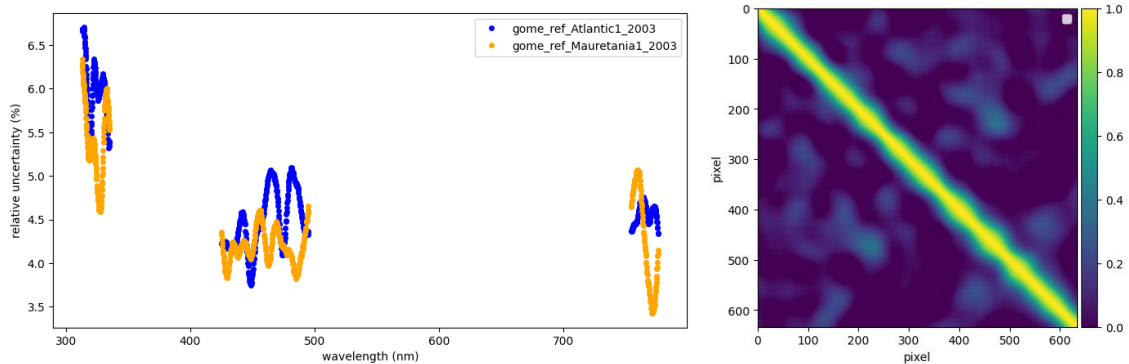


Figure 33: *Left: Combined uncertainties on reflectance for the 2 example input files for GOME. Right: error-correlation matrix with respect to spectral pixels for the Atlantic1 input file. The errors for the different wavelengths are highly correlated, especially within the same band.*

4 Limitations of approach

There are a number of assumptions and limitations to the approach used. In some cases, this is due to paucity of information from the documentation about some of the uncertainty sources, and especially their error correlation. In other cases, it is because a simplified approach was followed, such as using simplified measurement functions, rather than the full FDR processing chain (which would be computationally too expensive for the Monte Carlo approach followed). In this section, we list some of the main assumptions and limitations of this work.

- The most significant limitation is that the information available from the literature and GOME and SCIAMACHY documentation is rather limited in terms of the different sources of uncertainty, details of the sensor calibration, and especially the error correlation associated with each of the included terms. This means that the uncertainties listed and documented in [RD-07] have used best judgement, but this required many assumptions. It is also likely a number of uncertainty contributions have been missed, resulting in the uncertainties in this report being underestimated. Some of the uncertainties (e.g. on the SCIAMACHY reflectances) do look rather low considering the sensors were launched more than 20 years ago.
- Another limitation is that detailed error correlation matrices for each of the relevant dimensions was not available. Instead, we decomposed the uncertainties into multiple components based on whether their correlation was random or systematic. Using an error correlation matrix would have allowed for more accurate results, especially for components which are partly correlated. However, error correlation matrices were simply not available.
- For the radiance uncertainties, only uncertainty components that also apply to reflectance were included. This means that the radiance uncertainty budget is not complete. However, the main measurand of interest is the reflectance, for which the uncertainty budget is as complete as possible (see other caveats).
- The measurement functions were also simplified to the ones listed in [RD-07]. These are roughly the same measurement functions as used in the FDR processing, but a simplified version of it. Doing the full FDR processing as part of Monte Carlo approach such as the one used here, will be too costly computationally. The approach followed is still expected to yield the correct conclusions, but there will be small differences to the results if the full processing chain was used. The differences also mean that it is difficult to do an independent validation of the uncertainties themselves (such as comparing the FDR4ATMOS irradiances to the TSIS-1 solar irradiance model [RD-08] and check if the differences are within the uncertainty budget of TSIS-1 combined with the uncertainties presented in this document).
- The uncertainties were analysed for a limited number of scenes. These scenes showed similar results, and it is expected (but not guaranteed) that these uncertainties will be the same for every scene.
- Two uncertainty components that are known to be potentially scene dependent have been omitted from the example computations of reflectance: these are the effects of inhomogeneous scenes and polarisation effects. Inhomogeneous scenes may introduce small additional uncertainties on scan angle dependencies. The polarisation correction for radiance uses a set of algorithmic steps that are very complex to realistically simulate in a Monte-Carlo, including effects from inhomogeneous scenes that may

influence the correct synchronisation between main channel and PMD measurements. In the literature there have been validation studies of GOME and SCIAMACHY polarisation retrieval, that indicate that errors on the retrieval of polarisation may be substantial (several percent). However, these are lump-sum errors that include all sorts of causes for uncertainty. Therefore, they are of limited use for an uncertainty propagation model described by the measurement functions of [RD-7]. Note that for DOAS Level 2 retrieval, errors in the L1b polarisation correction are not significant, as these are spectrally broadband.

5 Future plans and recommendations

The FDR4ATMOS project allowed the assessment of the dominant uncertainties in the GOME and SCIAMACHY L1b reflectance and irradiance products within the bands relevant to the retrieval of O₃, SO₂ and NO₂ species, allowing for a fresh, metrologically rigorous, assessment of the product uncertainties. However, the project highlighted some limitations to analysis undertaken, with the following recommendations for future progress:

- A thorough assessment of all remaining identified uncertainty contributors. Many were difficult to assess due to a lack of evidence within the literature as to their magnitudes and correlations. Further assessment would provide further information for an evidenced assessment and should validate the judgements made in this project's prioritisation exercise.
- The example files have shown good consistency in the uncertainties at the extremes of the mission timescales. Further analysis of data over a range of surface and atmospheric parameters may provide more information for specific use cases.
- Scene variability within the harmonisation process produced a significant uncertainty source in the GOME reflectance data and additional efforts to optimise this could improve the FDR product.

Appendix A: GOME / SCIAMACHY L1b FDR Uncertainty analysis: Measurement Function, and Uncertainty Effects Table (FDR4ATB.TN.DLR.016)



Msm. Function and Uncertainties
FDR4ATB-TN-DLR-016
Issue 1.1
31 July 2024
Page 42 of 117



GOME / SCIAMACHY L1b FDR Uncertainty analysis: Measurement Function, and Uncertainty Effects Table

FDR4ATMOS Task B

FDR4ATB.TN.DLR.016
Issue 1.1
31. July 2024

	Name	Signature
Prepared	S. Slijkhuis, DLR-IMF	
Checked	G. Lichtenberg, DLR-IMF	
Approved	A. Dehn, ESA-ESRIN	

*Deutsches Zentrum für Luft- und Raumfahrt e.V. – DLR
Institut für Methodik der Fernerkundung
Oberpfaffenhofen
Germany*

Document Change Record

Version	Date	Changes	Originator
0.1 (Draft)	29.06.2021	Original version	S.Slijkhuis, DLR-IMF
0.2 (Draft)	28.08.2021	Extensive but not complete description of measurement functions	S.Slijkhuis, DLR-IMF
0.3 (Draft)	20.10.2021	Smaller improvements everywhere; taking into account project member comments	S.Slijkhuis, DLR-IMF
0.4 (Draft)	22.12.2021	Reworked irradiance section to more clearly distinguish between errors and uncertainties; taking into account project member comments. For irradiance, uncertainties were taken out of measurement functions (other sections to follow this approach).	S.Slijkhuis, DLR-IMF
0.5 (Draft)	22.08.2022	Updated radiance/reflectance section (not R12 polarisation)	S.Slijkhuis, DLR-IMF
0.5b (Draft)	22.09.2022	Updated spectral calibration section	S.Slijkhuis, DLR-IMF
0.6 (Draft)	15.02.2023	Added for GOME FDR the harmonisation of Irradiance to SCIAMACHY; modification of I8.	S.Slijkhuis, DLR-IMF
0.7 (Draft)	08.08.2023	Updated Radiance Section incl. Harmonisation	S.Slijkhuis, DLR-IMF
1.0	09.01.2024	Final edits	S.Slijkhuis, DLR-IMF
1.1	31.07.2024	Rewordings after internal review	S.Slijkhuis, DLR-IMF

Table of Content

Appendix A: GOME / SCIAMACHY L1b FDR Uncertainty analysis: Measurement Function, and Uncertainty Effects Table (FDR4ATB.TN.DLR.016)	41
1 Overview	47
1.1 Purpose and Scope	47
1.2 Documents.....	47
1.2.1 Applicable documents	47
1.2.2 Reference documents	47
1.3 Abbreviations and Acronyms.....	48
1.4 Terms and definitions.....	49
1.5 Document Overview	50
1.6 Document Status.....	51
2 Introduction to the GOME/SCIAMACHY uncertainty analysis	52
2.1 Uncertainties	52
2.2 Correlation scales	52
3 Uncertainties on the irradiance product	54
3.1 General calibration equation	54
3.2 Processing Chain Diagram.....	54
3.3 Instrument Measurement function	61
3.3.1 I1 - Memory effect.....	61
3.3.2 I2 - Non-linearity.....	61
3.3.3 I3 - Dark signal	62
3.3.4 I4 - Statistical Uncertainty (noise).....	63
3.3.5 I5 – Pixel-to-pixel gain.....	63
3.3.6 I6 – Electronic gain	64
3.3.7 I7 – Etalon.....	64
3.3.8 I8 – Straylight	65
3.3.9 I9 – Radiance response	66
3.3.10 I10 – Diffuser BSDF.....	70
3.3.11 I11 – Degradation.....	71
3.3.12 I12 – Polarisation	73
3.3.13 I13 – Harmonisation	73
3.4 Summary of Effect Tables	73
4 Uncertainties on the reflectance product	78
4.1 General calibration equation	78
4.2 Processing Chain Diagram.....	79
4.3 Instrument Measurement function	84
4.3.1 R1 - Memory effect.....	84
4.3.2 R2 - Non-linearity	84
4.3.3 R3 - Dark signal	85
4.3.4 R4 - Statistical Uncertainty (noise).....	86
4.3.5 R5 – Pixel-to-pixel gain.....	86
4.3.6 R6 – Electronic gain	87
4.3.7 R7 – Etalon.....	87
4.3.8 R8 – Straylight	87
4.3.9 R9 – Radiance response	89

4.3.10	I10 – Diffuser BSDF	92
4.3.11	R11 – Degradation	92
4.3.12	R12 – Polarisation correction	94
4.3.13	R13 – Harmonisation	96
4.4	Summary of Effect Tables	96
5	Uncertainties on the polarisation.....	102
5.1	Introduction	102
5.2	Processing Chain	102
5.3	Instrument Measurement function	105
5.3.1	P1 – PMD integration and synchronisation.....	105
5.3.2	P2 – PMD Non-linearity.....	106
5.3.3	P3 – PMD Dark signal	106
5.3.4	P4 – PMD Statistical Uncertainty.....	106
5.3.5	P5.....	107
5.3.6	P6 – PMD Electronic gain	107
5.3.7	P7 – PMD Etalon.....	107
5.3.8	P8 – PMD Straylight.....	107
5.3.9	P9 – Greek Keydata / MMEs.....	107
5.3.10	P10 – PMD: Diffuser BSDF.....	108
5.3.11	P11 – PMD Degradation correction	108
5.3.12	P12 – Polarisation values.....	108
5.3.12.1	The Virtual Sum.....	108
5.3.12.2	In-band correction factor	109
5.3.12.3	Theoretical point	109
5.4	Polarisation quantitative uncertainty estimates.....	110
6	Spectral uncertainties	111
6.1	Introduction	111
6.2	Processing Chain	111
6.3	Instrument Measurement function	112
6.3.1	S1 – SLS line positions.....	112
6.3.2	S2 – Polynomial fit.....	113
6.3.3	S3 – Apply spectral calibration	113
6.3.4	S4 – Doppler shift.....	114
6.3.5	S5 – ISRF	114
7	Geolocation uncertainties.....	115
7.1	Introduction	115
7.2	Processing chain	115
7.3	Geolocation Uncertainty components.....	116
7.3.1	G1 – Orbit position.....	116
7.3.2	G2 – Line-of-sight.....	116
7.3.3	G3 – Geometrical geolocation.....	116
7.3.4	G4 – Apparent pixel shift.....	116

1 Overview

1.1 Purpose and Scope

In this document we describe the GOME and SCIAMACHY uncertainties on Level 1b Earth reflectances and solar irradiances, following the methodology laid down by the European Union's FIDUCEO project [R1]. In particular, we provide the relevant instrument measurement functions and uncertainty effects tables.

The "Measurement Functions" are analytical expressions that describe step by step components of the measurement process and associated uncertainties, as well as external inputs (e.g. model data) and their uncertainties as used in Level 1b data processing.

The "Effect Tables" contain a quantitative description of each uncertainty from the measurement functions. This includes the magnitude of each uncertainty effect, but also spectral and/or temporal correlation scales, the form of the correlation function, and the maturity of the analysis.

The full Effect Tables are separate files available on the FDR4ATMOS website. A summary table with the most relevant effects has been included in this document.

The scope of this document is limited to fulfil the requirements of the FDR4ATMOS project. This leads to the following limitations:

- Wavelength bands are in GOME/SCIAMACHY channels 2, 3, 4 only, restricted to Level 2 retrieval windows of 313-340 nm, 425-495 nm, and 750-780 nm, respectively.
- For the reflectance product, the focus will be on uncertainties that influence the quality of the operational Level 2 products. For the FDR reflectance product this implies in particular a focus on reflectance (Sun-normalised radiance); and a focus on the effects relevant to DOAS retrieval rather than a retrieval using absolutely calibrated radiances. In particular, the effects of atmospheric polarisation, which is spectrally broad-band and not relevant to DOAS, are not covered extensively.
- For the GOME products, the uncertainty quoted in the effects table are after harmonisation to the SCIAMACHY irradiance.

1.2 Documents

1.2.1 Applicable documents

1.2.2 Reference documents

- [R1] FIDUCEO project, <http://www.fiduceo.eu>
- [R2] GOME/ERS-2 Level 0 to 1b ATBD, GOME-DLR-L1-ATBD, Issue 7, 20.06.2016 (available from <https://earth.esa.int/web/sppa/mission-performance/esa-missions/ers-2/gome/products-and-algorithms/products-information>)
- [R3] SCIAMACHY L0-1c Processing ATBD - Algorithm Theoretical Baseline Document for Processor V.9, ENV-ATB-DLR-SCIA-0041, Iss.7, 2018-11-23
- [R4] SCIAMACHY L1b product error analysis, ENV-TN-DLR-SCIA-0134, Issue 2, 27.11.2018
- [R5] SCIAMACHY keydata error analysis, SRON-SQWG3-TN-2016-002, Issue 1, 9.02.2018

- [R6] J. M. Krijger, R. Snel, G. van Harten, J. H. H. Rietjens, and I. Aben. Mirror contamination in space I: mirror modelling. *Atmospheric Measurement Techniques*, 7(10):3387–3398, Oct 2014. ISSN 1867-8548. doi:10.5194/amt-7-3387-2014. URL <http://dx.doi.org/10.5194/amt-7-3387-2014>
- [R7] FDR4ATMOS ATBD, D-B2-01, Issue 1
- [R8] FDR4ATMOS: General guidance on a metrological approach to fundamental data records (FDR). D-B1-07 Issue 1.0
- [R9] K. Bramstedt, Scan-angle dependent degradation correction with the scanner model approach, Technical Note, IUP-SCIA-TN-Mfactor, Issue: 1, 2014. URL https://www.iup.uni-bremen.de/sciamachy/mfactors/mfactor-TN-3-1_20140428.pdf
- [R10] Patricia Liebing. New Polarization Algorithm Theoretical Basis Document for L0-1 V9 (IUP-SCIA-TN-2015-01-PL). Technical Report issue 2.3.1, Institute of Environmental Physics (IUP), 10 March 2017
- [R11] I. Aben, M. Eisinger, E. Hegels, R. Snel, C. Tanzi, "GOME Data Quality Improvement GDAQI Final Report", SRON report TN-GDAQI--003SR/2000, 29.9.2000
- [R12] S. Slijkhuis, CHEOPS-GOME Study on Seasonal effects on the ERS-2/GOME Diffuser BSDF, CH-TN-DLR-GO-0001, Issue 1, 9 May 2004 (summary version on <http://adsabs.harvard.edu/full/2005ESASP.572E..25S>)
- [R13] M. Coldewey-Egbers, S. Slijkhuis, B. Aberle, D. Loyola, A. Dehn: "The Global Ozone Monitoring Experiment: review of in-flight performance and new reprocessed 1995-2011 level 1 product", *Atmos. Meas. Tech.*, 11, p.5237, 2018, <https://www.atmos-meas-tech.net/11/5237/2018>

1.3 Abbreviations and Acronyms

A list of abbreviations and acronyms which are used throughout this document is given below:

ACT	Across-Track (perpendicular to flight direction)
ALT	Along-Track (in flight direction)
ASM	Azimuth Scan Mirror (on SCIAMACHY)
BOL	Begin Of Life (first measurement in space)
BSDF	Bi-directional Scattering Distribution Function
BU	Binary Unit (ADC "counts")
CKD	Calibration Key Data
DLR	Deutsches Zentrum für Luft- und Raumfahrt e.V.
DOAS	Differential Optical Absorption Spectroscopy
ESA	European Space Agency
ESM	Elevation Scan Mirror (on SCIAMACHY)
FPA	Focal Plane Assembly
FOV	Field of View
FWHM	Full Width Half Maximum
GDF	General Distribution Function (for UV polarisation)
ILOS	Instantaneous Line of Sight
ISRF	Instrument Spectral Response Function (1-dimensional)
IR	Infra-red

IT	Integration Time
IUP	Institute of Environmental Physics, Bremen University
LC	Leakage Current
LED	Light Emitting Diode
LLSPA	Long-loop Sensor Performance Analysis
MEC	Memory Effect Correction
MME	Mueller Matrix Element
NIR	Near Infra-red
NL	Non-Linearity
NRT	Near-Real Time
OBM	Optical Bench Module
PET	Pixel Exposure Time
PMD	Polarization Measurement Device
PRNU	Pixel Response Non-Uniformity
PSF	Point spread Function (2-dimensional)
SAA	South Atlantic Anomaly
SCIAMACHY	Scanning Imaging Absorption Spectrometer for Atmospheric Chartography
SF	Slit Function = ISRF
SMR	Sun Mean Reference
SRON	Space Research Organisation of The Netherlands
SWIR	Short-Wave Infra-Red
SZA	Sun Zenith Angle
TOA	Top of Atmosphere
UTC	Universal Time Co-ordinate
UV	Ultra-Violet
VIS	Visible
WLS	White Light Source

1.4 Terms and definitions

Band (spectral-)

one of 4 (or 6) spectral bands referring to parts of an array detector:

band 1a and 1b cover the short-wavelength and long-wavelength part of channel 1 respectively,

band 2a and 2b cover the short-wavelength and long-wavelength part of channel 2,

band 3 and 4 are identical to channel 3 and 4.

In addition there are 4 'straylight' bands: two shortwave of band 1a, one longwave of band 1b, and one shortwave of band 2a. These 'straylight' bands are not part of the Level 1b data (but for the standard/original GOME data they are available on the Level 1a product).

Channel

one of the 4 spectral channels containing an array detector, sometimes an expression like 'channel 1a' is used for 'band 1a' etc.

Cluster (SCIAMACHY only)

a group of detector pixels within one channel, that have a specific readout configuration

Data Packet

one unit of scientific instrument data (e.g. for GOME generated every 1.5 second)

FPA crosstalk

a phenomenon for GOME which may cause a variation in detector signal related to the switching of coolers for the Focal Plane Assembly (detector housing).

Ground pixel

the footprint on the Earth's surface during one integration time.

Integration time pattern

specifies the integration time of each of the 6 bands

Level 1b Product

a data set (usually one orbit or a subset thereof) which contains the fully calibrated GOME/SCIAMACHY (ir)radiance spectra.

Pixel

here one spectral element on the detector is meant (as exception, depending on the context, this may also be shorthand for 'ground pixel').

Pixel (sub-)type

denotes a certain geometry in the scan pattern [ground pixel]. For GOME pixel type 0,1,2,3 refer to the East, Nadir, West and Backscan ground pixel, respectively. For SCIAMACHY, we have the same basic scan pattern but it can be subdivided again, depending on the cluster integration time.

Virtual pixel

a wavelength interval on the PMD detector which corresponds to the wavelength interval of the corresponding channel array detector pixel.

Virtual channel boundary

the pixel or wavelength which separates band 1a from 1b (or 2a from 2b)

1.5 Document Overview

Section 2 presents a short introduction to the uncertainties for GOME and SCIAMACHY.

Section 3 describes the Measurement Functions for solar Irradiance. It starts with an introduction to the overarching equation, followed by an overview table of the various terms in all measurement functions on sub-level. A figure depicting the processing chain it given, to illustrate the steps that have to be taken to calculate end-to-end uncertainties on the Irradiance. A subsection with the detailed mathematical equations is followed by subsection with a summary Effects Table. The latter provides quantitative uncertainties for the more significant measurement functions. The full Effects Table with all measurement function items will be digitally available on the FDR4ATMOS website.

Section 4 is similar to section 3, but for the Radiance.

Sections 5,6,7 give a verbal description for the Measurement Functions for polarisation, spectral calibration and Geolocation. Detailed mathematical formulae and effect tables are not provided here, for reasons described in Section 2.



1.6 Document Status

Issue 1.0 is the final delivery of the FDR4ATMOS Task B for the first project phase. Most of the document was compiled by Sander Slijkhuis (DLR), with input from several FDR4ATMOS team members, notably Melanie Coldewey-Egbers (DLR) and Klaus Bramstedt (IUP Bremen). The Effect Tables for SCI-AMACHY have been generated by Klaus Bramstedt.

2 Introduction to the GOME/SCIAMACHY uncertainty analysis

2.1 Uncertainties

The methodology of breaking down contributions to the uncertainties using measurement functions and effect tables follows the guidelines document [R8]. Uncertainties on a given measurement function item are given in units of one standard deviation (in the physical unit of that item).

We may discern the following types of uncertainties (although these are not separately treated here):

- uncertainties due to algorithm steps in level 0-1b processing
- uncertainties on CKD and other input data to the L0-1b processing
- uncertainties in the measurement process that are not covered by above.

A detailed description of the L1b calibration and an overview of associated errors may be found in the instrument ATBDs [R2][R3] and in existing error analyses documents [R4][R5].

Uncertainties on on-ground CKD have mostly been taken from TPD (now named TNO) instrument calibration documentation (internal GOME / SCIAMACHY project documents). Note that these quote 2σ uncertainties, while this FDR uses 1σ uncertainties.

In the current uncertainty analysis, we strive to describe all known instrument effects, although we cannot derive a quantitative number on all uncertainties. Uncertainties that are highly dependent on the input scene also have not been quantified. Especially those in the Reflectance data products, that are related to uncertainties in the atmospheric polarisation, or related to inhomogeneous illumination of a scene.

The FDR uncertainty analysis is restricted to uncertainties that influence the quality of the ESA Level 2 products of O_3 , NO_2 and SO_2 . This limits the applicability to the following wavelength ranges:

- 313-340 nm (channel 2)
- 425-495 nm (channel 3)
- 750-780 nm (channel 4)

2.2 Correlation scales

For practical purpose in Level 2 retrievals, uncertainties have different impacts depending on their spectral correlations. Most Level 2 retrievals employ spectrally broad "closure terms" which implies that the retrievals are insensitive to broad-band calibration errors. However, these retrievals may be sensitive to errors that vary on small spectral scales (typically pixel-to-pixel effects, or effect on spectral scales that are a smallish fraction of the spectral width of the fitting window). The latter may be subdivided into uncertainties that are random with each measurement, and those that are not.

Correlation scales will be indicated in the Effects Tables, which are a set of external files complementary to this document and available at <<link to landing page>>. However, for user convenience, we include here a summary of the effect tables with the more significant effects (including well-known effects that are numerically insignificant).

In spectrometers designed for [very] high signal-to-noise, like GOME and SCIAMACHY, the uncertainties on the broad-band scale are typically at least an order of magnitude larger than those on the scale of a



few pixels. However, that does not imply that the broad-band uncertainties are dominant for Level 2 retrieval errors (see above). Therefore, it may be very important for users to pay attentions to these correlation scales, and ignore uncertainties on scales that are not relevant to the Level 2 retrieval used.

3 Uncertainties on the irradiance product

3.1 General calibration equation

As explained in the GOME ATBD [R2], the general calibration equation for calibrated irradiance $I(\lambda_i)$ may be written as:

$I(\lambda_i) = \frac{S_i - SS_i - DS_i - MEC_i}{BPDF_0(\lambda_i) \cdot m_{BPDF,t}(\lambda_i) \cdot (RR_{0,i}/PPG_{0,i})(\lambda_i) \cdot PPG_{t,i} \cdot m_t(\lambda_i) \cdot E_t(\lambda_i)}$	Eq.(3-1)
--	-----------

with

- S_i measured signal at detector pixel i
- λ_i wavelength of detector pixel i
- $I(\lambda_i)$ incident radiation as function of wavelength
- SS_i straylight signal at detector pixel i (depending on all signals in the channel)
- DS_i dark signal of detector pixel i
- MEC_i correction term for memory effect or non-linearity of detector pixel i
- $BPDF_0(\lambda_i)$ bi-directional scattering distribution function of the diffuser; includes neutral density filter for SCIAMACHY
- $(RR_{0,i}/PPG_{0,i})(\lambda_i)$ smooth part of the radiance response function as function of wavelength, for unpolarised input
- $PPG_{t,i}$ pixel-to-pixel part of response function at detector pixel i
- $m_t(\lambda_i)$ degradation monitoring factor as function of wavelength
- $E_t(\lambda_i)$ etalon change as function of wavelength
- $m_{BPDF,t}(\lambda_i)$ BPDF degradation monitoring factor

where subscript 0 denotes the quantity at a reference time $t = 0$ and subscript t denotes the quantity at the time of measurement.

SCIAMACHY has several measurement modes for solar irradiance. For the FDR, the mode with ESM diffuser is used. This mode also contains a neutral density filter (NDF). In the measurement function description, the NDF is taken implicitly in $BPDF_0(\lambda_i)$ although the NDF is given as separate item in the Effects Tables datafile.

Note that the equation has multiplicative terms in the denominator, and additive terms (coloured red in the general equation) in the numerator. The distinction between multiplicative and additive terms is significant for the calculation of uncertainties. The additive terms generally give rise to uncertainties on small wavelength scales. Multiplicative terms may occur on all wavelength scales.

3.2 Processing Chain Diagram

The Level 0 to 1b processing chains are described in detail in the GOME and SCIAMACHY ATBDs [R2][R3]. This has been taken as basis for the uncertainty analysis here, but there are additional contributions which are not in the ATBDs, such as on-ground calibration uncertainties. Also, there are uncertainties

related to effects that have been noticed in-flight (or may be expected from first principles) but that are not corrected in Level 0-1b processing.

The processing chain diagram for the *uncertainties* follows the sequence for the error propagation (with as starting point the sequence of Level 0-1b processing steps). The numbering of the steps is accordingly.

The processing for GOME and SCIAMACHY is similar, but not identical. However, the numbering of the processing steps for the uncertainty analysis has been kept identical for both instruments. This implies that not all steps are necessarily used for each instrument. This will be visible as obsolete entries in the Effects Tables.

The numbering has also been kept identical for the Irradiance product and the Reflectance product. Also here, not all effects are statistically significant for each product, as indicated in the Effects Tables.

An overview of the uncertainty processing steps and numbering is shown in Table 3-1. The table lists for completeness some effects that are expected to be insignificant, but also omits possible effects known from other instruments that are expected to be insignificant (there is some arbitrariness here).

Table 3-1 Overview of generic processing steps and numbering for the irradiance product. The last column indicates if the item is applicable to GOME (G) and/or SCIAMACHY (S); an X denotes that the item is not applicable to irradiance. DET=Detector

#	main elements	#	contributing elements	#	sub-items	
I1	DET Memory Effect	I1.1	on-ground CKD			S
		I1.2	In-orbit CKD changes			S
		I1.3	determine previous readout	I1.3.1	without co-adding	S
				I1.3.2	with co-adding	S
I2	DET non-linearity	I2.1	due to saturation			GS
		I2.2	electronic	I2.2.1	OG CKD	GS
				I2.2.2	In-orbit changes	GS
I3	DET Dark Signal	I3.1	statistical uncertainty			GS
		I3.2	separation in LC + FPN	I3.2.1	FPN	S
				I3.2.2	LC	S
		I3.3	additional background	I3.3.1	Cross-talk	G
				I3.3.2	SAA background	X
				I3.3.3	Red Grass	S
		I3.3	detector temperature			
I4	DET statistical	I4.1	shot noise			GS

#	main elements	#	contributing elements	#	sub-items	
	uncertainty					
		14.2	readout noise			GS
		14.3	digitisation noise			GS
15	DET QE: PPG	15.1	noise on LED/WLS measurements			GS
		15.2	High-pass filtering			GS
16	DET: electronic gain					1)
17	Detector window etalon	17.1	calculate: filtering			2) S
		17.2	apply:	17.2.1	ice layer growth	S
				17.2.2	spectral calibration	S
18	Stray light	18.1	ghost CKD			GS
		18.2	"uniform" CKD			GS
		18.3	spatial stray light			GS
		18.4	"In-orbit change (degradation of optical elements)			GS
19	Radiance Response	19.1	OG CKD Nadir	19.1.1	calib.standards	GS
				19.1.2	distance measurements	GS
				19.1.3	noise on CKD	GS
		19.2	OG CKD Scan angle	19.2.1	Setup & measurement accuracy	GS
				19.2.2	"polarisation shift"	GS
				19.2.3	Noise on scan angle CKD	
		19.3	Apply	19.3.1	spectral calibration	GS
				19.3.2	OBM temperature	GS
				19.3.3	Representative scan angle	X
110	Diffuser BSDF	110.1	OG CKD default direction	110.1.1	calib.standards	GS
				110.1.2	distance measurements	GS
				110.1.3	noise on CKD	GS

#	main elements	#	contributing elements	#	sub-items	
		I10.2	Elev / Azi dependence	I10.2.1	OG CKD	GS
				I10.2.2	accuracy solar angles	GS
				I10.2.3	Elev summation window	G
		I10.3	Diffuser Speckles ESM			GS
		I10.4	Neutral Density Filter			S
I11	Degradation correction path ESM					
		I11.1	Errors on reference meas.		Errors on reference meas.	GS
		I11.2	Smoothing errors		Smoothing errors	GS
		I11.3	Method limitations	I11.3.1	scan angle dependence	G
				I11.3.2	layer optical constants	S
				I11.3.3	neglect OBM pol.change	GS
				I11.3.4	other effects	GS
		I11.4	BSDF degradation			GS
		I11.5	OG to first in-orbit meas.			GS
I12	Polarisation					
I13	Harmonisation					
		I13.1	Solar variability			G
		I13.2	Smoothing			G
		I13.3	Time dependence			G

1) Included in I9. 2) for GOME included in I9

The processing chain diagram for GOME is shown in Figure 34; the diagram for SCIAMACHY is in Figure 35.

- For the various symbols in the diagram: see Table 1 from DB1-07
- Schematic: CKD uncertainties include uncertainties in the application of CKD (as shown in figure), but also include uncertainties in their calculation (which in reality is a different process)
- The diagram differentiates between “broadband” uncertainties and “pixel-to-pixel” uncertainties. For Level 2 applications this is important, since “broadband” uncertainties usually can be accommodated by fitting a closure term (polynomial in DOAS). However, the effect tables will not make that differentiation. Instead, spectral correlation scales will be indicated. The Level 1b user then has to decide which correlation is relevant to his/her application.
- In the FDR, the GOME irradiances will be aligned to the SCIAMACHY irradiances. This will generally not modify the uncertainties that spectrally correlate on the scale of a few pixels, but it



will modify the broadband uncertainties. Of the latter, many GOME uncertainties will vanish (be aligned with the SCIAMACHY uncertainties) but some may persist on spectral scales smaller than the spectral scale on which the alignment is performed. Currently this is 3/2/5 nm for channels 2/3/4 respectively.

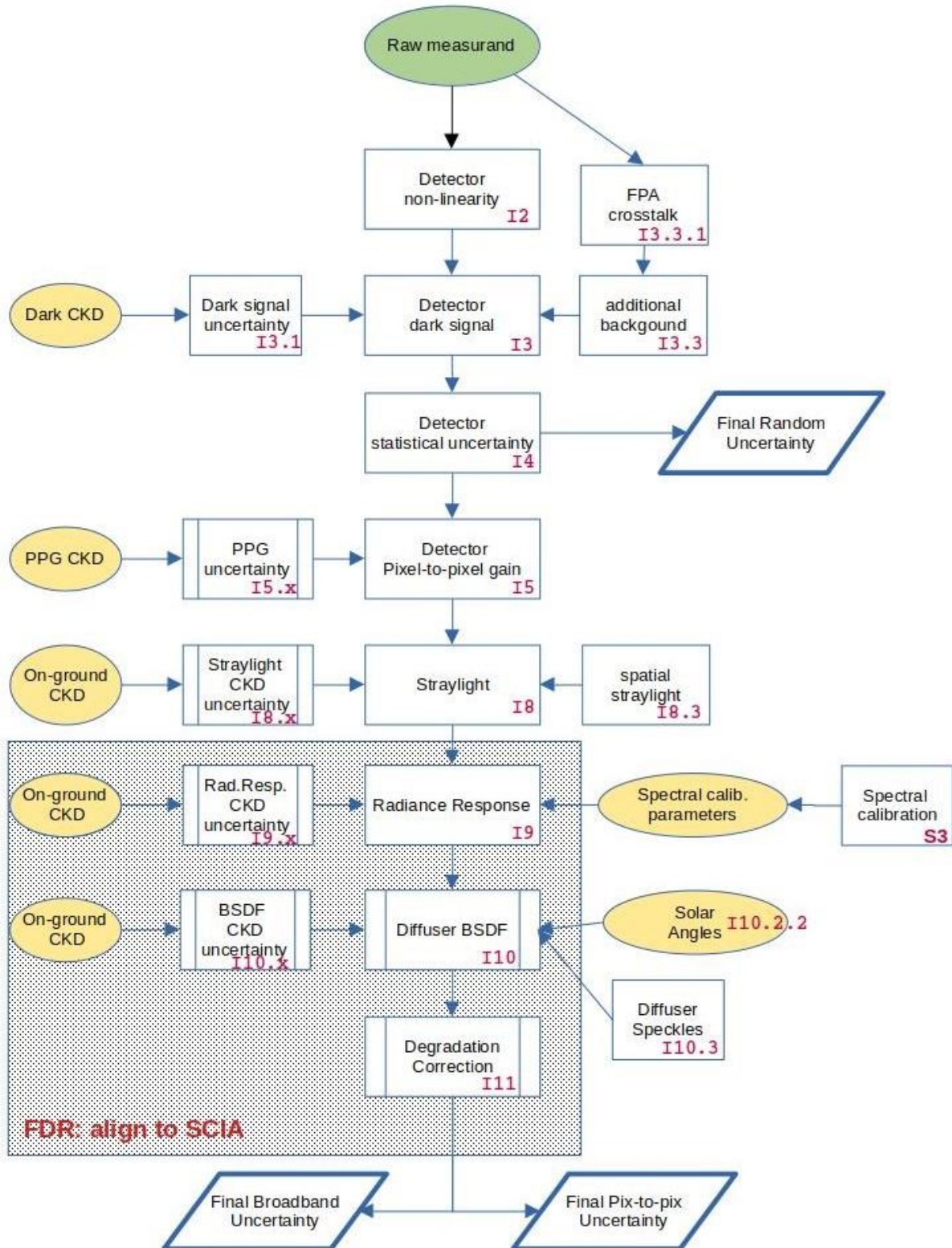


Figure 34 Processing chain diagram for GOME irradiance uncertainties

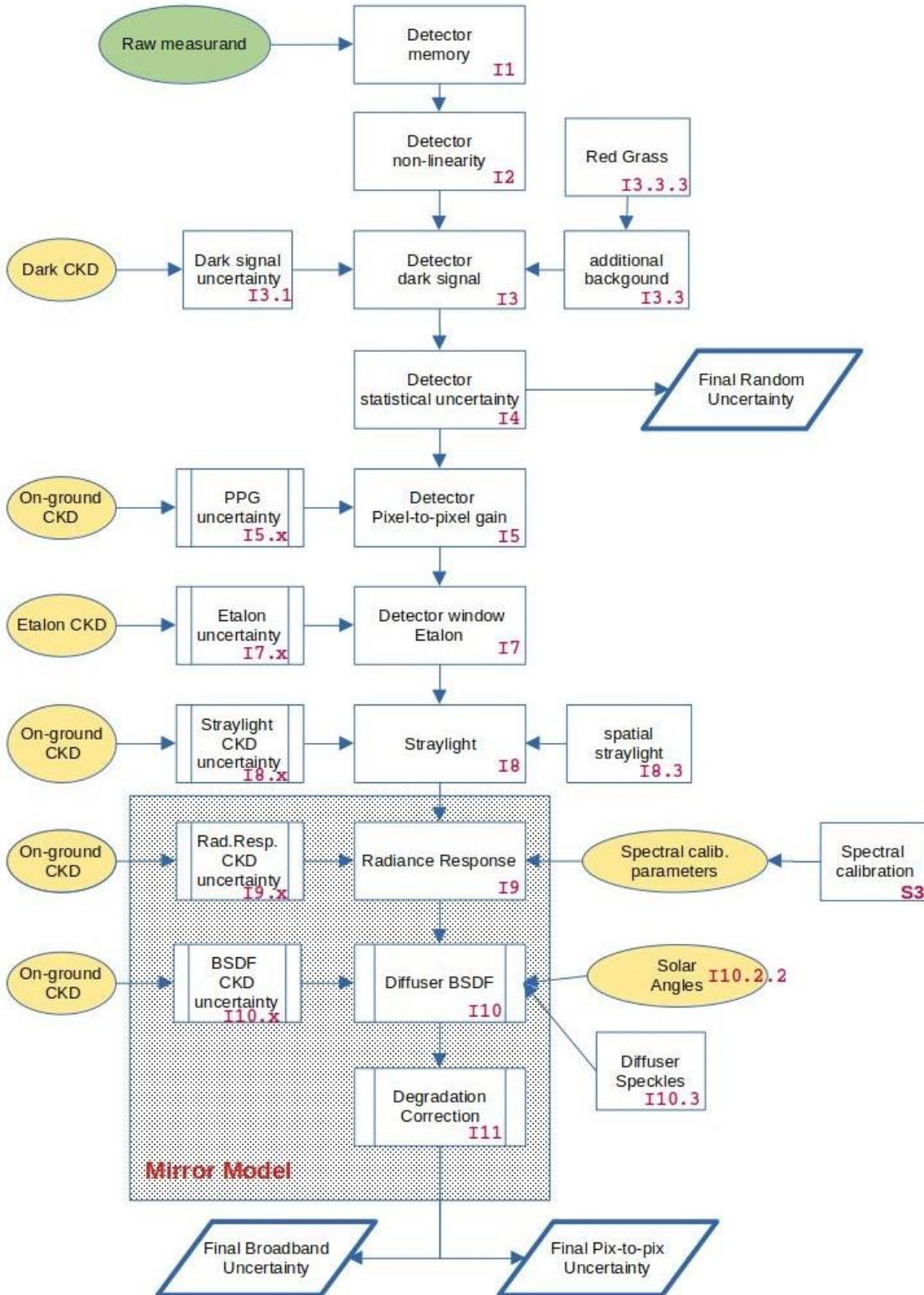


Figure 35 Processing chain diagram for SCIAMACHY irradiance uncertainties

3.3 Instrument Measurement function

- Order of equations in this section is according to the main element numbering (see Table 3-1) using as overarching function the general calibration equation (see Section 3.1).
- Numbering in Processing chain diagram and Effects table is indicated in red: [**Ix.y.z**]

3.3.1 I1 - Memory effect

This only applies to the main channels of SCIAMACHY.

Memory effect is described by the term MEC_i in the general calibration function (Eq.3-1). This term may be expanded as follows; the index k stands for the current readout.

$$MEC_i(k) = f_i(S_{measured}(i, k - 1)) + 0$$

The function f is calibrated for each channel as a function (lookup table) of signal level (in this case the signal of the previous readout). Although it may be dependent on pixel number, it could only be calibrated on-ground assuming that all pixels in the channel have the same memory effect. The MEC_i has the following uncertainties:

- $\varepsilon_{MEC}(i)$. the calibration uncertainty on the function f [**I1.1**]
- ε_S accounts for the fact that the previous signal may not be known: this happens in the case of co-adding when signals vary. For the irradiance product this may be neglected, as the solar signals do not change significantly during the measurement sequence. [**I1.3**]

There might be a possibility that the function f "degrades" (is not constant over time) [**I1.2**]

The +0 term accounts for model errors like:

- unknown if the same function f is strictly valid for all pixels in one channel;
- a known but not quantified effect that a residual memory signal is not only added to the next readout, but also to further readouts (although "exponentially" decaying).

3.3.2 I2 - Non-linearity

(this subsection is schematic, no quantitative uncertainty is associated here)

- Saturation **I2.1**: flagged not corrected, in practice doesn't occur for irradiance. In principle: also below the flagging threshold some effect may be present.
- GOME: see doc TPD-ERS-GO MIR = (ESA) ER-TR-TPD-GO-0032, Iss.1, 3-11-1994
- SCIAMACHY: see doc SCIAMACHY channel 2 non-linearity, SRON-SQWG3-TN-2015-002, Iss. 1, 14.01.2016
- SCIAMACHY linearity: electronic non-linearity **I2.2** is established for channels 6-8 and thus not relevant for the FDR. However, during on-ground calibration, it was difficult to attribute the observed signal anomaly during a non-linearity measurement to actual non-linearity (i.e. a dependence on the measured signal level) or to a memory effect (i.e. a dependence on the signal level of the previous measurements). A certain amount of memory effect was clearly seen, and therefore the whole anomaly was declared a memory effect. However, it cannot be excluded that this is incorrect.

3.3.3 I3 - Dark signal

SCIAMACHY

The dark signal term in Eq.(3-1) can be expanded as:

$$DS(i) = f_{coadd} \cdot (FPN(i) + PET(i) \cdot LC(i, T)) \quad Eq.(3-2)$$

where

$f_{coadd}(i)$	coadding factor for the cluster containing detector pixel i
$FPN(i)$	Fixed Pattern Noise (=offset) for detector pixel i
$PET(i)$	pixel exposure time (single-readout integration time) at detector pixel i
$LC(i, T)$	leakage current of detector pixel i at detector temperature T

with the following additive uncertainties:

$\epsilon_{FPN(i)}$	due to a calibration error on FPN(i) [I 3.2.1]
$\epsilon_{LC(i,T)}$	due to calibration error and temperature dependence on LC(i,T) [I 3.2.2]
ϵ_{SAA}	on LC(i,T) due to particle flux in SAA (value per channel) [I 3.3.2]
ϵ_{RG}	Red Grass [I 3.3.3]

The FPN and LC are obtained from the dark signal measured at several exposure times, where the offset and slope of the linear fit of dark signal versus exposure time are the FPN and LC, respectively. This can only be done if the detector temperature is kept constant, because LC depends on detector temperature. This should be the case (each detector is always operated at a pre-set temperature) but small temperature fluctuations due to lag in the feedback control loop are always possible.

Red Grass is an electronics issue that may suddenly trigger an odd-even offset on the spectrum. The cause of this trigger is unknown, it might be occurring when a high signal level is reached but this is not clear. Red Grass is unlikely to occur on the dark signal itself, but it may be considered as a background on the irradiance when it occurs. Therefore we include it here.

GOME

During on-ground calibration of GOME, it appeared that cross-talk was present which invalidates the expression from Eq.(3-2). The calibration approach has been to measure dark signals for each "integration time pattern" i.e. each combination of integration time of the 4 channels that is used for scanning measurements, solar observation, or in-orbit calibration measurements.

The cross-talk is not constant in time, but depends on switching in the FPA-temperature control loop. There is an additional calibration algorithm for this which is described in [R2].

There is also an additional calibration algorithm to reduce the dark signal error in the SAA, based on the signal in a "straylight" band at the start of channel 1. However, that is only applied to channel 1 (which has the longest integration time and is more susceptible to the effect) and thus not used for the FDR.

The dark signal term in Eq.(3-1) including error terms can then be expanded as:

$$DS(i) = DS_{cal}(i, IT, T) + \varepsilon_{DS(i)} + \varepsilon_{SAA} + C_{crosstalk} + \varepsilon_{crosstalk}$$

where

$DS_{cal}(i, IT, T)$ calibrated dark signal for the integration time pattern and detector temperature, for detector pixel i .

$C_{crosstalk}(t)$ time-dependent cross-talk correction (one value per channel)

with the following additive uncertainties

$\varepsilon_{DS(i,T)}$ uncertainty on the assigned dark signal [I 3.1]

ε_{SAA} uncertainty due to particle flux in SAA (one value per channel) [I 3.3.2]

$\varepsilon_{crosstalk}$ uncertainty on cross-talk correction [I 3.3.1]

As for SCIAMACHY, the detector temperature effect is probably negligible, but added for completeness. Since dark signal is not calibrated as function of temperature, we include any such effect in the +0 term.

The FPA cross-talk scales approximately with integration time and is only applied for integration times ≥ 12 seconds. The irradiance measurements are much shorter than that. The measurement function thus may be reduced to:

$$DS(i) = DS_{cal}(i, IT) + 0 \quad \text{Eq. (3-3)}$$

with the additive uncertainties as above.

3.3.4 14 - Statistical Uncertainty (noise)

Noise is calculated as in the respective ATBDs, as the rms sum of readout noise, shot noise, and digitisation noise.

$$\sigma_{Stat} = \frac{1}{N_e} \sqrt{S_e + \sigma_R^2 + \varepsilon_D^2} \quad \text{Eq. (3-4)}$$

where

N_e number of electrons for 1 BU

S_e signal of a pixel (without electronic offset / FPN) in electrons = $S[\text{BU}] \cdot N_e$

σ_R noise on the detector readout in electrons

ε_D uncertainty due to digitisation = $0.5 \cdot N_e$

The noise on an average of measurements, due to co-adding or in the calculation of an averaged irradiance spectrum, is reduced by the square root of the number of measurements.

The subtraction of electronic offset from the signal, and the uncertainty in the determination of detector readout noise cause an uncertainty on σ_{Stat} itself. However, this may be neglected

3.3.5 15 – Pixel-to-pixel gain

Uncertainties on pixel-to-pixel gain (PPG) are basically determined by two things:

- noise on the calibration measurements [I 5.1]
- calculation method of the PPG [I 5.2]

In the general calibration equation Eq.(3-1), PPG occurs twice: as a correction on Radiance Response during on-ground calibration, $PPG(t=0)$, and $PPG(t)$ measured in-flight. Since the former may be subject to wavelength shifts, these terms do not necessarily cancel even if they were to be identical.

It will be assumed here that errors on $PPG(t=0)$ are contained in the “noise on Radiance Response” uncertainty ([I 9.1.3]) since the CKD were not smoothed, whereas the $PPG(t=0)$ correction is intended to provide smooth (= wavelength-dependent but not pixel-dependent) CKD.

GOME:

The in-flight PPG is obtained as the residual of a triangular smoothing (running average) through (time-)averaged LED measurements. Measurement noise may play a role in the PPG uncertainty, as well as the width/shape of the smoothing kernel. It was found that the PPG amplitude increases over the years (on average). Since the LED signals are not affected by degradation of the optics, it is unlikely that the amplitude increase is connected to an increase in uncertainty on PPG.

SCIAMACHY:

The noise on the WLS measurements was deemed too large to reliably calculate an in-flight PPG. The PPG from the on-ground calibration was taken as proxy for $PPG(t)$ (see [R3]). Since SCIAMACHY has the same detectors as GOME, the best guess may be that uncertainties on $PPG(t)$ are similar. Noise on the WLS measurements would be an upper limit to the uncertainty.

3.3.6 16 – Electronic gain

The electronic gain is not expected to vary significantly. In GOME and SCIAMACHY there is no way to characterise this independently. The term will be treated as part of the radiance response [I 9].

3.3.7 17 – Etalon

GOME:

GOME does not have a WLS that could be used for an etalon correction. The changing etalon is in channel 2 and 3 a significant part of the irradiance calibration error. As illustration, Figure 36 shows for channel 2 the ratio of irradiance spectra in 1997 and 2002 w.r.t. the first spectrum in each year (spectra at 14 days intervals).

The uncertainty caused by changing etalon structures is difficult to separate from other radiometric changes. Therefore we will include this uncertainty together with other effects as lump-sum in Section 3.3.11 I11 – Degradation”.

Note that Figure 36 is for GOME as stand-alone instrument. In the FDR, after alignment to SCIAMACHY, most of this structure will disappear. However, since this alignment involves a smoothing in wavelength, a small residual may remain.

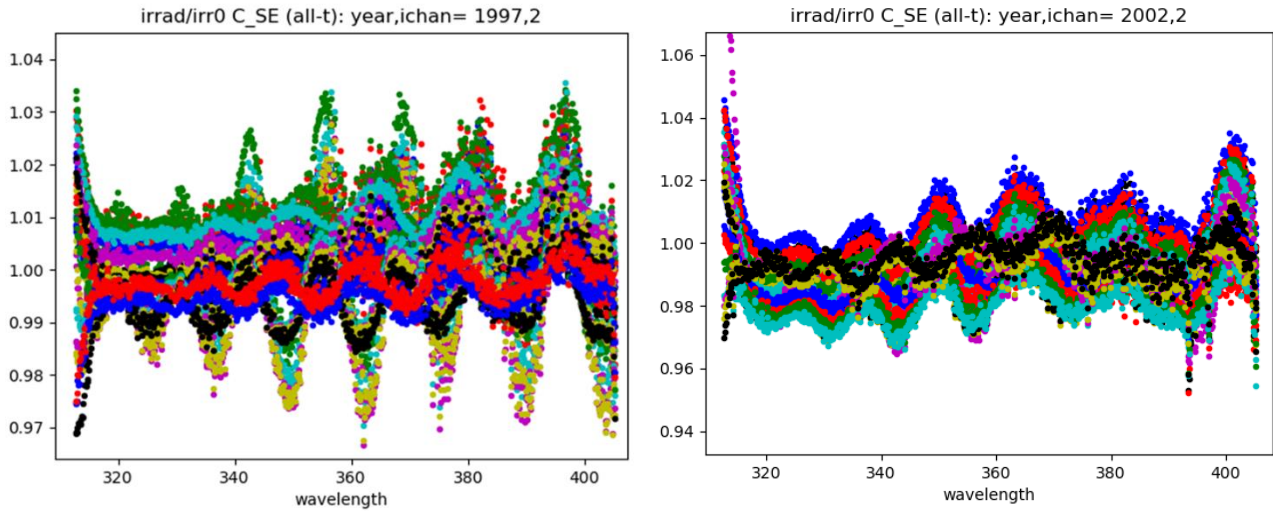


Figure 36 Etalon in GOME channel 2 (before harmonisation in the FDR), see text.

SCIAMACHY:

Since L1b processing version 8, the etalon correction is implicitly included in the degradation correction using m-factors (which are generated daily). In L1b processing, the m-factor from the previous Sun calibration is used. This time delay may occasionally introduce calibration errors if the etalon changes rapidly (usually only after instrument decontamination or switch-off).

The etalon change between on-ground calibration and the in-orbit reference date for the m-factors is since L1b processing version 9 incorporated in the general on-ground to in-orbit change of radiance response.

This will be included in Section 3.3.11 I11 – Degradation”.

3.3.8 I8 – Straylight

The straylight signal term in Eq.(3-1) may be expanded as:

	$SS_i = \sum_i FST(i) \cdot FR(i) + \sum_j ST(i, j) \cdot S(j) + 0$	Eq.(3-5)
--	---	-----------

...where

- $FST(i)$ straylight operator for out-of-field straylight, for detector pixel i
- $ST(i, j)$ straylight operator for spectrometer straylight from pixel j onto pixel i
- $FR(i)$ out-of-field radiance
- $S(j)$ signal of pixel j

with multiplicative uncertainties

- $\epsilon_{FST}(i)$ uncertainty on the out-of-field straylight
- $\epsilon_{stray}(i, j)$ uncertainty on the spectrometer straylight (split into components below)

The out-of-field straylight component FST is irrelevant for irradiance, as there is no other bright light source than the Sun.

Out-of-band straylight (originating from wavelengths outside the channels) is in principle possible, but since GOME/SCIAMACHY is a double monochromator design it is expected to be comparatively small. Depending on the origin of the straylight, it may increase due to contamination of the optics over time.

GOME:

For GOME, the straylight operator is split into a uniform component and a single ghost. The ghost straylight is not expected to be influenced by optics degradation, but the uniform component may be. Further errors on the uniform straylight may arise from uncertainties on the straylight intensity CKD and the fact that the straylight is not really uniform but has in reality a wavelength dependence. Errors on the calculated ghost straylight may arise from uncertainties on the ghost intensity CKD and the position of the ghost (the ghost is a fraction of the spectrum mirrored around a “central” pixel).

We then have in Eq.(3-5):

$$ST(i, j) = ST_{stray-uniform} + defoc(ST_{stray-ghost} \cdot \delta_{ij}(j = 2 \cdot i_c - i)) + ST_{stray-degrad}(i, j, t) \quad Eq.(3-6)$$

where

$ST_{stray-uniform}$	coefficient for uniform straylight
$ST_{stray-ghost}$	coefficient for ghost straylight
$\delta_{ij}(j = 2 \cdot i_c - i)$	delta function which is 1 when pixel $j = 2 \cdot i_c - i$ and else 0
i_c	a “central” pixel number for the mirror function (different for each channel, number between 0 and 1023, usually around 500)
defoc	a function describing defocussing of the ghost

with multiplicative uncertainties

$\epsilon_{stray-uniform}$	uncertainty on $ST_{stray-uniform}$ [I 8.1]
$\epsilon_{stray-ghost}$	combined uncertainty on $ST_{stray-ghost}$, defoc, and i_c [I 8.2]
$\epsilon_{stray-degrad}(t)$	uncertainty due to increase in straylight with time (e.g. due to optics contamination) [I 8.4]

Note that in effect these uncertainties may be evaluated as fraction of the calculated Level 1b straylight, rather than as fraction of the input signal at each pixel.

SCIAMACHY:

The straylight calculation for SCIAMACHY is similar to that of GOME, except that for the uniform straylight part of $ST(i, j)$ there is a matrix, and there are several focussed ghosts. An error assessment on CKD [R4] recommended to use a fixed fraction of the *calculated straylight* intensity as formal error, such that similar expressions for the GOME straylight uncertainties may be taken for SCIAMACHY as well.

3.3.9 I9 – Radiance response

The radiance response, and all the components from which it is calculated, is applied as a multiplicative factor on the signal. Its errors shall be treated accordingly.

The radiance response is the term $(RR_{0,i}/PPG_{0,i})(\lambda_i)$ in the general calibration equation. Subscript 0 denotes on-ground calibration. The division by PPG shall ensure that when the wavelength calibration

changes, the radiance response may be interpolated in wavelength without having to care about a pixel dependence. In principle, errors in PPG cause an error in spectral interpolation. For practical purposes, this may be neglected as PPG is already very small itself.

Errors in the wavelength calibration do cause errors in radiance response; the corresponding relative uncertainty is

$$\varepsilon_{RRs} = \frac{\partial R}{\partial \lambda} \cdot \varepsilon_{\lambda} / R$$

Where R is the radiance response and ε_{λ} the spectral calibration uncertainty [I 9.3.1].

The radiance response may be dependent on temperature T of the optical bench; the corresponding relative uncertainty is

$$\varepsilon_{RRt} = \frac{\partial R}{\partial T} \cdot (T - T_0) / R$$

Where R is the radiance response and T_0 the optical bench temperature for which the CKD are valid [I 9.3.2].

The uncertainties on the on-ground CKD are as follows.

GOME

The radiance response was calibrated at one specific scan angle α_c . (approximately nadir) The scan angle dependency $\chi(\alpha)$ was separately measured. For the system as designed, with all optics in one plane, one would expect that χ is a simple multiplicative factor that depends only on wavelength. However, GOME seems to suffer from a similar polarisation shift as SCIAMACHY which may be diagnosed from the jumps in χ at the channel boundaries.

The radiance response in the measurement function may be written as (R and χ implicitly dependent on λ and T):

$R = R(\alpha_c) \cdot \chi(\alpha) + 0$	Eq.(3-7)
--	-----------

with (in addition to ε_{RRs} and ε_{RRt}) the following multiplicative uncertainties on $R(\alpha_c)$:

δ_{Lref} is a (mostly systematic) uncertainty on the NIST reference lamp calibration [I 9.1.1]

δ_{Rdist} is a systematic uncertainty on the distance between NIST lamp and instrument [I 9.1.2]

σ_R is a noise term on $R(\alpha_c)$ [I 9.1.3]

and the following multiplicative uncertainties on $\chi(\alpha)$:

ε_{χ} is an uncertainty for measurement setup and calibration accuracy of $\chi(\alpha)$ [I 9.2.1]

δ_{Rps} is an uncertainty due to polarisation shift in the instrument [I 9.2.2]

σ_{χ} is a noise term on $\chi(\alpha)$ [I 9.2.3]

The +0 term accounts for uncertainties due to lamp stability and a possible etalon effect depending on input beam inhomogeneity, as well as several uncertainties associated with the processing of the on-ground calibration measurements (e.g. dark signal and straylight subtraction).

The CKD for radiance response were in channels 1 and 2 after launch corrected for an air-to vacuum shift, while in channel 3 a correction for outgassing of the dichroic filter was applied. The uncertainties associated with this correction are described in Section 3.3.11 "I11 – Degradation" but note that in Level 0 to 1 processing they are implemented as an implicit part of CKD and not part of the degradation

correction algorithm.

GOME after FDR alignment to SCIA

After FDR harmonisation to SCIAMACHY, systematic offsets δ_{Lref} and δ_{Rdist} for GOME will vanish, while the noise terms will remain. Short wavelength range uncertainties on $\chi(\alpha)$ and $R(\alpha_c)$ might remain. These will be accommodated by a “harmonisation uncertainty” term. This is a lump sum for residual effects in radiance response, diffuser BSDF, and degradation correction. For radiance response, it replaces [I 9.3.2] [I 9.2.1] [I 9.2.2] .

In addition, the uncertainties on Radiance Response from SCIAMACHY have to be added.

SCIAMACHY

In the on-ground calibration there was a separate calibration for the OBM (which here was done in thermal vacuum) and one of the scanner unit (angular dependence) which was done in ambient. In the original calibration plan there were radiance response CKD, diffuser BSDF CKD, and “greek keydata” which during calibration were derived from ratios of measurements, thereby cancelling out several systematic error components. For Level 0 to 1 processing these CKD were pre-processed into Mueller matrix elements (see [R3]).

In recent versions of the Level 0 to 1 processor, the Mueller matrix elements and in particular their polarisation-dependent function of scan angle make use of a “SCIAMACHY Scan Mirror Model” which has the advantage that it can account for degradation of the polarisation properties of the scan mirror [R3][R6][R9].

In the Mueller matrix formalism, the detected signal (excluding the additive terms in the general calibration equation) may be written as function of input (ir)radiance I as (see [R9]):

$S_{det} = M_1^{OBM} \cdot \vec{\mu}^{OBM} \cdot \bar{K}^{sc}(\alpha, d) \cdot \begin{pmatrix} 1 \\ q \\ u \\ v \end{pmatrix} \cdot I$	Eq.(3-8)
--	-----------

where the rightmost 2 terms constitute the Stokes vector of the incoming light, and

M_1^{OBM} the radiance response of the OBM

$\vec{\mu}^{OBM} = (1 \quad \mu_2^{OBM} \quad \mu_3^{OBM} \quad \mu_4^{OBM})$ the polarisation sensitivity of the OBM (see [R3])

$\bar{K}^{sc}(\alpha, d)$ the 4 × 4 Mueller matrix of the scan unit model (see [R6])

The scan mirror model has 2 layers on top of the aluminium mirror surface: an Aluminium Oxide layer with fixed thickness and a “contamination” layer with variable thicknesses d . The Mueller matrix elements further depend on incidence angles α on the ASM and ESM and/or the corresponding diffuser. Fixed model inputs are the optical constants of Aluminium, Aluminium Oxide, and the contamination layer. In-orbit measurements from Sun and WLS are used to adjust d inflight (corresponding uncertainties are described in Section 3.3.11 I11 – Degradation”).

The mirror model makes a fit to on-ground calibration measurements to derive a parameter for optical constants including on-ground contamination of the scan mirror. As such, similar on-ground calibration uncertainties as for GOME are still present in the mirror model (albeit indirectly for the scan angle dependencies).

The mirror model is a “model” in the sense that it makes assumptions on how the contamination is layered, and it assumes that the “polarisation shift” in the OBM is caused by a retarding element, which

is a probable cause but not necessarily the only cause. These assumptions may lead to non-negligible unknown uncertainties (although less than neglecting degradation in scan angle polarisation as is done for GOME). These inherent model uncertainties add to the uncertainties on on-ground CKD.

Light from the Sun (and also from the WLS) is unpolarised, such that $q = u = v = 0$.
Eq.(3-8) may then be written as:

$$S_{det} = I \cdot M_1^{OBM} \cdot \sum_{j=1}^4 \mu_j^{OBM} \cdot K_{j1}^{sc}(\alpha, d) \quad \text{Eq.(3-9)}$$

The irradiance product using Sun over ESM diffuser employs the reflection of the ASM mirror and the BSDF of the ESM diffuser. Since ASM and ESM are not orthogonal, the BSDF factor cannot be separated out (as for GOME). Therefore the equation above calculates directly the irradiance response. On-ground calibration errors on BSDF are included here and not in the next section (as for GOME).

Using $\chi(\alpha)$ as a shorthand symbol for the summation term in Eq.(3-9) we may cast the error calculation into a similar form as used for GOME.

The irradiance response IR in the measurement function, which is the equivalent of the term: $BSDF_0 \cdot (RR_{0,i}/PPG_{0,i})$ in the general calibration equation, may then be written as (M_1^{OBM} and χ implicitly dependent on λ and T):

$$IR = M_1^{OBM} \cdot \chi(\alpha) + 0 \quad \text{Eq.(3-10)}$$

with (in addition to ε_{RRs} and ε_{RRt}) the following multiplicative uncertainties on M_1^{OBM} :

- δ_{Lref} a (mostly systematic) uncertainty on the NIST reference lamp calibration [I 9.1.1]
- δ_{Rdist} a systematic uncertainty on the distance between NIST lamp and instrument [I 9.1.2]
- σ_R a noise term [I 9.1.3]

and the following multiplicative uncertainties on $\chi(\alpha)$:

- ε_χ is an uncertainty for the calibration accuracy of $\chi(\alpha)$ as discussed below
- σ_χ is a noise term on $\chi(\alpha)$ [I 9.2.3]

The +0 term accounts for several uncertainties associated with the processing of the on-ground calibration measurements (e.g. dark signal and straylight subtraction).

Since δ_{Lref} and δ_{Rdist} are by far the dominant uncertainties on M_1^{OBM} for the spectrally broadband errors, we may consider other broadband effects in the +0 term. Having said that, varying the lamp distance or input source in SCIAMACHY on-ground calibration also gave rise to slightly modified etalon structures, and it is unknown if this +0 term is really insignificant.

The uncertainty on $\chi(\alpha) = \sum_{j=1}^4 \mu_j^{OBM} \cdot K_{j1}^{sc}(\alpha, d)$ may be broken down into a complex of several components:

- On-ground measurement setup and calibration accuracy of the Mueller matrix elements of the scan mirror (the original measured elements to which the scanner model is fitted) [I 9.2.1]
- An uncertainty due to polarisation shift in the instrument [I 9.2.2]
This is the measurement accuracy on the polarisation sensitivity parameters of the OBM μ_j^{OBM} and the uncertainty in the OBM retarder model

- An uncertainty in the parameters of the scan mirror model as fitted to the measured mirror properties [I 9.2.3]

Note that the scan mirror model has no noise, but the term is σ_{ξ} is non-zero because the calibrated polarisation parameters of the OBM have noise.

3.3.10 I10 – Diffuser BSDF

GOME

The BSDF of the calibration unit for Sun irradiance has been calibrated on-ground. The CKD describe the BSDF as separate factors for wavelength dependence, solar azimuth dependence, and solar elevation dependence. Solar azimuth and elevation are here in a coordinate frame relative to the instrument’s irradiance port. Solar azimuth changes as function of day-of-year according to the analemma. Elevation changes with position in orbit, where the Sun is for a short period every orbit visible through the irradiance port. The unobstructed FOV in solar elevation is around $\pm 1.5^\circ$. The L1b processor averages the Solar spectra over this elevation range.

Since the elevation-dependence of the BSDF was found to be linear with elevation angle, the averaging of spectra results in a cancelling of the BSDF elevation term. However, uncertainties remain because of geolocation/timing uncertainties, und uncertainty in the attitude of the spacecraft.

After a few years in-orbit, data analysis showed that the calibrated azimuth-dependence was inaccurate, and an improved function was derived for the CKD (the “smoothed BSDF” from [R12]). Following the logic of this document, that would be described here as “in-orbit degradation” effect, but as is reduces instead of enlarges the uncertainty, we include this correction in the on-ground CKD.

The measurement function, which is the term $BSDF_0(\lambda_i)$ in the general calibration equation Eq.(3-1), may be written as:

$$BSDF_0 = P_1(\lambda_i) \cdot P_2(\alpha_{azi}) + 0 \quad \text{Eq.(3-11)}$$

where $P_1(\lambda_i)$ and $P_2(\alpha_{azi})$ are polynomial functions in wavelength (per channel) and solar azimuth (in the diffuser coordinate frame), respectively. In Level 0 to 1b processing the polynomial in azimuth is in fact (for historical reasons) the quadratic function from on-ground CKD multiplied with a correction factor from a pre-calculated LUT. The +0 term accounts for the fact that the separation of variables might not strictly apply.

The following sources of uncertainty may be identified; all are multiplicative.

- $\delta_{BSDFref}$ uncertainty on on-ground calibration standard (in this case the BSDF of a reference diffuser) and light source stability [I 10.1.1] (for the centre azimuth/elevation position)
- The noise term [I 10.1.3] is zero, as the wavelength-, azimuth-, and elevation dependence was fitted by polynomials for the CKD
- $\epsilon_{BSDF-azi}$ uncertainty on the azimuth dependence of the BSDF CKD [I 10.2.1]
- $\epsilon_{Sun-azi}$ uncertainty on the solar azimuth (geolocation) [I 10.2.2]
- $\epsilon_{BSDF-elev}$ uncertainty on averaging over elevation caused by uncertainty in solar elevation (geolocation) [I 10.2.3]

- $\epsilon_{Speckle}$ uncertainty related to diffuser speckles (see SCIAMACHY below) [I 10.3].
 The SMR averaging over solar elevation angles may somewhat subdue this effect.

GOME after FDR alignment to SCIAMACHY

After FDR harmonisation to SCIAMACHY, the “harmonisation uncertainty” term (see Section 3.3.9 I9 – Radiance response) replaces all of the above effects except [I 10.3]. In addition, the uncertainties on BSDF from SCIAMACHY have to be added.

SCIA

The errors on BSDF as incorporated in the “mirror model” have been listed in the previous Section 3.3.9 /SCIAMACHY.

One additional multiplicative error is associated with speckle patterns that arise in ground aluminium diffusers when the “hills and valleys” in the surface are not completely randomly distributed. The diffuser speckle pattern depends on azimuth and elevation angles of the incident light.

In Level 1 processing a LUT predicts the speckles. However, an uncertainty will remain with the speckle prediction that may add to the Pixel-to-pixel uncertainty [I 10.3]. The irradiance response may then be written as

$$IR = IR9 \cdot (1 + \Delta_{Speckle}) \quad \text{Eq.(3-12)}$$

where IR9 is the irradiance response from the mirror model (Section 3.3.9) and $(1 + \Delta_{Speckle})$ is the L1b correction for speckles, with multiplicative uncertainty

$\epsilon_{Speckle}$ the uncertainty on L1b diffuser speckles correction [I 10.3].

3.3.11 I11 – Degradation

GOME:

The degradation correction in GOME Level 0-1b processing is based on the following assumptions [R2]:

- the Sun may be taken as constant, the degradation is calculated from the ratio of Sun measurements compared to reference time of 3 July 1995.
- the degradation is a smooth function of wavelength, calculated as a polynomial function per channel
- the degradation is a smooth function of time, implemented as SAVGOL fitting of each coefficient in the wavelength polynomial
- changing etalon/dichroic structures are not corrected (but will vanish in the reflectance)

The measurement function for degradation correction consists then of the terms from the general calibration equation Eq.(3-1)

$$m_{BSDF,t}(\lambda_i) \cdot m_t(\lambda_i)$$

where

$$m_{BSDF,t}(\lambda_i) \quad \text{BSDF degradation monitoring factor}$$

$m_t(\lambda_i)$ RR degradation monitoring factor as function of wavelength

The degradation correction has for the irradiance the following uncertainties:

- fitting leaves (large) etalon/dichroic/small-scale structures:
 $\epsilon_{Sun-smooth}$ uncertainty due to spectral smoothing [I 11.2]
- on-ground to orbit changes [I 11.5]:
 - air-to-vacuum correction (see e.g. [R11])
 - Ch.3 : dichroic outgassing with wavelength shift of transmission function
These were largely corrected in Radiance Response keydata version 8.3 but have residual uncertainties
- $\epsilon_{Sun-measurement}$ uncertainty on the solar measurement due to additive calibration errors and due to the assumption that the Sun remains constant over time [I 11.1]
Since the degradation correction uses strong smoothing, the additive errors effectively vanish, while in channel 2,3,4 the Sun may be regarded constant except in strong coronal-active lines. However, these are outside the FDR wavelengths (Ca-K and H- α)
- Ambiguity between degradation of Radiance Response and degradation of BSDF [I 11.4]. This is irrelevant for GOME irradiance, since only the total degradation counts.

GOME after FDR alignment to SCIA

After FDR harmonisation to SCIAMACHY, the “harmonisation uncertainty” term (see Section 3.3.9 19 – Radiance response) replaces all of the above effects except [I 11.1] .

In addition, the uncertainties on Degradation from SCIAMACHY have to be added.

SCIAMACHY

The degradation correction for SCIAMACHY is implemented in 2 steps:

- update of the scan mirror model
- calculate m-factors for the OBM (residual after update of the mirror model)

Both are based on the comparison of the measured and calibrated signal of a light source (WLS or Sun) at the measurement time versus the measured signal (calibrated without degradation correction) at a reference time (in orbit).

The uncertainties in this procedure may be broken down into the following components:

- $\epsilon_{Sun-measurement}$ uncertainty on the measurement due to additive calibration errors and due to the assumption that the Sun remains constant over time [I 11.1]
- $\epsilon_{Sun-smooth}$ uncertainty due to spectral smoothing of the m-factors [I 11.2]
- $\Delta\delta$ uncertainty on the thickness of the contamination layer [I 11.3.2]
- $\epsilon_{OBM-pol-const}$ uncertainty due to assumption that the μ_j^{OBM} from Eq.(3-8) remain constant in time [I 11.3.3]. In L1b Version 10 this is (partly) corrected by deriving a separate OBM m-factor for each light path, but that results in an error on the calculation of δ .

Note that uncertainties with the mirror model itself still count (but these should not be added to those of Eq.(3-10), rather should that equation be re-calculated with the updated value of δ to be precise).

In addition to the above degradation in-flight, there are also uncertainties in instrument degradation between the on-ground calibration and the date of the in-orbit reference [I 11.5]. This degradation was derived based on WLS measurements; a correction was made for different temperature of the WLS due to gravity-induced turbulence which “cools” the WLS filament on-ground. The associated

uncertainty, $\varepsilon_{OG \rightarrow IF}$ includes but is not limited to the uncertainty in on-ground/inflight WLS measurements, an uncertainty in the WLS temperature correction, and an uncertainty if the correction method captures all the physics involved (e.g. the OBM light path degradation is not identical for Sun and WLS).

3.3.12 I12 – Polarisation

As the Solar Irradiance is unpolarised, this is not an issue.

3.3.13 I13 – Harmonisation

FDR Harmonisation of GOME Irradiance to SCIAMACHY Irradiance is done by multiplying with a “harmonisation factor” that is taken as the smoothed ratio of SCIAMACHY Irradiance to GOME Irradiance:

$I(\lambda_i, t)_{FDR}^{GOME} = I(\lambda_i, t)^{GOME} \cdot SMOOTH \left(\frac{I(\lambda_i, t_{ref})^{SCIA}}{I(\lambda_i, t)^{GOME}} \right)$	Eq.(3-13)
---	------------

with

- λ_i wavelength of detector pixel *i*
- t time of GOME measurement (in this case number of days)
- t_{ref} reference time for SCIAMACHY measurement
- $I(\lambda_i, t)$ Irradiance measured for day *t* as function of wavelength
- $SMOOTH$ function for smoothing over wavelength (in this case gaussian kernel)

Uncertainties are present due to solar variability [I 13.1] and spectral features not captured by the smoothing function [I 13.2]. Partly, the latter is intentional, since GOME and SCIAMACHY have different spectral resolution and the slit functions of both instruments are not known well enough to adjust irradiances on a spectral scale less than a few nm. The uncertainty in solar variability may be neglected, since the Sun is quite stable at the FDR wavelengths, and the time difference between GOME and SCIAMACHY irradiance measurements is only ~0.5 hours.

The use of one reference time for SCIAMACHY implies that it is tacitly assumed that the SCIAMACHY degradation correction is valid. For the GOME-FDR uncertainty, the uncertainty on SCIAMACHY degradation has to be taken into account. Also the SCIAMACHY uncertainties on radiance response and BSDF need to be accounted for.

3.4 Summary of Effect Tables

The following Table lists the most relevant entries of the GOME and SCIAMACHY Irradiance Effect Tables, for those measurement function items that are applicable and where uncertainties have been determined. The full tables are available at the FDR4ATMOS website.

Some entries in the Effect Tables refer to data files. These are dependent on input spectra and have been generated for internal use. For experienced users, one example, for 2003, is made available at the FDR4ATMOS website.

Table 3-2 Summary of GOME FDR Irradiance Effect Table. Abbreviations: S=spectral, T=temporal, INS=insignificant

Item	Uncertainty	Correlation scale	Remark
I2.1	INS	S: whole channel	Irradiance measurements remain well below saturation limit
I3.1	INS	S: random T: 1 orbit, then change	Noise averaged over many measurements
I3.3.1	INS	S: whole channel T: very high correlation with FPA cooler switches	In ch.2 depending on integration time
I3.3.2	N/A for Irradiance		Irradiance is not measured inside SAA
I4.1	Depends on signal, very roughly 0.5 BU at signal of 10000 BU for 2003)	S: random T: random	Use Eq.(3-4) with N_meas and S[BU] on datafile
I4.2	INS: $\sim 3 \text{ BU} / \sqrt{N_{\text{meas}}}$	S: random; T: random	N_meas ~ 35
I4.3	INS: $< 1 \text{ BU} / \sqrt{N_{\text{meas}}}$		
I5.1+I5.2	See data file; typically $3e-5$, $2e-5$, $2e-5$ for channels 2,3,4	S: random T: 100% correlated until next LED measurement	LED measurement: typically 1 per month beginning of mission; infrequent at end of mission
I7			Included in I9 Radiance Response
I8.1	Signal dependent, see data file, typically for 2003: 0.05 % for 313-315 nm 0.02 % for 315-340 nm 0.07 % for 412-500 nm 0.03 % for 750-790 nm	S: whole channel for ghost intensity errors; ~ 3 pixels for ghost centre errors and defocussing errors (depends on input spectrum) T: at least several months	Ghosts in-between channels are neglected because they have much lower intensity
I8.2	Signal dependent. It amounts to 0.025% of the mean intensity in each channel (corrected for dark signal; average over 1024 pixels)	S: whole channel	Straylight in-between channels is negligible, even for channel 2 with much higher input intensity from other channels

Item	Uncertainty	Correlation scale	Remark
I8.3	INS		Intensity of Earthshine over diffuser is extremely low compared to direct Sunlight
I9.1.3	ch2: 1.6e-4 ch3: 1.9e-4 ch4: 2.4e-4		Relative number
I9.3.1	$\frac{\partial R}{\partial \lambda} / R$, see data file		Uncertainty in wavelength calibration that aliases into the radiance response
I10.3	Tentatively the SCIAMACHY value of 0.1% is used, but the actual value is unknown.	S: typical ~10 pixels T: daily change with yearly repeat	
I11.1	Uncertainty on the SMR itself. May be assumed as covered by the other uncertainty sources.		
I13	See data file, estimated at 0.1%		Note that broadband SCIAMACHY irradiance uncertainties have to be added, to obtain the full irradiance uncertainties

Table 3-3 Summary of SCIAMACHY FDR Irradiance Effect Table. Abbreviations: S=spectral, T=temporal, INS=insignificant

Item	Uncertainty	Correlation scale	Remark
I1.1, I1.2, I1.3	~3 BU random and ~1 BU systematic	T: one measurement S: a few pixel	Irradiance: signal high and variation low.
I3.1	INS	T: one orbit S: random	Negligible for averaged high signal of irradiance
I3.2.1	~0.1 BU	T: fixed	
I3.2.2	~0.5 BU	T: 1 day	
I3.3.3	INS	S: odd-even pixel effect	
I3.4	INS		Negligible for UV-vis
I4.1	0.5 BU	random	ATBD (eq. 3.71). For irradiance, divided by SQRT(176)

Item	Uncertainty	Correlation scale	Remark
I4.2	0.1 BU	random	Defined in ATBD, (3.52)
I4.3	0.038 BU	random	0.5BU/sqrt(176)
I8.1	INS	S: few pixels	Full matrix approach: error included in I8.2. Ghosts only in NIR.
I8.2	10BU	T: correction matrix fixed S: few pixels	Uncertainty is estimated with 10% of straylight for all channels.
I8.3	INS		Earthshine over diffuser is extremely low
I9.1.1	0.8%	T: fixed S: all pixels	Total uncertainty (1 σ)
I9.1.2	1-1.5%	T: fixed S: all pixels	
I9.1.3	~0.1%	T: fixed S: 1 pixel	
I9.2.1	0.2 – 0.3%	T: fixed S: fixed	
I9.3.1	INS	S: 1 pixel	Uncert. wavelength calibration that aliases into the radiance response
I9.3.2	INS	T: One orbit S: per channel	OBM temperature stabilized
I10.1.1	0.8%	T: fixed S: all channels	Total uncertainty
I10.1.2	1-1.5%	T: fixed S: all channels	
I10.1.3	0.1%	T: fixed S: 1 pixel	
I10.3	0.1%	T: Yearly repetition S: 3-10 pixels	
I11.1	2-3%	T: fixed S: all channels	Uncertainty of single ESM measurement



Item	Uncertainty	Correlation scale	Remark
			(2003/02/26).
I11.2	INS	T: week S: 10 pixels	Degradation is smooth, both in time and spectral direction.
I11.3.2	INS	T: week S: all channels	Thickness is the main parameter of the degradation correction. In V10, the OBM residual m-factor covers most errors here.
I11.3.4	INS		Optical properties of contamination assumed constant.
I11.4	INS		Covered by mirror model assuming contamination layer on ESM Diffuser
I11.5	0.14%	T: fixed S: all channels	WLS measurements based correction; additionally the WLS measurement uncertainty to be taken into account

4 Uncertainties on the reflectance product

Uncertainties for the reflectance product (the ratio of radiance with irradiance) are here described as uncertainties on radiance; the uncertainties on irradiance have to be added to these in the final error propagation.

However, uncertainties common to radiance and irradiance are not considered here, because they will cancel in the reflectance. Additive errors do not cancel, multiplicative errors often cancel partly – this will be described on case-by-case basis.

4.1 General calibration equation

As explained in [R2], the general calibration equation for calibrated radiance $I(\lambda_i)$ may be written as:

$$I(\lambda_i) = \frac{S_i - SS_i - DS_i - MEC_i}{c_{pol}(\lambda_i, p_t(\lambda_i)) \cdot (RR_{0,i}/PPG_{0,i})(\lambda_i) \cdot PPG_{t,i} \cdot m_t(\lambda_i) \cdot E_t(\lambda_i)} \quad \text{Eq.(4-1)}$$

where subscript 0 denotes the quantity at a reference time $t = 0$ and subscript t denotes the quantity at the time of measurement, and

S_i	measured signal at detector pixel i
λ_i	wavelength of detector pixel i
$I(\lambda_i)$	incident radiation as function of wavelength
SS_i	straylight signal at detector pixel i (depending on all signals in the channel)
DS_i	dark signal of detector pixel i
$(RR_{0,i}/PPG_{0,i})(\lambda_i)$	smooth part of the radiance response function as function of wavelength, for unpolarised input
$c_{pol}(\lambda_i, p_t(\lambda_i))$	polarisation correction factor as function of wavelength and input polarisation
$PPG_{t,i}$	pixel-to-pixel part of response function at detector pixel i
$m_t(\lambda_i)$	degradation monitoring factor as function of wavelength
$E_t(\lambda_i)$	etalon change as function of wavelength

Note that the equation has multiplicative terms in the denominator, and additive terms (coloured red in general equation) in the numerator. The distinction between multiplicative terms and additive terms is significant for the calculation of uncertainties. The additive terms generally give rise to uncertainties on small wavelength scales. Multiplicative terms may occur on all wavelength scales.

Since for the Level 2 retrievals only the Sun-normalised radiance matters (i.e. Earth measurement divided by Sun calibration measurement), multiplicative terms that are common to radiance and irradiance will cancel in Sun-normalised radiance, but additive terms do not cancel.

The cancellation of terms in Sun-normalised radiance may be hampered by time-dependent effects, e.g. wavelength shifts during the course of one day (the interval between solar measurements).

4.2 Processing Chain Diagram

For the reflectance processing chain diagram, the same general remarks apply as for irradiance, see Section 3.2.

The numbering has been kept identical for the Irradiance product and the Reflectance product. Also here, not all effects are statistically significant for each product, as indicated in the Effects Tables.

An overview of the uncertainty processing steps and numbering is shown in Table 4-1. The table lists for completeness some effects that are expected to be insignificant, but also omits possible effects known from other instruments that are expected to be insignificant (there is some arbitrariness here).

Table 4-1 Overview of generic processing steps and numbering for the reflectance product. The last column indicates if the item is applicable to GOME (G) and/or SCIAMACHY (S), an X denotes that the item is not applicable to reflectance.

#	main elements	#	contributing elements	#	sub-items	
R1	DET Memory	R1.1	OG CKD			S
		R1.2	In-orbit CKD changes			S
		R1.3	determine previous readout	R1.3.1	without co-adding	S
				R1.3.2	with co-adding	S
R2	DET non-linearity	R2.1	due to saturation			GS
		R2.2	electronic	R2.2.1	OG CKD	GS
				R2.2.2	In-orbit changes	GS
R3	DET Dark Signal	R3.1	statistical uncertainty			GS
		R3.2	separation in LC + FPN	R3.2.1	FPN	S
				R3.2.2	LC	S
		R3.3	additional background	R3.3.1	Cross-talk	G
				R3.3.2	SAA background	X
				R3.3.3	Red Grass	S
		R3.3	detector temperature			
R4	DET statistical uncertainty	R4.1	shot noise			GS
		R4.2	readout noise			GS
		R4.3	digitisation noise			GS

#	main elements	#	contributing elements	#	sub-items	
R5	DET QE: PPG	R5.1	noise on LED/WLS measurements			GS
		R5.2	High-pass filtering			GS
R6	DET: electronic gain					1)
R7	Detector window etalon	R7.1	calculate: filtering			2) S
		R7.2	apply:	R7.2.1	ice layer growth	S
				R7.2.2	spectral calibration	S
R8	Stray light	R8.1	ghost CKD			GS
		R8.2	"uniform" CKD			GS
		R8.3	spatial stray light			GS
		R8.4	"In-orbit change (degradation of optical elements)			GS
		R8.5	Solar straylight			GS
R9	Radiance Response	R9.1	OG CKD Nadir	R9.1.1	calib.standards	GS
				R9.2.	distance measurements	GS
				R9.3.	noise on CKD	GS
		R9.2	OG CKD Scan angle	R9.2.1	Setup & measurement accuracy	GS
				R9.2.2	"polarisation shift"	G
				R9.2.2a	scanner model: OBM	S
				R9.2.2.b	scanner model: fit to original scanner CKD	S
				R9.2.3	Noise on scan angle CKD	GS
		R9.3	Apply	R9.3.1	spectral calibration	GS
				R9.3.2	OBM temperature	GS
				R9.3.3	Representative scan angle	GS
I10	Diffuser BSDF					GS
R11	Degradation correction					

#	main elements	#	contributing elements	#	sub-items	
		R11.1	Errors on reference meas.			GS
		R11.2	Smoothing errors			GS
		R11.3	Method limitations	R11.3.1	scan angle dependence	G
				R11.3.2	layer optical constants	S
				R11.3.3	neglect OBM pol.change	GS
				R11.3.4	other effects	GS
		R11.4	BSDF degradation			GS
		R11.5	OG to first in-orbit meas.			GS
R12	Polarisation correction	R12.1	OG CKD	R12.1.1	Broad-band	
				R12.1.2	noise on CKD	
		R12.2	CKD degradation			
		R12.3	PMD polarisation values			3)
		R12.4	theoretical point			3)
		R12.5	wavelength interpolation	R12.5.1	GDF	
				R12.5.2	poly using PMD points	
				R12.5.3	Absorption line structure	
R13	Harmonisation					
		R13.1	Scene variability			G
		R13.2	Smoothing errors			G
		R13.3	Time dependence			G

1) Included in R9. 2) for GOME included in R9 3) input from Polarisation section

The processing chain diagram for GOME and SCIAMACHY reflectance is shown in Figure 37 and Figure 38, respectively. The term “differential uncertainty” in the figures denote the uncertainty that remains for multiplicative terms that (almost) cancel in the ratio of radiance to irradiance.

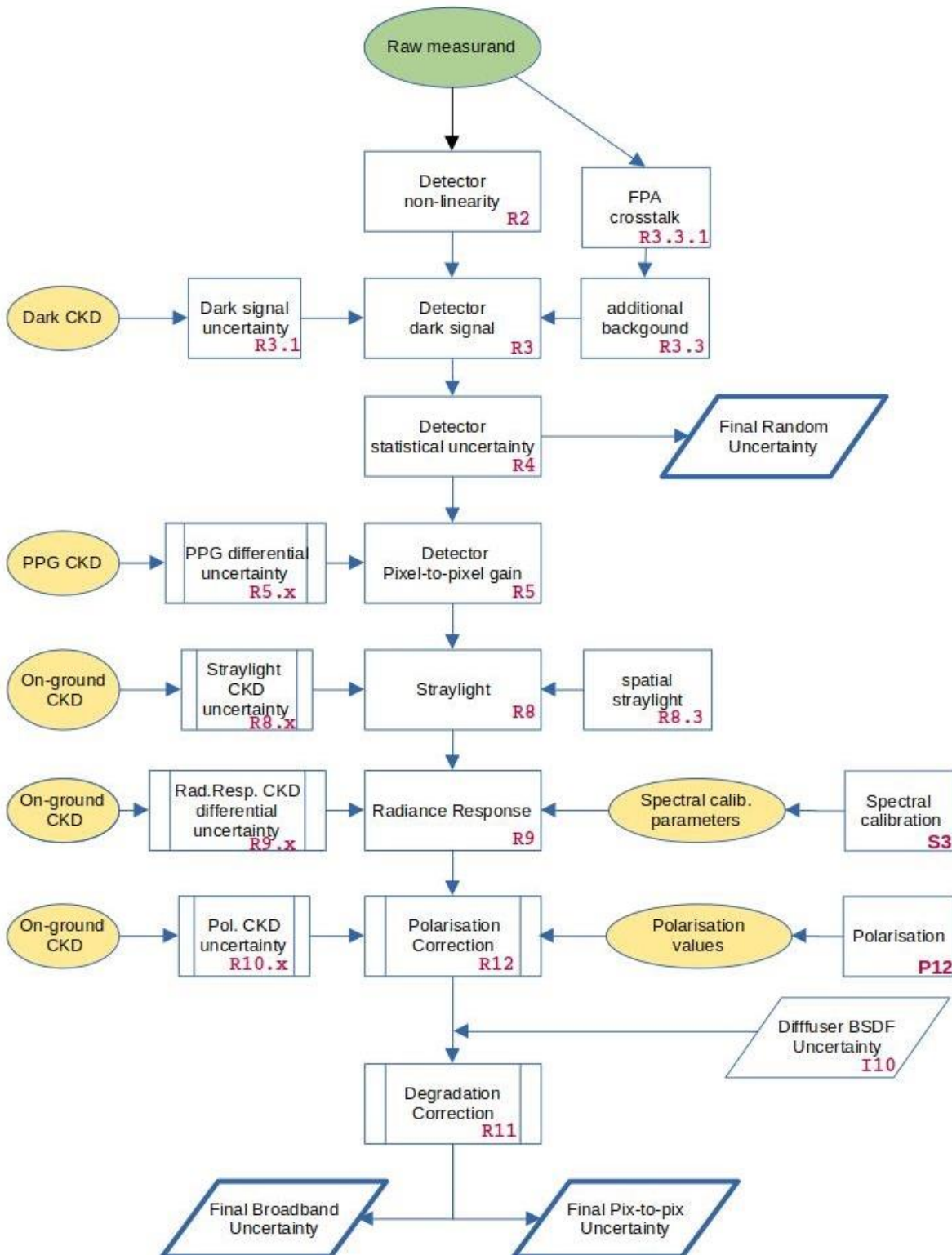


Figure 37 Processing chain diagram for GOME reflectance uncertainties. The FDR alignment to SCIAMACHY currently only covers Radiance Response plus Degradation Correction for 2003.

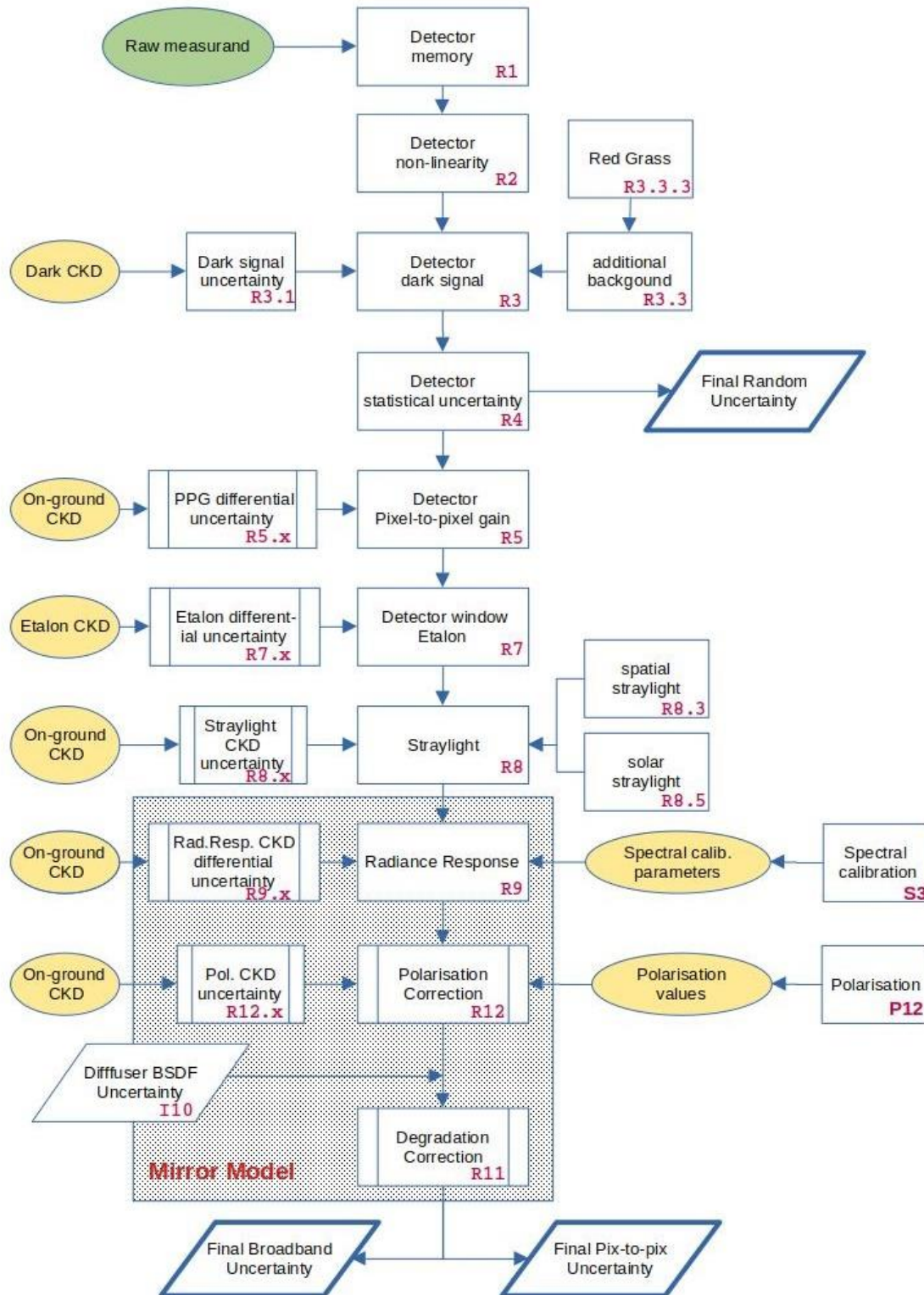


Figure 38 Processing chain diagram for SCIAMACHY reflectance uncertainties

4.3 Instrument Measurement function

- Order of equations in this section is according to the main element numbering (see Table 3-1) using as overarching function the general calibration function (see Section 3.1).
- Numbering in Processing chain diagram and Effects table added in red: [**Rx.y.z**]

4.3.1 R1 - Memory effect

This only applies to the main channels of SCIAMACHY.

Memory effect is described by the term MEC_i in the general calibration function (Eq.3-1).

This term may be expanded as follows; the index k stands for the current readout.

$$MEC_i(k) = f_i(S_{measured}(i, k - 1)) + 0$$

The function f is calibrated for each channel as a function (look-up table) of signal level (in this case the signal of the previous readout). Although it may be dependent on pixel number, it could only be calibrated on-ground assuming that all pixels in the channel have the same memory effect. The MEC_i has the following uncertainties:

- $\varepsilon_{MEC}(i)$. the calibration uncertainty on the function f [**R1.1**]
- ε_{fS} accounts for the fact that the previous signal may not be known: this happens in the case of co-adding when signals vary. [**R1.3.2**]

There might be a possibility that the function f "degrades" (is not constant over time) [**R1.2**]

Over co-added heterogeneous scenes, the measured signal for each readout (before co-adding) is estimated using the PMD readouts; the PMD corresponding to each channel is used. However, this will be associated with errors due to spectral mismatches between PMD and channel wavelengths, synchronisation errors between PMDs and channels/pixels [**P1**], and noise on PMD measurements [**P4**]. Note that the uncertainty ε_{fS} depends both on the function f and on the uncertainty on the previous signal. It is therefore difficult to provide a general uncertainty estimate for this quantity.

The +0 term accounts for uncertainties like:

- Uncertain if the same function f is strictly valid for all pixels in one channel
- a known but not quantified effect that a residual memory signal is not only added to the next readout, but also to further readouts (although "exponentially" decaying).

4.3.2 R2 - Non-linearity

(this subsection is schematic, no quantitative uncertainty is associated here, for references see Section 3.3.2)

- Non-linearity near detector saturation is flagged, not corrected. However, below the flagging threshold some effect might be present.
- GOME: only a figure in on-ground calibration documentation, no quantitative numbers.
- SCIAMACHY linearity: electronic non-linearity **R2.2** is established for channels 6-8 and thus not relevant for this FDR. However, during on-ground calibration it was difficult to attribute the observed signal anomaly during a non-linearity measurement to actual non-linearity (i.e. a

dependence on the measured signal level) or to a memory effect (i.e. a dependence on the signal level of the previous measurements). A certain amount of memory effect was clearly seen, and therefore the whole anomaly was declared a memory effect. However, it cannot be excluded that this is incorrect.

4.3.3 R3 - Dark signal

SCIAMACHY

The dark signal term in Eq.(3-1) can be expanded as:

$$DS(i) = f_{coadd} \cdot (FPN(i) + PET(i) \cdot LC(i, T)) \quad Eq.(4-2)$$

where

$f_{coadd}(i)$	coadding factor for the cluster containing detector pixel i
$FPN(i)$	FPN (=offset) for detector pixel i
$PET(i)$	pixel exposure time (single-readout integration time) at detector pixel i
$LC(i, T)$	leakage current of detector pixel i at detector temperature T

with the following additive uncertainties:

$\varepsilon_{FPN(i)}$	on FPN(i) due to calibration [R 3.2.1]
$\varepsilon_{LC(i, T)}$	on LC(i, T) due to calibration and temperature dependence [R 3.2.2]
ε_{SAA}	on LC(i, T) due to particle flux in SAA (value per channel) [R 3.3.2]
ε_{RG}	Red Grass [R 3.3.3]

The FPN and LC are obtained from the dark signal measured at several exposure times, where the offset and slope of the linear fit of dark signal versus exposure time are the FPN and LC, respectively. This can only be done if the detector temperature is kept constant, because LC depends on detector temperature. This should be the case (each detector is always operated at a pre-set temperature) but small temperature fluctuations due to lag in the feedback control loop are always possible.

GOME

During on-ground calibration of GOME it appeared that cross-talk was present which invalidates the expression from Eq.(3-2). The calibration approach has been to measure dark signals for each "integration time pattern" i.e. each combination of integration time of the 4 channels that is used for scanning measurements, solar observation, or in-orbit calibration measurements.

The cross-talk is not constant in time, but depends on switching in the FPA-temperature control loop. There is an additional calibration algorithm for this which is described in [R2]. The FPA cross-talk scales approximately with integration time and is only applied for integration times ≥ 12 seconds. This excludes its use in the FDR, but the uncertainty due to cross-talk still remains.

There is also an additional calibration algorithm to reduce the dark signal error in the SAA, based on the signal in a "straylight" band at the start of channel 1. However, that is only applied to channel 1 (which has the longest integration time and is more susceptible to the effect) and thus not used for the FDR.

In analogy to the irradiance case, the dark signal term in Eq.(4-1) can then be written as:

$$DS(i) = DS_{cal}(i, IT) + 0 \quad \text{Eq. (4-3)}$$

where

$DS_{cal}(i, IT)$ calibrated dark signal for the integration time pattern
 with the following additive uncertainties:

- $\epsilon_{DS(i,IT)}$ on the assigned dark signal [R 3.1]
- ϵ_{SAA} due to particle flux in SAA (value per channel) [R 3.3.2]
- $\epsilon_{crosstalk}$ uncertainty on cross-talk correction [R 3.3.1]

where the latter two scale with integration time

As for SCIAMACHY, a detector temperature effect is probably negligible. Since dark signal is not calibrated as function of temperature, we include any such effect in the +0 term.

4.3.4 R4 - Statistical Uncertainty (noise)

Noise is calculated as in the respective ATBDs, as the rms sum of readout noise, shot noise, and digitisation noise.

$$\sigma_{Stat} = \frac{1}{N_e} \sqrt{S_e + \sigma_R^2 + \epsilon_D^2} \quad \text{Eq. (4-4)}$$

where

- N_e number of electrons for 1 BU
- S_e signal of a pixel (without electronic offset / FPN) in electrons = $S[\text{BU}] \cdot N_e$
- σ_R noise on the detector readout in electrons
- ϵ_D uncertainty due to digitisation = $0.5 \cdot N_e$

The noise on an average of measurements, due to co-adding, is reduced by the square root of the number of measurements.

The subtraction of electronic offset from the signal, and the uncertainty in the determination of detector readout noise cause an uncertainty on σ_{Stat} itself. However, this may be neglected

Because of the large value of N_e , the signal-dependent noise ($\sqrt{S_e/N_e^2}$) only becomes dominant at fairly large signals, for GOME above a value of ~16,000 BU.

Note that instrument [optical] degradation may significantly degrade the signal-to-noise ratio, especially at the low wavelengths of channel 2, where degradation may be very large and signals low (thus dominated by detector readout noise).

4.3.5 R5 – Pixel-to-pixel gain

Pixel-to-pixel gain (PPG) effects on the reflectance are usually very small. If irradiance and radiance were to have the same spectral calibration, PPG would cancel out in the reflectance. If PPG were error-free, an uncertainty involving the PPG term would only arise via an uncertainty in spectral calibration. If PPG has an uncertainty itself (which is the case), the propagation of the PPG uncertainty into the reflectance comprises a division of Eq. (4-1) after a spectral calibration (including spectral calibration

uncertainty) by Eq.(3-1) after a spectral calibration (including spectral calibration uncertainty and Doppler shift of the solar measurement). And it includes uncertainties on both PPG(t) and PPG_0. There is no shortcut to cancel anything out of the equation. However, the radiance response provided in the calibration keydata is Radiance Response corrected by PPG_0. It is assumed here that PPG_0 uncertainties are already accounted for in the uncertainty on Radiance Response.

The multiplicative uncertainty

$$\varepsilon_{PPG}(i)$$

which is identical for irradiance and for radiance on a pixel basis (but does not cancel out in reflectance which is on a wavelength basis) will be provided in the Effect Tables.

4.3.6 R6 – Electronic gain

The electronic gain is not expected to vary significantly. In GOME and SCIAMACHY there is no way to characterise this independently. The term will be treated as part of the radiance response [R 9].

For the reflectance, gain will cancel out in the ratio of radiance to irradiance, unless it were to vary on timescales of less than a day.

4.3.7 R7 – Etalon

For the reflectance, etalon will cancel out in the ratio of radiance to irradiance, unless it were to vary on timescales of less than a day. There also may be a very small etalon residual if the wavelength calibration shifts, either through Doppler-effect on the irradiance or due to spectral calibration errors.

The relative error on the etalon term $E_t(\lambda_i)$ in the general calibration equation Eq.(4-1) is then

$$\varepsilon_{E_t(\lambda_i)} = \frac{\partial E_t(\lambda_i)}{\partial t} \cdot \Delta t + \frac{\partial E_t(\lambda_i)}{\partial \lambda_i} \cdot \varepsilon_{\lambda} + 0 \quad \text{Eq.(4-5)}$$

where

- $\frac{\partial E_t(\lambda_i)}{\partial t}$ the etalon growth rate [R 7.2.1]
- Δt the time between radiance measurement and irradiance measurement
- $\frac{\partial E_t(\lambda_i)}{\partial \lambda_i}$ the spectral gradient of the etalon (largest near the nodes) [R 7.2.2]
- ε_{λ} combined effect of uncertainties in Doppler shift and spectral calibration.

Note that a changing spectral calibration alone is not thought to have an effect, as etalon (as an interference effect) depends on wavelength and the pixel location should be irrelevant.

These residual Etalon effects are expected to be broad/band and insignificant for Level 2 DOAS retrieval.

4.3.8 R8 – Straylight

The straylight signal term in Eq.(4-1)Eq.(3-1) may be expanded as:

	$SS_i = \sum_i FST(i) \cdot FR(i) + \sum_j ST(i, j) \cdot S(j) + 0$	Eq.(4-6)
--	---	-----------

where

$FST(i)$ straylight operator for out-of-field straylight, for detector pixel i

$ST(i, j)$ straylight operator for spectrometer straylight from pixel j onto pixel i
 $FR(i)$ out-of-field radiance
 $S(j)$ signal of pixel j

with multiplicative uncertainties

$\varepsilon_{FST}(i)$ on the out-of-field straylight [R 8.3]
 $\varepsilon_{ST}(i, j)$ on the spectrometer straylight (split into components below)
 $\varepsilon_{straydegrad}(t)$ due to increase in straylight with time (due to optics contamination)
 [R 8.4]

The out-of-field straylight component FST is set to zero in Level 0-1b processing. For GOME and for SCIAMACHY Nadir this may be a fair approximation (in fact some out-of-field straylight was measured for GOME by scanning a light source across and beyond the slit; there might be noticeable straylight for a dark scene surrounded by clouds). For SCIAMACHY Limb it is known that there is a non-negligible contribution from out-of-field straylight, especially for the higher tangent height measurements where the signal from the limb itself is very low (see Section 3.5 of [R4]). A complication is that the out-of-field radiance is not directly measured: even if a correction in Level 1b would be possible, there would be a significant uncertainty on that correction.

Out-of-band straylight (originating from wavelengths outside the channels) is in principle possible, but since GOME/SCIAMACHY is a double monochromator design it is expected to be comparatively small. Depending on the origin of the straylight, it may increase due to contamination of the optics over time.

GOME:

For GOME, the straylight operator is split into a uniform component and a single ghost. The ghost straylight is not expected to be influenced by optics degradation, but the uniform component may be. Further errors on the uniform straylight may arise from uncertainties on the straylight intensity CKD and the fact that the straylight is not really uniform but has in reality a wavelength dependence. Errors on the calculated ghost straylight may arise from uncertainties on the ghost intensity CKD and the position of the ghost (the ghost is a fraction of the spectrum mirrored around a "central" pixel).

We then have:

	$ST(i, j) = ST_{stray-uniform} + defoc \left(ST_{stray-ghost} \cdot \delta_{ij}(j = 2 \cdot i_c - i) \right) + ST_{stray-degrad}(i, j, t)$	Eq.(4-7)
--	---	-----------

where

$ST_{stray-uniform}$ coefficient for uniform straylight
 $ST_{stray-ghost}$ coefficient for ghost straylight
 $\delta_{ij}(j = 2 \cdot i_c - i)$ delta function which is 1 when pixel $j = 2 \cdot i_c - i$ and else 0
 i_c a "central" pixel number for the mirror function (different for each channel, number between 0 and 1023, usually around 500)
 $defoc$ a function describing defocussing of the ghost

$ST_{stray-degrad}(i, j, t)$ coefficient for time-dependent additional straylight due to optics degradation (unknown but zero at time of on-ground calibration) with multiplicative uncertainties

- $\varepsilon_{stray-uniform}$ uncertainty on $ST_{stray-uniform}$ [R 8.1]
- $\varepsilon_{stray-ghost}$ combined uncertainty on $ST_{stray-ghost}$ and i_c [R 8.2]
- $\varepsilon_{stray-degrad}(t)$ uncertainty due to increase in straylight with time (e.g. due to optics contamination) [R 8.4]

Note that in effect these uncertainties may be evaluated as fraction of the calculated Level 1b straylight, rather than as fraction of the input signal at each pixel.

SCIAMACHY:

The straylight calculation for SCIAMACHY is similar to that of GOME, except that for the uniform straylight part of $ST(i, j)$ there is a matrix, and there are several focussed ghosts. An error assessment on CKD [R4] recommended to use a fixed fraction of the *calculated straylight* intensity as formal uncertainty, such that similar uncertainty expressions as for the GOME straylight may be taken for SCIAMACHY as well.

The ghosts may be polarised, so that uncertainties on the polarisation correction may play a role in the error propagation. However, for the UV-VIS channels of the FDR, ghosts may be considered unpolarised according to the CKD.

For SCIAMACHY Limb measurements (currently not in the FDR), there may also be straylight from the Sun around sunrise [R 8.5] (this may be regarded as a special case of out-of-field straylight).

4.3.9 R9 – Radiance response

The radiance response, $(RR_{0,i}/PPG_{0,i})(\lambda_i)$ in Eq.(4-1), and all the components from which it is calculated, is applied as a multiplicative factor on the signal. Its uncertainties shall be treated accordingly.

The radiance response calibration is part of both, the irradiance and the radiance calculation. Everything else being equal, it would cancel in the calculation of the reflectance. However, there generally will be differences in scan angle, and there may be secondary effects due to differences in spectral calibration and/or temperature.

We may discern between uncertainties on the [on-ground] measurement of CKD, and uncertainties associated to the application of the CKD in Level 0-to-1 processing. We start with the latter.

The uncertainty in reflectance due to uncertainty in spectral calibration is:

$$\varepsilon_{RRs} = \frac{\partial R}{\partial \lambda} \cdot \varepsilon_{\lambda} / R \tag{Eq.(4-8)}$$

where R is the radiance response CKD and ε_{λ} the spectral calibration uncertainty [R 9.3.1].

The radiance response may be dependent on temperature T of the optical bench; the corresponding relative uncertainty is

$$\varepsilon_{RRt} = \frac{\partial R}{\partial T} \cdot (T^{Rad} - T^{Irrad}) / R \tag{Eq.(4-9)}$$

where R is the radiance response and $(T^{Rad} - T^{Irrad})$ the difference in optical bench temperature between the radiance measurement and the previous irradiance measurement [R 9.3.2].

Scan angle related uncertainties arise due to the selection of a representative scan angle in Level 0-to-1 processing [R 9.3.3]. This is a consequence of detector readout synchronisation errors and scene inhomogeneity while the scan angle changes continuously during the exposure time.

The detector pixels are read out sequentially, which implies that each detector pixel “sees” a ground scene that is slightly advanced compared to that of the previous detector pixel. The instrument clock pulse triggers the readout of the first detector pixel (in each channel). Following this clock signal, Level 0-to-1 processing uses in the application of radiance response the scan angle for the middle of the integration time of the first detector pixel. All other pixels use a slightly “wrong” scan angle.

For a homogeneously illuminated ground pixel, this is a deterministic error.

However, often scenes are not completely homogeneous. In that case, the correct effective scan angle should be weighted with intensity (wavelength-dependent).

Level 0-to-1 processing applies a “channel jump” correction, using [the faster] PMD readouts that may correct the sequential readout error. The uncertainty due to inhomogeneous scenes may be reduced, but assumes a linear wavelength-independent intensity gradient with scan angle

The uncertainties due to the on-ground CKD are as follows. There is a difference in calibration concept between GOME and SCIAMACHY.

GOME:

The radiance response was calibrated at one specific scan angle α_c . (approximately nadir) The scan angle dependency $\chi(\alpha)$ was separately measured. For the system as designed, with all optics in one plane, one would expect that χ is a simple multiplicative factor that depends only on wavelength. However, GOME seems to suffer from a similar polarisation shift as SCIAMACHY which may be diagnosed from the jumps in χ at the channel boundaries.

The measurement function for radiance response is as for the Irradiance product, Eq.(3-7), see section 3.3.9:

$$R = R(\alpha_c) \cdot \chi(\alpha) + 0 \quad \text{with implicit wavelength and temperature dependence.}$$

with (in addition to ε_{RRs} and ε_{RRt}) the following multiplicative uncertainties on $R(\alpha_c)$:

δ_{Lref} is a (mostly systematic) uncertainty on the NIST reference lamp calibration

δ_{Rdist} is a systematic uncertainty on the distance between NIST lamp and instrument

σ_R is a noise term on $R(\alpha_c)$ [R 9.1.3]

and the following multiplicative uncertainties on $\chi(\alpha)$:

ε_χ is an uncertainty for measurement setup and calibration accuracy of $\chi(\alpha)$ [R 9.2.1]

δ_{Rps} is an uncertainty due to polarisation shift in the instrument [R 9.2.2]

σ_χ is a noise term on $\chi(\alpha)$ [R 9.2.3]

The “radiance response function” for reflectance (= radiance divided by irradiance) may be written as:

$R^{Refl} = \frac{R(\alpha_c, \lambda^{Rad}, T^{Rad}) \cdot \chi(\alpha^{Rad}, \lambda^{Rad}) + 0}{R(\alpha_c, \lambda^{Irrad}, T^{Irrad}) \cdot \chi(\alpha^{Irrad}, \lambda^{Irrad}) + 0}$	Eq.(4-10)
--	-----------

where for the uncertainties a few things have to be observed:

- the scan-angle independent part $R(\alpha_c)$ falls out of the equation, except for the uncertainty in the spectral calibration of radiance and irradiance (and temperature) as given by Eq.(4-8) and Eq.(4-9). This implies that δ_{Lref} and δ_{Rdist} vanish from the above list of reflectance uncertainties.
- The noise term σ_R [R 9.1.3] [I 9.1.3] does not cancel because of possible differences in spectral calibration.
- The uncertainty terms ε_χ and δ_{Rps} are already for 2 different scan angles (namely w.r.t. the angle α_c) and should not be taken twice in the ratio Radiance / Irradiance. Similar holds for the noise term σ_ξ .

Probably δ_{Rps} itself depends on scan angle (larger for “East” viewing angles) but since it is difficult to quantify this is currently neglected.

GOME after FDR alignment to SCIA

After FDR harmonisation to SCIAMACHY, spectrally broadband uncertainties in ε_χ and δ_{Rps} for GOME reflectance should vanish, while the noise terms will remain. Short wavelength range uncertainties in ε_χ and δ_{Rps} and might remain (but should not, as these functions are thought to be spectrally smooth). Remaining uncertainties in ε_χ and δ_{Rps} will be included in a “harmonisation uncertainty” term [R 13]. This is a lump sum for residual effects in radiance response, diffuser BSDF, and degradation correction.

SCIAMACHY:

The measurement function for reflectance in SCIAMACHY, is similar to that of GOME, except that the scan angle dependence in Eq.(4-10) is calculated via the “Scan mirror model”. See Section 3.3.9 “I9 – Radiance response” for a description.

Following Eq.(3-9), the “radiance response function” for unpolarised reflectance is:

$\frac{R^{Rad}}{R^{Irrad}} = \frac{M_1(\lambda, \alpha, \delta)^{Rad}}{M_1(\lambda, \alpha, \delta)^{Irrad}} = \frac{M_1^{OBM}(\lambda^{Rad}, T^{Rad}) \cdot \sum_{j=1}^4 \mu_j^{OBM}(\lambda^{Rad}, T^{Rad}) \cdot K_{j1}^{sc-Rad}(\lambda^{Rad}, \alpha^{Rad}, d) + 0}{M_1^{OBM}(\lambda^{Irrad}, T^{Rad}) \cdot \sum_{j=1}^4 \mu_j^{OBM}(\lambda^{Irrad}, T^{Rad}) \cdot K_{j1}^{sc-Irrad}(\lambda^{Irrad}, \alpha^{Irrad}, d) + 0}$	Eq.(4-11)
---	------------

Similar to GOME, we have the following multiplicative uncertainties:

- σ_R is a noise term on M_1^{OBM} [R 9.1.3] [I 9.1.3]
- ... σ_μ is a noise term on μ_j^{OBM} [R 9.2.3] [I 9.2.3]
- ε_χ is an uncertainty for the scan-angle dependent part of the mirror model (the summation term in the equation above)

The uncertainty ε_χ may be broken down into several components:

- measurement setup and calibration accuracy of the SCIAMACHY scan unit for Nadir [R 9.2.1] and for Irradiance configuration [I 9.2.1] It relates to the parameters ELEV_s and ELEV_p for Nadir mode, and BSDF_s and BSDF_p for Sun mode, from the original on-ground calibration plan of TNO. (may partially cancel in reflectance but currently unclear)
- an uncertainty due to polarisation shift in the instrument. This is the on-ground measurement uncertainty on the polarisation sensitivity parameters of the OBM $\mu_j^{OBM}(j=2,3,4)$. It relates to the

parameters OBM_s_p, eta, and zeta from the original on-ground calibration plan of TNO [R 9.2.2a] [I 9.2.2a] (may partially cancel in reflectance but currently unclear). Note that in this section we only consider the errors on the M_1 component, not those associated with the end-to-end polarisation sensitivity.

- an uncertainty in the fit of scan mirror model parameters to SCIAMACHY scan unit measurements [R 9.2.2b] [I 9.2.2b].

Further, there is the fundamental uncertainty in the validity of the OBM retarder assumption, and the uncertainty in the assumptions on optical properties of the scan mirror layer materials. For the BOL (Begin of Life) radiance response this plays a minor role (in addition to [R 9.2.2b]), since the model parameters are fitted to the on-ground calibration measurements and thus the quality of the fit is the only thing that matters as far as BOL model concept is concerned.

However, for correction of in-flight degradation the model concept is important (it is accounted for in section 4.3.11 “R11 – Degradation”).

The scan mirror model also contains a function for calculating diffuser speckles. For compatibility with the GOME measurement function this is described in Section 4.3.10 “I10 – Diffuser BSDF”.

4.3.10 I10 – Diffuser BSDF

The uncertainty of the BSDF may be taken from the Irradiance, see section 3.3.10 “I10 – Diffuser BSDF”. For GOME, all uncertainties associated to Diffuser BSDF [I 10] also apply to the reflectance. For SCIAMACHY, most BSDF effects are accounted for in the scan mirror model according to Eq.(4-11). In addition, the uncertainty on diffuser speckle correction [I 10.3] applies.

4.3.11 R11 – Degradation

For practical purposes (mainly for GOME), we may split the degradation in reflectance in three factors:

- Radiance / Irradiance response in the viewing direction towards the Sun
- Scan angle dependency
- Influence on the Polarisation correction

The latter is discussed in Section 4.3.12 “R12 – Polarisation correction”.

All uncertainties in this section are multiplicative.

GOME:

Degradation as calculated in L1b assumes that there is no difference for the Sun light path and the radiance light path, hence degradation cancels in the reflectance. However, even this assumption has some uncertainties:

- Wavelength calibration and Temperature difference between Sun and Radiance measurements have the same effect as discussed in Section 4.3.9R9 – Radiance response. However, the effect increases with time because (especially in ch.2) the spectral gradient in the radiance response becomes [much] steeper with increasing degradation. In the Effect Tables this may be accounted for using [R 9.3.1] [R 9.3.2] and specifying the effect as time-dependent

- Although BSDF degradation was not detected within the measurement uncertainties, it could have taken place and cause a small additional degradation in the Sun light path [R 11.3.4].

Not accounted for in L1b is that degradation, which probably mainly occurs on the scan mirror, will alter the polarisation dependence of the scan mirror as function of scan angle – due to the polarisation sensitivity of the optical bench, this results in an additional scan-angle dependent degradation component (even for unpolarised radiance) [R 11.3.1]. And also the optical bench itself might change its polarisation properties [R 11.3.3], giving rise to an additional scan angle dependence.

The degradation between on-ground calibration and in-orbit reference day [R 11.5] was in GOME primarily due to an in-air to vacuum effect, that has been corrected by adapting the on-ground CKD (albeit with substantial uncertainty). Assuming that the air-to-vacuum effect does not significantly change the BSDF, there is no effect on reflectance. The uncertainty on this assumption should be taken into account.

Other uncertainties common to degradation of both radiance and irradiance, such as [R 11.1] [R 11.2] may be considered to cancel in the reflection.

GOME after FDR alignment to SCIAMACHY

After FDR harmonisation to SCIAMACHY, the “harmonisation uncertainty” term [R 13] replaces all of the above (where effects from [R 11.3.1] and [R 11.3.3] will remain the major contributors, see FRD4ATMOS ATBD [R7]).

In addition, the uncertainties on Degradation from SCIAMACHY have to be added.

SCIAMACHY:

The scan mirror model employed in L1b/c processing is expected to account for most of the scan-angle dependent degradation (it was designed to do exactly that) such that most uncertainties are already counted via Eq.(4-11). As mentioned in Section 4.3.9 “R9 – Radiance response”, there are uncertainties related to the mirror model concept itself, and to the derivation of the contamination layer thickness. That the scan mirror model is not perfect follows from the fact that, using different light paths, different OBM degradation is calculated. But only the light paths in front of the OBM differ; and OBM degradation should be independent of light path. A possible explanation is that as the OBM degrades, also its polarisation properties change which is not accounted for in the model.

The uncertainties may be broken down into the following components:

- $\Delta\delta$ uncertainty on the thickness of the contamination layer [R 11.3.2]
- $\varepsilon_{OBM-pol-const}$ uncertainty due to assumption that the μ_j^{OBM} from Eq.(3-8) remain constant in time [R 11.3.3]
- $\varepsilon_{model-layering}$ uncertainty of the scan mirror layering model (which optical constants may change) [R 11.3.4]

In the reflectance, there is the same issue as for GOME with wavelength calibration and Temperature difference between Sun and Radiance measurements.

Other uncertainties common to degradation of both radiance and irradiance, such as [R 11.1] [R 11.2] [R 11.2] may be considered to cancel in the reflection.

4.3.12 R12 – Polarisation correction

The polarisation correction in Eq.(4-1) is in terms of the Mueller matrix formalism given by the correction factor

$c_{pol}(\lambda_i, p_t(\lambda_i)) = 1 + \mu_2(\lambda_i, \alpha) \cdot q(\lambda_i) + \mu_3(\lambda_i, \alpha) \cdot u(\lambda_i)$	<i>Eq.(4-12)</i>
--	-------------------

where

- λ_i wavelength of detector pixel i
- α scan angle
- $p_t(\lambda_i)$ polarisation state of the incoming light in the instrument
- $q(\lambda_i)$ fractional polarisation Q/I perpendicular to the optical plane
- $u(\lambda_i)$ fractional polarisation U/I at 45° to the optical plane
- μ_2, μ_3 fractional Mueller matrix elements M_2/M_1 and M_3/M_1 , respectively

The fractional polarisation parameters are calculated from PMD measurements (3 wavelength points for the FDR wavelengths), plus a theoretical point near 300nm. The corresponding uncertainties are described in Section 5 [P 1]-[P 12].

Then an interpolation in wavelength is made, using a special parametrisation (named “GDF”) between the theoretical point and a “GDF end point”, as well as an interpolation between GDF end point and the first PMD point [R2][R3].

Uncertainties in the polarisation correction due to this interpolation originate broadly from the following:

- GDF parameters: the GDF is determined by 2 params, shortest wavelength λ_0 and wavelength of steepest gradient λ_m .
 These are calculated from LUT with as parameters viewing/solar geometry, surface (cloud) reflectivity at 380 nm, Ozone vertical column (taken from earlier L2 product)
 [R 12.5.1]
- In channel 2 wavelengths from around 290-320 nm (from λ_0 to GDF end) the uncertainty due to wavelength interpolation is dominated by the GDF [R 12.5.1]
- In channel 2 the GDF attachment to PMD-A is uncertain (but mainly over clouds where polarisation is small) [R 12.5.2]
- In channel 3 the uncertainty on wavelength interpolation is dominated by the assumption of a polynomial through the PMD points [R 12.5.2]
- For GOME channel 4, some sort of extrapolation must be made for wavelengths beyond the 3rd PMD point (SCIAMACHY still has information from channel 5) [R 12.5.2]
- For clear sky, strong terrestrial absorption lines (O3, O2-A band) may be stronger polarised than the near-by continuum [R 12.5.3]

The uncertainties may be split into two components: pixel-to-pixel and broadband uncertainties. Since the wavelength interpolation using a smooth function does not generate pixel-to-pixel uncertainties, these come only from noise on Keydata [R 12.1.2]:

$\sigma_{c_{pol}}(\lambda_i, p_t(\lambda_i)) = \sigma_{\mu_2}(\lambda_i, \alpha) \cdot q(\lambda_i) + \sigma_{\mu_3}(\lambda_i, \alpha) \cdot u(\lambda_i)$	<i>Eq.(4-13)</i>
---	-------------------

The broad-band uncertainties on the interpolated polarisation values are assumed to be dominant over uncertainties on the CKD, such that the broadband uncertainty on the polarisation correction may be written as [R 12.1.1]:

$\varepsilon_{c_{pol}}(\lambda_i, p_t(\lambda_i)) = \mu_2(\lambda_i, \alpha) \cdot \varepsilon_q(\lambda_i) + \mu_3(\lambda_i, \alpha) \cdot \varepsilon_u(\lambda_i)$	<i>Eq.(4-14)</i>
--	-------------------

This equation neglects possible errors due to instrument degradation – these are accounted for in Section 4.3.11.

GOME:

GOME uses a formalism that rewrites the Mueller matrix formalism to one that uses the fraction of polarisation parallel to the slit, $p(\lambda_i)$ instead of $q(\lambda_i)$. There is a simple transformation between the two, $p(\lambda_i) = 0.5 \cdot (1 + q(\lambda_i))$

Level 1 processing assumes that [the sensitivity to] the 45° component $\mu_3(\lambda_i, \alpha) = 0$. The uncertainty on the polarisation correction factor can be expressed in terms of “Greek keydata” as:

$\varepsilon_{c_{pol}}(\lambda_i, p_t(\lambda_i)) = \frac{1 - \eta(\lambda_i, \alpha)}{1 + \eta(\lambda_i, \alpha)} \cdot 2 \cdot \varepsilon_p(\lambda_i) + 0$	<i>Eq.(4-15)</i>
---	-------------------

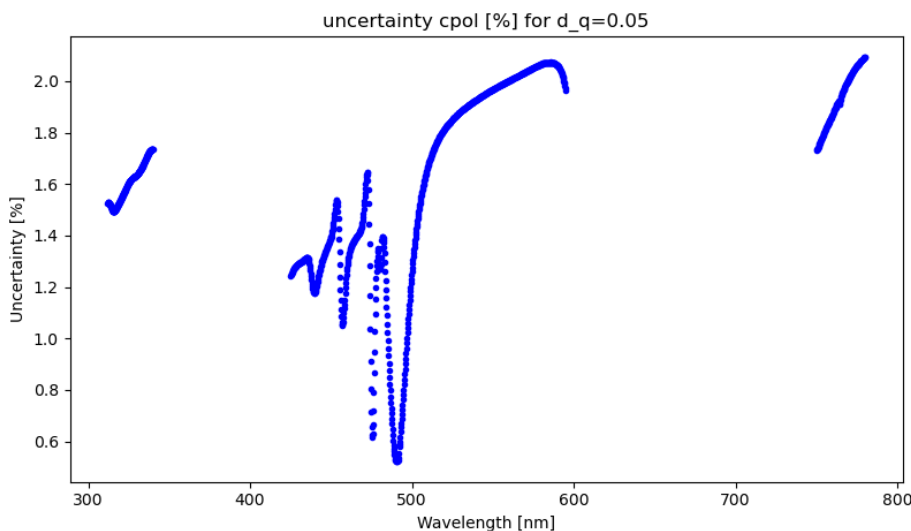


Figure 39 Uncertainty $\varepsilon_{c_{pol}}$ of GOME in % for an uncertainty in $q(\lambda_i)$ of 0.05.

where the +0 term incorporates the uncertainty due to neglecting the 45° component. Several Level 2 validation studies after L1b processing upgrades of GOME have shown that the influence of the polarisation correction on the Level 2 DOAS products is very small, even if the uncertainties on the absolute radiance level may be significant. The probable cause is that DOAS fits a polynomial that compensates for broadband radiance errors as they arise from the (GDF) wavelength interpolation. For smaller spectral scales, Level-2 DOAS also fits η as auxiliary cross-section. In channel 3 that η fit has

significant issues, not because of uncertainties in $p(\lambda_i)$, but because degradation (outgassing) of the dichroic results in unknown changes in η .

4.3.13 R13 – Harmonisation

FDR Harmonisation of GOME radiance to SCIAMACHY radiance is done by multiplying with a “harmonisation factor” that is taken as the smoothed ratio of SCIAMACHY radiance to GOME radiance:

$I(\lambda_i, t)_{FDR}^{GOME} = I(\lambda_i, t)^{GOME} \cdot SMOOTH \left(\frac{I(\lambda_i, t_{ref})^{SCIA}}{I(\lambda_i, t_{ref})^{GOME}} \right)$	Eq.(4-16)
---	------------

with

- λ_i wavelength of detector pixel i
- t measurement time
- t_{ref} reference time for collocated measurements (approximate match)
- $I(\lambda_i, t)$ radiance measured at t as function of wavelength
- $SMOOTH$ function for smoothing over wavelength (in this case polynomial fit)

Initially the smoothing employed a Gaussian kernel, but since the harmonisation factors showed a very smooth behaviour, that method was replaced by a polynomial fit. The latter implies that DOAS retrievals should be invariant to the harmonisation process.

The harmonisation factor is derived from analysis of the reflectance of dedicated calibration sites, that are quasi-simultaneously measured by SCIAMACHY.

The use of a reference time for GOME implies that it is tacitly assumed that the GOME degradation correction is valid. For this FDR version, measurements throughout 2003 were used as reference. However, this may lead to substantial systematic errors, especially at the shorter UV wavelengths, and especially for the years 2006-2011 [R 13.3]. The GOME Radiance/Reflectance Effect Tables list [R 13.3] as uncertainty with a random correlation, although we know that a major part of the uncertainty is a systematic error that may be correctable with further analysis. For such a correction, Eq.(4-16) needs to use the actual measurement time instead of a reference time. However, the spectral shape of such a correction is not known at present, but we do know it varies strongly (at least in channel 2). Due to that unknown variability, we assign the uncertainty as random effect.

Uncertainties are present due to scene variability [R 13.1] and spectral features not captured by the smoothing function [R 13.2]. Partly, the latter is intentional, since GOME and SCIAMACHY have different spectral resolution and the slit functions of both instruments are not known well enough to adjust radiances on a spectral scale less than a few nm. The uncertainty in scene variability appears to be significant.

The use of one reference time for SCIAMACHY implies that it is tacitly assumed that the SCIAMACHY degradation correction is valid. For the GOME-FDR uncertainty, the uncertainty on SCIAMACHY degradation has to be taken into account. Also the SCIAMACHY uncertainties on radiance response and BSDF need to be accounted for.

4.4 Summary of Effect Tables

The following Table lists the most relevant entries of the GOME and SCIAMACHY Radiance Effect Tables,

for those measurement function items that are applicable and where uncertainties have been determined. The full tables are available at the FDR4ATMOS website. Uncertainties that have 100% correlation between radiance and irradiance are not taken into account, since the FDR product contains reflectances.

Some entries in the Effect Tables refer to data files. These are dependent on input spectra and have been generated for internal use. For experienced users, one example, for Mauretania 2003 Radiance, is made available at the FDR4ATMOS website.

Table 4-2 Summary of GOME FDR Radiance Effect Table, without components common to radiance and irradiance. Abbreviations: S=spectral, T=temporal, INS=insignificant.

Item	Uncertainty	Correlation scale	Remark
R2.1	Depends on pixel signal but was not sufficiently calibrated	S: Channel 3: whole channel Channel 2,4: dependent on spectral shape of scene, scale typically >100 pixels T: scene-dependent	Flagged in Level 1b for high signals (those expected to be affected)
R3.1	INS	S: random T: 1 orbit, then change	Noise averaged over many measurements
R3.3.1	INS but dark measurements suggest occasional spikes up to 10 BU	S: whole channel T: very high correlation with FPA cooler switches, typically irregular triangular pattern with ~24s repeat time	Scales with integration time, deemed insignificant for IT=1.5s.
R3.3.2	Depends on location inside SAA. Not included in the example calculation of uncertainty (uncertainty data files)	S: one channel but with random spikes on individual pixels	Note that calibration measurements (dark, spectral, Sun) are not affected as SAA data are discarded (when present at all)
R3.4	INS		Generally, dark current (LC) doubles with every ~7 degrees of temperature increase. Assuming a temperature stabilisation ± 0.1 °C yields a deviation of LC of 1% which may be neglected
R4.1	Depends on signal, see data files for examples	S: random T: random	
R4.2	~4 BU	S: random; T: random	The noise in one scanning

Item	Uncertainty	Correlation scale	Remark
			measurement is included in R4.1 if signal taken after FPN subtraction
R4.3	$1./\text{SQRT}(3)=0.58$ BU		
R5.1+R5.2	INS (PPG largely cancels for reflectance)	S: random T: 100% correlated until next LED measurement	LED measurement: typically 1 per month beginning of mission; infrequent at end of mission
R7			Included in R9 Radiance Response
R8.1	Signal dependent, see data file, typically for 2003 (straylight / input[BU]): 0.04 % for 313-315 nm 0.02 % for 315-340 nm 0.07 % for 412-500 nm 0.02 % for 750-790 nm outside O2A band	S: whole channel for ghost intensity errors; ~3 pixels for ghost centre errors and defocussing errors (depends on input spectrum) T: at least several months	Ghosts in-between channels are neglected because they have much lower intensity In O2-A band straylight relative to signal much higher.
R8.2	Signal dependent. It amounts to 0.025% of the mean intensity in each channel (corrected for dark signal; average over 1024 pixels)	S: whole channel	Straylight in-between channels is negligible, even for channel 2 with much higher input intensity from other channels
R9.1.3	provided on data file (per pixel), typically $2e-4$	S: random T: On which pixel CKD noise is mapped depends on spectral calibration.	This will approximately be a fixed pattern that shifts with spectral calibration
R9.2.3	On data file, $\sim 2.5e-5$ (relative uncertainty)		
R9.3.1	$\frac{\partial R}{\partial \lambda}/R$, see data file		Uncertainty in wavelength calibration that aliases into the radiance response
I10	See Effect Table for Irradiance		
R11	Accounted for in harmonisation factor		
R13	Note that broadband SCIAMACHY radiance uncertainties have to be added, to obtain the full radiance uncertainties		

Item	Uncertainty	Correlation scale	Remark																
R13.1	Typically ~4 %		Uncertainty derived from PIC sites (Ocean showed significantly higher variability, probably due to larger effect of foam and/or of residual clouds).																
R13.2	INS		Insignificant compared to R13.1 and R13.3																
R13.3	For 2003 per viewing angle (East, Nadir, West): <table border="1" data-bbox="368 824 683 1025"> <thead> <tr> <th></th> <th>E</th> <th>N</th> <th>W</th> </tr> </thead> <tbody> <tr> <td>Ch.2</td> <td>5%</td> <td>4%</td> <td>2%</td> </tr> <tr> <td>Ch.3</td> <td>5%</td> <td>2%</td> <td>1%</td> </tr> <tr> <td>Ch.4</td> <td>5%</td> <td>2%</td> <td>1%</td> </tr> </tbody> </table>		E	N	W	Ch.2	5%	4%	2%	Ch.3	5%	2%	1%	Ch.4	5%	2%	1%	S: unknown, probably a few nm T: probably months. In the effect tables the correlation function is given as random, although we have systematic errors. This has been done because the spectral shape of the reflectivity error is unknown, but known to be variable in time, see e.g. Fig.8 of [R13]	The uncertainty depends on time and viewing (scan) angle. In Channel 2 the scan angle dependence of the harmonisation factor is significant. In Channels 3,4 it is within the scene variability uncertainty. Wavelength dependence has not been studied in detail and uncertainties are provided as one value per channel. For beginning of channel 2 this may be a significant underestimation
	E	N	W																
Ch.2	5%	4%	2%																
Ch.3	5%	2%	1%																
Ch.4	5%	2%	1%																

Table 4-3 Summary of SCIAMACHY Radiance Effect Table. Abbreviations: S=spectral, T=temporal, INS=insignificant

Item	Uncertainty	Correlation scale	Remark
R1.1, R1.2, R1.3	~3BU	T: one measurement S: a few pixel	Additive term, variable with signal. Mostly uncorrelated.
R3.1	INS	T: one orbit S: random	
R3.2.1	INS	T: fixed per orbit phase	
R3.2.2	0.3BU	T: orbit phase segment	
R3.3.2	INS		No quantitative analysis, only SAA region (flagged in L1B product)
R3.3.3	INS	S: odd-even pixel effect	Very small

Item	Uncertainty	Correlation scale	Remark
R3.4	INS	T: random S: channel	Negligible for UV-VIS
R4.1	~1-6 BU	random	ATBD (eq. 3.71)
R4.2	~0.1 BU	random	Defined in ATBD, (3.52)
R4.3	0.5 BU	random	
R8.1	INS	T: fixed S: few pixels	Full matrix approach: error included in 18.2. Ghosts only in NIR.
R8.2	1-10 BU	T: fixed S: few pixels	Uncertainty is estimated with 10% of straylight for all channels. signal dependent!
R8.3	INS		Spatial (out of field) straylight is expected to be small.
R 9.1.3	~0.1%	T: one day S: 1 pixel	
R 9.2.1	0.2 - 0.3%	T: fixed S: fixed	
R9.3.1	0.07%	T: daily S: 1 pixel	Uncert. wavelength calibration that aliases into the radiance response
R9.3.2	INS	T: orbit phase segment S: per channel	OBM temperature stabilized
R 11.1	2-3%	T: fixed S: all channels	Uncertainty of nadir light path solar measurement (sub-solar, 2003/02/26).
R11.2	INS	T: week S: 10 pixels	Degradation is smooth, both in time and spectral direction.
R11.3.2	INS	T: week S: all channels	Thickness is the main parameter of the degradation correction. In V10, the OBM residual m-factor covers most errors here.
R11.3.3	INS		OBM polarization changes are unknown,



Item	Uncertainty	Correlation scale	Remark
			most likely small.
R11.3.4	INS		Optical properties of contamination assumed constant.

5 Uncertainties on the polarisation

5.1 Introduction

The PMDs are somewhat different from the detector channels, as they provide only broad-band intensities (very approximately 100-200 nm wide wavelength bands), measure only one linear polarisation direction, and the detectors are not accurately integrating over a well-defined integration time but they “continually” sample the signal of a light-sensitive diode. Nevertheless, their calibration may be described by a similar structure as used for the main channel (ir)radiances.

For the PMDs, there is no calibrated (ir)radiance response. Instead, there are “Greek Keydata” that describe ratios of PMD polarisation directions or PMD-to-channel intensities. These are used to derive the polarisation of the incoming light. For GOME, only the fraction of intensity polarised perpendicular to the slit is calculated, while for SCIAMACHY also the 45° component is derived.

As a consequence, we do not have a “general calibration function” similar to Eq.(3-1), Eq.(4-1). Instead, the polarisation parameters are calculated using a “virtual sum” equation that will be detailed in Section 5.3.12.

The virtual sum equation observes that the intensity $I(\lambda_i)$ from Eq.(4-1), integrated over the PMD spectral range, should be equal to the intensity derived from the PMD signals integrated over the channel integration time. The intensity from the PMDs is there expressed by a similar equation as for the main channels. However, this intensity is not explicitly calculated, but the atmospheric polarisation parameters are solved from the ratio of PMD signals (corrected for additive terms) to channel signals (corrected for additive terms). The instrument throughput and polarisation properties needed to solve the virtual sum are given by the “Greek Keydata”, which for SCIAMACHY have been converted to Mueller Matrix Elements (MMEs).

5.2 Processing Chain

An overview of the uncertainty processing steps and numbering is shown in Table 5-1. The numbering has been kept close to that of the Irradiance and the Reflectance products. Also here, not all effects are statistically significant, as will be indicated in the Effects Tables.

Table 5-1 Overview of generic processing steps and numbering for the polarisation measurements. The last column indicates if the item is applicable to GOME (G) and/or SCIAMACHY (S), an X denotes that the item is not applicable to the PMDs.

#	main elements	#	contributing elements	#	sub-items	
P1	PMD “integration” and synchronisation	P1.1	due to filter constants			GS
		P1.2	PMD clock synchronisation			S
		P1.3	PMD and det.pixel synchronisation			GS

#	main elements	#	contributing elements	#	sub-items	
P2	PMD non-linearity	P2.1	due to saturation			GS
		P2.2	electronic	R2.2.1	OG CKD	GS
					R2.2.2	In-orbit changes
P3	PMD Dark Signal	P3.1	statistical uncertainty			GS
		P3.2	electronic offset stability			GS
		P3.3	additional background	R3.3.1	Cross-talk	S
				R3.3.2	SAA background	GS
		P3.4	PMD temperature			
P4	PMD statistical uncertainty	P4.1	shot noise			GS
		P4.2	readout noise			GS
		P4.3	digitisation noise			GS
P6	PMD: electronic gain	6.1				1)
		6.2	amplifier stage "a"			S
P7	PMD etalon					X
P8	PMD Stray light	P8.1	Spectral straylight			GS
		P8.2	out-of-band light			3)
		P8.3	spatial stray light			GS
		P8.4	In-orbit change (degradation of optical elements)			GS
		P8.5	Solar straylight			S
P9	"Greek Keydata"	P9.1	OG CKD Nadir	P9.1.1	Setup & measurement accuracy	GS
				P9.1.2	"polarisation shift"	G
				P9.1.3	noise on CKD	X
		P9.2	OG CKD Scan angle	P9.2.1	Setup & measurement accuracy	GS
				P9.2.2	"polarisation shift"	G
		P9.3	Apply	P9.3.1	spectral calibration	X
				P9.3.2	OBM temperature	GS

#	main elements	#	contributing elements	#	sub-items	
				P9.3.3	"channel jump" correct.	X
				P9.3.4	Representative scan angle	GS
P10	Diffuser BSDF for PMD	P10.1	OG CKD default direction			G
		P10.2	Elev / Azi dependence			G
P11	PMD Degradation correction					
		P11.1	Errors on reference meas.			GS
		P11.2	Smoothing errors			X
		P11.3	Method limitations	P11.3.1	scan angle dependence	G
				P11.3.2	layer optical constants	S
				P11.3.3	neglect OBM pol.change	GS
				P11.3.4	other effects	GS 3)
		P11.4	BSDF degradation			G
		P11.5	OG to first in-orbit meas.			GS
P12	Polarisation values	P12.1	OG CKD			4)
		P12.2	CKD degradation			5)
		P12.3	PMD Virtual Sum	P12.3.1	Polarised spectrum shape	GS
				P12.3.2	In-band correction factor	GS
				P12.3.3	cluster readout scaling	S
				P12.3.4	PMD effective wavelength	G
		P12.4	theoretical point			GS

1) Implicit in P9. 2) Implicit in P12.3.2. 3) for GOME: Q-factor included in P12.3.2

4) moved to P9. 5) moved to P11

The end results of the uncertainty Processing Chain are the uncertainties on PMD polarisation values. These follow from solving the virtual sum equation [P12.3]. The error propagation is thus not linear from [P1] to [P12], but must take into account the uncertainties on all terms as they are present in the virtual sum.

For both instruments, an independent polarisation value for the "theoretical point" is calculated [P12.4].

5.3 Instrument Measurement function

5.3.1 P1 – PMD integration and synchronisation

The PMDs are photodiodes whose voltage is “continually” sampled with a certain readout frequency (16 Hz for GOME and 40Hz for SCIA). To avoid that only an instantaneous signal is measured, the PMD signals are “integrated” by sending the signal through an electronic filter that preserves a certain amount of signal with time.

The calibration equations for deriving the polarisation parameters assume that the PMDs integrate exactly as the main channels (i.e. that the filter function is rectangular with a width equal to the channel integration time). But this is not the actual case. We may write:

	$S_{PMD}(t_{readout}) = \int_{t_{start}}^{t_{readout}} S_{PMD_inst}(t) \cdot F(t) \cdot dt$	Eq.(5-1)
--	--	-----------

where

$S_{PMD}(t_{readout})$ PMD signal as measured at time $t_{readout}$

$S_{PMD_inst}(t)$ “instantaneous” PMD signal before filtering

$F(t)$ filter function (throughput versus time)

with additive uncertainties:

$\varepsilon_F(t)$ difference between $F(t)$ and the assumed rectangular filter
[P1.1]

$\varepsilon_{S_{PMD}}$ difference between measured PMD signal and the one assumed from a rectangular filter

In the following we will use S_{PMD} as shorthand for $S_{PMD}(t_{readout})$ i.e. we always refer to the measured PMD signal

Note that, in the on-ground calibration of the [Greek] Keydata, input intensities are used that are constant in time. In that case the filter shape is irrelevant. Filter shape errors only become relevant over scenes that are inhomogeneous in the scanning direction (in particular partially clouded scenes, or scenes with large contrast in surface albedo e.g. sea / sand transitions).

As errors due to PMD integration and synchronisation only are related to inhomogeneous scenes, it will be difficult to assign a general uncertainty figure to the product. At statistical value for the “average scene” may be given, but it is questionable if that is a relevant number. On the other hand, that is what is often included in validation studies on the polarisation parameters.

GOME:

No documentation on PMD filter constants is known to the author.

SCIAMACHY:

The “integrating” filter is a third order Butterworth filter (internal communication Fokker Space 22.09.1997). The signal response of this filter with time has a fairly steep ascent with overshoot and

dampened-out oscillations (i.e. positive as well as negative values around the final value). Over scenes with e.g. alternating cloud cover this might in some cases lead to integrated signals that significantly deviate from the mean signal.

Apart from the uncertainties associated to filter response, inhomogeneous scenes may lead to L1b polarisation retrieval errors due to synchronisation issues between PMDs and main channels:

- Separate clocks for PMDs and main channels carry an uncertainty in clock synchronisation [P1.2]
- Sequential detector readout leads to synchronisation errors depending on the detector pixel number [P1.3] (larger relative errors for shorter integration times)

For the latter, there is only one detector pixel per channel where a “perfect” synchronisation may be achieved, this is specified in Level 0-1b processing configuration file.

5.3.2 P2 – PMD Non-linearity

GOME: missing info

SCIAMACHY: non-linearity is expected to occur for high signals. To cope with this, the PMD detector signals are amplified via two different electronic circuits “a” and “b”. Level 1b processing uses as default “b” but for high signals “a” is taken. In addition, there is cross-talk for “b”
 Uncertainty on the conversion factor and on the cross-talk.

5.3.3 P3 – PMD Dark signal

This is similar to the dark signal term for radiance. However, there is no dependence on integration time, as PMDs are always sampled at the same rate. Temperature dependence has not been calibrated and is accounted for by the +0 term in the measurement function. For each PMD(j) we may write:

$$DS^P(j) = DS_{cal}^P(j) + 0 \quad \text{Eq.(5-2)}$$

where

$DS_{cal}^P(j)$ calibrated dark signal for PMD j

with the following additive uncertainties:

$\varepsilon_{DS}^P(j)$ on the assigned dark signal [R 3.1]

ε_{SAA}^P due to particle flux in SAA (value per channel) [R 3.3.2]

SCIAMACHY:

For SCIAMACHY the PMD detector readouts are processed by 2 independent electronic circuits “a” and “b” with different gain and dark signal. The dark signals (“PMD zero offsets”) are calibrated for each of these 2 amplifier stages. Cross-talk is present for PMD amplifier stage “a”, but since the interfering signals are “constant” dark signals, this is implicitly accounted for in $DS_{cal}^P(j)$.

5.3.4 P4 – PMD Statistical Uncertainty

This is similar to the statistical uncertainty of the main channels (sections 3.3.4 and 4.3.4)

5.3.5 P5

Not applicable (skip number)

5.3.6 P6 – PMD Electronic gain

For the GOME and SCIAMACHY PMDs, there is no way to characterise electronic gain independently. The term is implicit in the “Greek Keydata” and may be implicit in the degradation correction. This assumes that no short-term variations (< 1 day) occur.

SCIAMACHY:

For SCIAMACHY, the PMD detector readouts are processed by two independent electronic circuits “a” and “b” with different gain factors. The CKD are derived for “b” (higher sensitivity). For high PMD signals, L1b uses “a” with a conversion factor.

5.3.7 P7 – PMD Etalon

Not applicable as the GOME/SCIAMACHY PMD detectors cannot spectrally resolve (for GOME-2 that would be different).

5.3.8 P8 – PMD Straylight

Straylight components that originate before the split-off of the PMDs and main channels are similar as for radiance. This applies in any case to out-of-field (spatial) straylight [R 8.3] [P 8.3] and to solar straylight [R 8.5] [P 8.5].

Spectral straylight from within the spectrometer [P 8.1] might also be present, but cannot be calibrated as the PMDs integrate the wavelength band into a single measurement point. In the main instrument channels, straylight may modify weak absorption lines, but the integrated straylight signal is very small compared to the total channel signal. Hence the contribution of spectral straylight is expected to be minor. In addition, for calibrated PMD quantities the spectral straylight in-orbit is probably not overwhelmingly different from that during on-ground calibration, and the latter is implicitly accounted for in the Keydata (although there may be some differences due to spectral shape of the input spectrum).

A larger source of uncertainty may be light from a spectral region covered by a PMD bandwidth, but not measured in the channel detectors. This is referred to as “out-of-band” straylight [P 8.2]. The correction for out-of-band straylight that is used in Level 1b processing is a correction for “missing” intensity which effectively results in a lump sum for all effects that lead to an offset of atmospheric polarisation values. This is implemented as a correction to the virtual sum and is described in Section 5.3.12 “P12 – Polarisation values”.

5.3.9 P9 – Greek Keydata / MMEs

Uncertainty components are listed in Table 5-1 (note applicability in last table column).

Since the PMDs integrate over a wide spectral bandwidth, any noise on Keydata is averaged out and can be neglected for the calculation of polarisation values. Noise on Keydata used for calculation of the radiance polarisation correction factor may play a role; this is accounted for in [R 12.1.2].

5.3.10 P10 – PMD: Diffuser BSDF

This is only relevant for GOME, where a correction term “Q” for the virtual sum is derived from self-calibration on the Sun (which provides an unpolarised input).

The uncertainties are similar to [I 10.1] and [I 10.2] where it has to be taken into account that the PMDs integrate over their broad bandwidth (e.g. noise is irrelevant).

5.3.11 P11 – PMD Degradation correction

GOME:

This is implicit in the Q-factor, but uncertainties due to

- Earth spectrum shape different from Sun spectral shape
- Different scan angles for Sun and Earth

SCIAMACHY:

This is implicit in the “in-band correction factor” C_{IB} , but uncertainties due to

- Systematic differences between modelled atmosphere and real atmosphere
- Temporal averaging of C_{IB} over long time scales

5.3.12 P12 – Polarisation values

The PMD virtual sum is the pivotal equation from which the PMD polarisation parameters are derived. The formal error propagation follows from the uncertainties on all terms in the virtual sum.

The virtual sum has a number of inputs:

- Greek Keydata or MMEs with uncertainties from on-ground calibration [P 9] and in-orbit degradation [P 11] .
- “in-band correction factor” as in-flight “calibration” of polarisation values [P 12.3.2] .
- assumptions on the spectral shape of the polarisation [P 12.3.1] .
- for SCIAMACHY: calculation and/or assumptions on $u(\lambda_i)$
- for SCIAMACHY: correction for cluster readout issue [P 12.3.3] .

Output is polarisation parameter q (for SCIAMACHY there may be an iteration for u as well).

For GOME an effective PMD centre wavelength is calculated, for SCIAMACHY this is fixed and accounted for in the in-band correction [R3].

In addition to the virtual sum calculation for PMDs, a value for the “theoretical point” (polarisation value and wavelength) is calculated. This provides a polarisation point for the UV interpolation in channels 1 and 2, as mentioned in Section 4.3.12.

5.3.12.1 The Virtual Sum

The following uncertainties are without the uncertainties from [P 9] that need to be taken into account

too.

GOME:

This uses a PMD virtual sum as described in ATBD [R2] to derive atmospheric polarisation at an effective “central wavelength” of each PMD.

- uncertainty on correction factor Q (see “in-band correction factor” below)
- significant uncertainty due to assumption that polarisation fraction is constant over PMD bandwidth
- uncertainty because the unknown instrument sensitivity to u is neglected

SCIAMACHY:

This uses a PMD virtual sum as described in [R10].

- Uncertainty on in-band correction factor [R10]
- Uncertainty on the applicability of wavelength-averaged MMEs (that replaces the GOME assumption of constant polarisation, with smaller uncertainty)
- Uncertainty on u . (depending on polarisation angle)

5.3.12.2 In-band correction factor

GOME:

The GOME algorithm requires that polarisation retrieved from Sun measurements is zero (self-calibration of PMD response on the Sun). This is achieved by adding an amount ($Q \cdot S_{PMD}$) to the “channel side” side of the virtual sum [R2]. This “Q-factor” corrects not only out-of-band straylight but also differential degradation between PMDs and main channels [P 12.3.2].

SCIAMACHY:

In older versions of the L1b algorithm, there was a Q-factor as for GOME. In the current L1b algorithm version [R3][R10], there is a pre-calculated “in-band correction factor” [P 12.3.2]. The in-band correction factor is pre-calculated in a LUT as function of time, such that it also implicitly corrects for degradation. The in-band correction factor has been empirically determined such that the polarisation fractions are (on average) zero where this is expected based on a radiative transfer model.

A mismatch between PMD signals and channel signals may occur because of the clustered readout. Some parts of the channel may be read out faster than the others. The spectrum of the cluster[s] with longer integration time is then unknown. This missing intensity is estimated by scaling the spectrum using the higher time sampling of the PMDs [P 12.3.3].

5.3.12.3 Theoretical point

This calculates the single scattering polarisation value, the highest single scattering wavelength, and the steepest gradient for the GDF (see Section 4.3.12).

Algorithm: see ATBDs [R2][R3] . Uncertainties in:

- Albedo



- O3 content
- Representative scan angle
- How representative is the radiative transfer LUT

5.4 Polarisation quantitative uncertainty estimates

It is not possible to derive a generally valid estimate on the uncertainty on polarisation values. The main reason is that uncertainties depend on scene inhomogeneity, as well as specific shape of the input spectrum. In addition, uncertainties on some vital components are not known with sufficient accuracy. Effect tables have not been generated for polarisation.

6 Spectral uncertainties

6.1 Introduction

The spectral uncertainties are divided into two categories:

- “spectral calibration” i.e. determination of the wavelength of each detector pixels
- Instrument Spectral Response Function (ISRF) i.e. the instrument response to a monochromatic input.

The definitions of the ISRF and the spectral calibration are linked. The wavelength assigned to a pixel in spectral calibration refers to the geometrical centre of a pixel. However, if the ISRF is not strictly symmetrical, a monochromatic input wavelength centred on the pixel (according to the real instrument dispersion) will result in a measurement that shows an intensity distribution with a centre-of-gravity that is slightly off-centre. Thus, it will appear that the wavelength is shifted, if the centre of the ISRF is defined as its centre of gravity. One could also define the centre of the ISRF as being its maximum value. Then no shift occurs but if the ISRF changes in-orbit the location of the maximum cannot be detected (unless if the instrument clearly oversamples the spectrum, which is not the case for GOME and SCIA). A centre-of-gravity can always be determined and thus that definition is used in the spectral calibration method of GOME and SCIAMACHY.

The determination of the ISRF has no direct relevance for the Level 1 calibrated [ir]radiance, but is important for Level 2 retrievals.

6.2 Processing Chain

An overview of the contributions to the spectral uncertainty is shown in Table 6-1. As with similar tables for [ir]radiance, not all effects are necessarily significant. This table serves to understand error contributions, but it will not be mirrored 1-to-1 in the Measurement Functions and Effect Tables. The reason for this is that the uncertainty will be expressed as lump sum that is not based on rigorous error propagation, but rather on practical experience.

Table 6-1 Overview of contribution to the uncertainty for the spectral calibration. The last column indicates if the item is applicable to GOME (G) and/or SCIAMACHY (S)

#	main elements	#	contributing elements	#	sub-items	
S1	Get SLS line positions	S1.1	determine centre-of-gravity			GS
		S1.2	line blends			GS
		S1.3	Low-signal lines			GS
		S1.4	etalon effects			GS
		S1.5	line shift on radiance slope			GS
S2	Polynomial fit	S2.1	fit quality due to uncertainty in line			GS

#	main elements	#	contributing elements	#	sub-items	
			positions (from S1)			
		S2.2	non-polynomial "truth"			GS
		S2.3	channel edges	S2.3.1	missing lines	GS
				S2.3.2	polynomial edge effect	GS
		S2.4	pixel-to-pixel variations			GS
S3	Apply spectral calib.	S3.1	Pre-disperser temperature			G
		S3.2	orbit dependence			S
		S3.3	inhomogeneous scenes			GS
S4	Doppler shift	S4.1	Radiance			GS
		S4.2	Sun			GS
S5	ISRF	S5.1	on-ground CKD			GS
		S5.2	change OG→ in-orbit			GS
		S5.3	in-orbit change			GS

The main source of uncertainty in spectral calibration lies in generation of the in-orbit CKD, which results from [S2] which uses as input [S1].

6.3 Instrument Measurement function

6.3.1 S1 – SLS line positions

For each SLS line used in spectral calibration, the line position is calculated as the first moment of the pixel distribution in each line (centre-of-gravity).

The determination of the centre-of-gravity carries uncertainties due to noise on the (few) pixels in each line, and also because the lines are undersampled [S1.1]. This is usually not a significant source of uncertainty, except for low-signal lines [S1.3]. More significant uncertainties may arise from line blends [S1.2], as different components in these lines may show different strength based on lamp temperature. A spectral line on a radiance response slope may also be shifted [S1.5], since in the first moment calculation one line wing will contribute more than the other.

It is not known if line shifts may occur due to etalon [S1.4] (akin to shift on radiance slope). If the cause of the etalon is interference by different wavelengths, etalon is not present on monochromatic spectral lines. But if etalon is caused by interference of various incidence angles on the detector, monochromatic lines are also affected.

6.3.2 S2 – Polynomial fit

Dispersion of a grating is strictly constant, which would result in a strictly linear function of wavelength versus detector-pixel if the optics were focussing perfectly on the detector. In practice, the wavelength scale on the detector follows from the intersection of a curved focal plane with a straight line (the detector). Usually, this may be approximated well by a polynomial function of wavelength versus detector pixel, but it needs not be strictly polynomial [S2.2]...

On a pixel-to-pixel scale, deviations from the polynomial may occur if the semiconductor material in the pixel (“doping”) is not completely homogeneous, or if the pixels are not completely identical in size [S2.4]. This would also be reflected in the PPG. Since PPG is very small for GOME and SCIAMACHY, the effect is probably insignificant.

Operational Level 1 processing calculates the spectral calibration polynomial using a SVD fit of the line positions with equal line weights (i.e. independent of uncertainty from noise, line strength and line stability) [S2.1]. For GOME, all instable lines (probably those with line blends) have been removed. This has significantly stabilised the fit. However, it is not known if having fewer lines might have introduced a systematic fit error.

A well-known issue with polynomial fits is that they tend to run away (be instable and badly constrained) near the channel edges [S2.3]. In SCIAMACHY Level 1 processing it was attempted to constrain this by effectively giving the outermost line (closest to either channel edge) double weight, and also by fitting Chebychev polynomials instead of normal ones. In practice this didn’t significantly help in constraining the fit near the channel edges.

6.3.3 S3 – Apply spectral calibration

Spectral calibration may change with instrument temperature. In GOME and SCIAMACHY, the main component sensitive to temperature [in this respect] is the predisperse prism.

For GOME, spectral calibration parameters are stored in the calibration database as function of temperature. The temperature reading of the predisperse prism is used in the application of spectral calibration to select the right parameters. Other possible effects are neglected [S3.1].

In SCIAMACHY, the optical bench is temperature-stabilised. Nevertheless, spectral calibration may change due to temperature gradients in the instrument. This is dependent on the amount and history of heating by the Sun, i.e. depends on position in the orbit. The spectral calibration parameters are stored in the calibration database for several different orbit phases. In the application of spectral calibration, orbit phase is used to select the right parameters. There is no interpolation in orbit phase and thus a “digitisation error” remains [S3.2].

An entirely different kind of uncertainty is associated to scene inhomogeneity [S3.3]. The image of the slit on the detector pixels is curved (this was demonstrated in orbit for SCIAMACHY, by using the planet Venus as a probe for measured intensity versus position of a point-source like Venus in the slit). If a scene has inhomogeneous intensity as function of slit height, the centre-of-gravity of this curved slit image may change, and hence an apparent spectral shift may be present in the spectrum.

6.3.4 S4 – Doppler shift

During solar calibration, the instrument is looking more or less in the flight direction (moving in an angle towards the Sun). This results in a blue-shifted solar spectrum (i.e. Fraunhofer lines are at shorter wavelengths than spectral calibration predicts). The shift is proportional to wavelength. For SCIAMACHY channel 8 at 2.4 μm , the shift may be as large as half a detector-pixel. For GOME and SCIAMACHY at the beginning of channel 1 (near 240 nm) it is 1/20th of a pixel. At 480 nm it is still 1/20th because there the detector pixels are 0.2 nm wide instead of 0.1 nm.

On the GOME Level 1b product, there is neither a correction nor a parameter describing the Doppler shift for Irradiance. In principle it is straightforward to calculate from the spacecraft velocity and the azimuth incidence angle of the Sun on the Diffuser (and the orientation of the Diffuser in the instrument). For SCIAMACHY, the Doppler shift is calculated on the Level 1 product for a wavelength of 500 nm (it scales linearly with wavelength). Uncertainties arise due to uncertainties in the instrument state vector and uncertainties in the exact viewing angles, but these are relatively small.

For nadir-looking instruments, there is no Doppler shift. There is for East and West viewing pixels a small velocity component in the viewing direction due to the velocity difference between Earth rotation and spacecraft velocity.

6.3.5 S5 – ISRF

The shape of the ISRF has been calibrated on-ground using a fit of a “trial function” on measured SLS lines. Since SCIAMACHY and GOME both under sample the spectrum (GOME more than SCIAMACHY) this has led to significant uncertainties on the ISRF CKD. The CKD trial functions have employed a symmetrical ISRF, although better fits may be achieved with asymmetrical functions – this is especially the case at the start (the short wavelength side) of channel 2.

A better ISRF determination has been made for GOME using a fit of solar spectra. Chance and Caspar have fitted the FWHM of a Gaussian. A further improvement for Channel 2 was made by Van Roozendaal et al. who fitted an asymmetrical Voigt profile. Note that for asymmetrical ISRFs, the convolution kernel may be the mirror image of the line profile. At short wavelengths in channel 2, the GOME line profiles have a “blue” wing.

References:

- C. Caspar, K. Chance, “GOME wavelength calibration using solar and atmospheric spectra”, Proc. Third ERS Symposium on Space at the Service of our Environment, ESA pub. SP-414, Vol.II, p.609, 1997
- M. Van Roozendaal, V. Soebijanta, C. Fayt, and J.-C. Lambert, “INVESTIGATION OF DOAS ISSUES AFFECTING THE ACCURACY OF THE GDP VERSION 3.0 TOTAL OZONE PRODUCT”, Chapter 6 of “ERS-2 GOME GDP 3.0 Implementation and Delta Validation”, ERSE-DTEX-EOAD-TN-02-0006 p.98, 2002, <https://earth.esa.int/eogateway/documents/20142/37627/ERS-2-GOME-GDP-3.0-Implementation-and-Delta-Validation.pdf>

7 Geolocation uncertainties

7.1 Introduction

In this section the uncertainty estimates are given for the geolocation data in the GOME/SCIAMACHY Level 1 products. The definition of geolocation for Radiance is w.r.t. a well-defined reference height, and a well-defined reference time for the measurement. For the Nadir radiance measurements of the FDR these are top of atmosphere (TOA) defined as 100 km above the WGS84 reference ellipsoid and readout time of the first detector pixel, respectively.

The quoted uncertainties are on this definition. However, even within this definition, the actual geolocation of the measurement may differ slightly from the geometrically calculated one due to light path effects in the atmosphere.

7.2 Processing chain

An overview of the uncertainty processing steps and numbering is shown in Table 7-1. The numbers [G1] and [G2] deal with uncertainties in the Level 0-1 processing. The uncertainties from these steps cannot be added by the usual error propagation rules, as they affect complex calculations in the orbit propagation software. Therefore, [G3.3] is intended to provide a lump-sum uncertainty on the purely geometrical geolocation calculations.

In addition to the uncertainties on the geometrical pixel boundaries, there are also uncertainties [G4] due to the fact that the spatial point-spread function (PSF) is not rectangular, and due to [uneven] illumination effects within the instrument slit. These are mentioned for completeness, but not included in the uncertainty budget as they are scene-dependent, and may be more a Level 2 issue than a Level 1 issue.

Table 7-1 Overview of generic processing steps and numbering for the geolocation. The last column indicates if the item is applicable to GOME (G) and/or SCIAMACHY (S)

#	main elements	#	contributing elements	#	sub-items	
G1	Orbit position	G1 .1	state vector			GS
		G1 .2	measurement time stamp			GS
		G1.3	orbit propagation S/W			GS
G2	Line-of-sight	G2.1	uncertainty in scanner encoder			GS
		G2.2	misalignment sat/instrum			GS
		G2.3	platform attitude (AOCS)			GS
G3	Geometrical geolocation	G3.1	orbit propagation			GS
		G3.2	surface height/			GS

#	main elements	#	contributing elements	#	sub-items	
			ref.ellipsoid			
		G3.3	detector readout			GS
G4	Apparent pixel shift					
		G4.1	light path			GS
		G4.2	scene heterogeneity			GS

7.3 Geolocation Uncertainty components

The default heading of this section, analogue to previous chapters, would be “Instrument measurement function”. However, geolocation in the GOME/SCIAMACHY L1b products is not based on measurements but purely on calculations. We therefore present here a description of the uncertainty components from Table 7-1.

7.3.1 G1 – Orbit position

The position of the satellite in the orbit is calculated by the orbit propagation software [G1.3] from the measurement time [G1.2] and the orbit state vector [G1.1]. All three items have their uncertainties.

For the measurement time stamp there is also a definition issue, because not all pixels of the detector are read out simultaneously. For GOME, the time stamp is at readout of the first detector pixel (subsequent pixels are sequentially read out a fraction of a second later). For SCIAMACHY, the readout is at “BCPS” which also coincides with readout of the first detector pixel. An “average time” for the complete spectrum (or a SCIAMACHY cluster) would be slightly later. However, we do not take this definition issue into the uncertainty budget.

7.3.2 G2 – Line-of-sight

This concerns the line of sight from instrument towards Earth / Sun / Moon. The uncertainties will be given in angular units. The items [G2.1] [G2.2] [G2.3] should be self-explaining.

7.3.3 G3 – Geometrical geolocation

Item [G3.1] is a lump-sum uncertainty on the purely geometrical geolocation calculations from inputs mentioned in section 7.2. TBD: Item [G3.3] addresses the time stamp definition as mentioned in section 7.3.1.

7.3.4 G4 – Apparent pixel shift

There are a number of reasons why, even with accurate geometrical geolocation, the measured radiance may come from a somewhat different location than one thinks:

- The projection of the slit on the Earth surface is not sharp, but a fraction of light outside the nominal pixel also falls on the detector (meant is not straylight, but light included in the optical



PSF). Actually, in the along-track direction it is the detector pixel size that limits the field-of-view, but that doesn't change the argument.

- Especially in low solar elevation (large solar zenith angles), a significant part of the atmospheric absorption may occur outside the pixel.
- Heterogeneity in the scan direction (across-track) may lead to a displacement of the centre-of-gravity. For scanning measurements, this will generally be negligible. However, for static nadir measurements (and SCIAMACHY limb measurements) this may be a significant effect.

We consider these items primarily as interpretation issues relevant for Level 2, rather than uncertainties in the measurements themselves. Therefore, this will not be included in the FDR uncertainty budget.